NASA
TP
1044
c.1

NASA Technical Paper 1044

LOAN COPY: RETUR
AFWL TECHNICAL LI
KIRTLAND AFB, N.

TECH LIBRARY KAFB, NM
0134262

Aerodynamic Characteristics at Mach Numbers From 0.33 to 1.20 of a Wing-Body Design Concept for a Hypersonic Research Airplane

James L. Dillon and Jimmy L. Pittman

DECEMBER 1977

NASA

TECH LIBRARY KAFB, NM
0134262

NASA Technical Paper 1044

Aerodynamic Characteristics at Mach Numbers From 0.33 to 1.20 of a Wing-Body Design Concept for a Hypersonic Research Airplane

James L. Dillon and Jimmy L. Pittman
Langley Research Center
Hampton, Virginia

National Aeronautics
and Space Administration

**Scientific and Technical
Information Office**

1977

SUMMARY

An experimental investigation of the static aerodynamic characteristics of a model of one design concept for the proposed National Hypersonic Flight Research Facility was conducted in the Langley 8-foot transonic pressure tunnel. The experiment consisted of configuration buildup from the basic body by adding a wing, center vertical tail, and a three-module or six-module scramjet engine. The free-stream test Mach numbers were 0.33, 0.80, 0.90, 0.95, 0.98, 1.10, and 1.20 at Reynolds numbers per meter ranging from 4.8×10^6 to 10.4×10^6. The test angle-of-attack range was approximately -4° to 22° at constant angles of sideslip of 0° and 4°; the angle of sideslip ranged from about -6° to 6° at constant angles of attack of 0° and 17°. The elevons were deflected 0°, -10°, and -20° with rudder deflections of 0° and 15.6°.

The basic configuration (without either engine) experienced a local pitch instability at an angle of attack of about 6° and a free-stream Mach number of 0.95; but, in general, the configurations with and without either scramjet engine exhibited large amounts of static longitudinal stability through the angle-of-attack range and positive effective dihedral for positive angles of attack. The concept was directionally unstable across the test free-stream Mach number range above an angle of attack of 14°. Rudder deflection caused effective control reversal at free-stream Mach numbers of 0.90, 0.95, and 0.98.

INTRODUCTION

Separate National Aeronautics and Space Administration (NASA) and U.S. Air Force (USAF) studies have shown the desirability of hypersonic flight for certain missions. These studies have included a commercial transport, military defense systems, and an air-breathing launch vehicle for future space systems (refs. 1 to 7). In further pursuing these objectives, the two agencies jointly conducted a study to define a research airplane which would serve as a hypersonic flight technology demonstrator (ref. 8). This joint research effort (ref. 9) is currently designated the National Hypersonic Flight Research Facility (NHFRF). Some of the guidelines for the NHFRF design concepts are:

(1) To achieve low cost, low risk status, the facility will use near state-of-the-art materials and the proven B-52 air-launch, rocket-boost, and glide-descent flight techniques.

(2) The facility will serve as a flying test bed for hypersonic cruise engine prototypes such as the integrated modular scramjet.

(3) The facility will have a removable payload bay for housing research experiments.

A typical mission profile for the proposed research airplane is shown in figure 1 to illustrate the angle of attack expected during transonic flight.

In the transonic regime, a 17° angle of attack is required during ascent in order to attain a high flight path angle for efficient rocket boost path and to minimize dynamic pressure; the 4° equilibrium angle of attack established at the cruise condition is maintained during descent. The supersonic and hypersonic portions of the profile will change with different experimental objectives but the transonic ascent-descent portion shown is probably representative for most research flights.

The purpose of the present study was to investigate experimentally at transonic speeds a wing-body concept developed in-house for the NHFRF. Longitudinal, lateral, and directional stability and control characteristics of the model were studied. These aerodynamic characteristics will be used to assess the acceptability and viability of the concept through simulator and mission studies. The parametric tests included configuration buildup and elevon and rudder deflection. Most of the study was conducted at Mach numbers of 0.80, 0.90, 0.95, 0.98, 1.10, and 1.20 over a Reynolds number per meter range of 9.3×10^6 to 10.4×10^6. Limited data were also taken at $M_\infty = 0.33$ and at a Reynolds number per meter of 4.8×10^6. The angle of attack varied from about -4° to 22° at constant angles of sideslip of 0° and 4°, while the angle of sideslip varied from about -6° to 6° at constant angles of attack of 0° and 17°. The elevons were deflected symmetrically to establish trim characteristics and asymmetrically for roll control. The rudder was also deflected for yaw control. Only those data and results pertinent to an overall assessment of this concept at transonic speeds are presented in the main body of the paper. The basic data are presented in the appendixes.

SYMBOLS

The longitudinal characteristics are presented about the stability axis, and the lateral-directional characteristics are presented about the body axis (fig. 2). The moment reference point was located at the design center of gravity (65 percent of the body length longitudinally) and on the model reference line vertically. Values are given in SI units. (Tables present values in both SI and U.S. Customary Units.) Measurements and calculations were made in U.S. Customary Units.

A_b base area of fuselage, m^2

A_r reference area, 0.0626 m^2

$\frac{A_{rudder}}{A_{total}}$ ratio of rudder area to total vertical tail area

b wing span, m

C_D drag coefficient, $\frac{D}{q_\infty A_r} - C_{D,b}$

$C_{D,b}$ base drag coefficient, $\frac{\text{Base drag}}{q_\infty A_r}$

$C_{D,o}$ drag coefficient at zero lift $(C_D)_{C_L=0}$ obtained by extrapolating C_L^2 plotted against C_D to $C_L = 0$

C_L lift coefficient, $\frac{L}{q_\infty A_r}$

C_{L_α} lift-curve slope, $\frac{\partial C_L}{\partial \alpha}$, per deg

C_l rolling-moment coefficient, $\frac{M_X}{q_\infty A_r b}$

C_{l_β} effective dihedral parameter $\frac{\Delta C_l}{\Delta \beta}$ obtained from values of C_l at $\beta \approx 0^\circ$ and 4°, per deg

$C_{l_{\delta_h}}$ rate of change of C_l with differential elevon deflection, $\left[(C_l)_{\delta_h=20} - (C_l)_{\delta_h=0}\right]/20$, per deg

$C_{l_{\delta_v}}$ rate of change of C_l with rudder deflection, per deg

C_m pitching-moment coefficient, $\frac{M_Y}{q_\infty A_r \ell}$

$C_{m,o}$ pitching-moment coefficient at zero lift

C_{m_α} pitching-moment curve slope $\frac{\partial C_m}{\partial \alpha}$, per deg

$\frac{\partial C_m}{\partial C_L}$ static longitudinal stability parameter, based on ℓ

C_n yawing-moment coefficient, $\frac{M_Z}{q_\infty A_r b}$

C_{n_β} directional-stability parameter $\frac{\Delta C_n}{\Delta \beta}$ obtained from values of C_n for $\beta \approx 0^\circ$ and 4°, per deg

$C_{n_{\beta_{dyn}}}$ dynamic directional-stability parameter, $C_{n_\beta} \cos \alpha - C_{l_\beta} \frac{I_Z}{I_X} \sin \alpha$

$C_{n_{\delta_h}}$ rate of change of C_n with differential elevon deflection, $\left[(C_n)_{\delta_h=20} - (C_n)_{\delta_h=0}\right]/20$, per deg

$C_{n_{\delta_v}}$ rate of change of C_n with rudder deflection, per deg

$C_{p,b}$ base-pressure coefficient, $\frac{p_b - p_\infty}{q_\infty}$

C_Y side-force coefficient, $\frac{F_Y}{q_\infty A_r}$

C_{Y_β} side-force parameter $\frac{\Delta C_Y}{\Delta \beta}$ obtained from values of C_Y for $\beta \approx 0^o$ and 4^o, per deg

$C_{Y_{\delta_h}}$ rate of change of C_Y with differential elevon deflection, $\left[(C_Y)_{\delta_h=20} - (C_Y)_{\delta_h=0}\right]/20$, per deg

$C_{Y_{\delta_v}}$ rate of change of C_Y with rudder deflection, per deg

c.g. design center of gravity, moment reference point

D drag, $F_N \sin \alpha + F_A \cos \alpha$

F_A axial force along X-axis, positive direction, -X

F_N normal force along Z-axis, positive direction, -Z

F_Y side force along Y-axis, positive direction, +Y

HL hinge line

h altitude, km

$\frac{I_Z}{I_X}$ ratio of moments of inertia about yaw and roll axes, respectively

L lift, $F_N \cos \alpha - F_A \sin \alpha$

L/D lift-drag ratio

ℓ length of model fuselage, m

M_∞ Mach number

M_X, M_Y, M_Z moments about X-, Y-, and Z-axes, respectively

p_b base pressure

p_∞ free-stream static pressure

q_∞ free-stream dynamic pressure, kN/m^2

X,Y,Z reference axes, unsubscripted indicate body axes

α angle of attack, deg

β angle of sideslip, deg

δ_e elevon deflection angle, positive when trailing edge is down, deg

Subscripts:

s stability axis system

t trim condition, $C_m = 0$

δ_h differentially deflected ailerons for roll control

δ_v deflected rudder for yaw control

Model nomenclature:

B body of fuselage

BF base fairing

BWV_{CS} basic configuration

E_3 three-module scramjet engine

E_6 six-module scramjet engine

V_{CS} center vertical tail, subsonic, diamond airfoil

W wing

DESIGN CONCEPT

This concept was based primarily on performance, stability, and control requirements over a Mach number range from 6 to 8 and the performance at touchdown speed, with a scramjet engine installed. Reference 10 has shown that vehicle performance is sensitive to the longitudinal location of the scramjet engine and to wing incidence because the engine produces moments that must be

counterbalanced by the wing and elevons. The scramjet engine also dictates the underbody shape of the vehicle since the airframe-integrated scramjet concept uses the forebody for precompressed air and the aftbody for a half-nozzle expansion ramp (ref. 11). This proposed scramjet engine package would probably require a minimum of three modules for a meaningful flight experiment whereas a six-module package represents the size required to produce positive net thrust minus drag at Mach 6. The center vertical tail was designed with a dual hinge line at approximately the two-thirds chord location. This design allows for a diamond airfoil for subsonic through supersonic speeds, a wedge airfoil for hypersonic speeds, and speed brake extension. Base fairings were added to determine the effect on drag of reducing the flat base area at touchdown speeds.

MODEL

A photograph of the cast model with its interchangeable parts is shown in figure 3. The modular design of the 0.033-scale test model permitted buildup of the basic model (fig. 4(a)) from the following components: body, cropped delta wing, center vertical tail, base fairing, and scramjet engine. The wing had 2.1° negative incidence and 10° positive dihedral. The airfoil was a modified circular arc with a leading-edge radius (normal to leading edge) of 0.064 cm followed by a 10° wedge section, and the elevons had a constant thickness at the hinge line of 0.814 cm and a 7.6° wedge angle. The wedge elevons were machined with a radius over approximately the aft one-third to give a trailing-edge thickness of 0.064 cm. The elevons could be deflected $\pm 20^{\circ}$. The diamond airfoil tail (fig. 4(b)) was the only one tested in this investigation. The base fairings are shown in figure 3. Two model scramjet engine packages consisting of three and six clustered modules were also tested (see figs. 3 and 4(c)). The proposed flight research engine has three internal fuel struts in each module whereas the model engine packages used in this test simulated the internal geometric contraction by use of one strut (ref. 12). The pertinent geometrical characteristics of the model for aerodynamic testing are listed in table I.

APPARATUS AND TEST

Tunnel and Test Conditions

The investigation was conducted in the Langley 8-foot transonic pressure tunnel (ref. 13). This facility is rectangular in cross section; the upper and lower walls are slotted longitudinally to allow continuous operation through the transonic speed range and, as a result, the effects of choking and blockage are negligible.

The aerodynamic forces and moments were measured by means of a six-component strain-gauge balance housed inside the model fuselage and attached to the tunnel sting support system. Base pressure was measured with forward facing pressure tubes located approximately 0.2 cm behind the fuselage base. Most of the tests were conducted at free-stream Mach numbers, Reynolds numbers per meter, and dynamic pressures as follows:

M_∞	Reynolds number		Free-stream dynamic pressure	
	per meter	per foot	kPa	lb/ft^2
0.80	9.3×10^6	2.83×10^6	22.4	468
.90	9.8	2.98	25.5	533
.95	10.0	3.04	26.9	562
.98	10.1	3.07	27.7	578
1.10	10.3	3.14	30.2	631
1.20	10.4	3.17	31.6	660

A limited amount of data were taken at $M_\infty = 0.33$, at a Reynolds number per meter of 4.8×10^6 (1.47×10^6 per foot), and at a free-stream dynamic pressure of 5.4 kPa (113 lb/ft^2).

The stagnation temperature and dew point were maintained at values to preclude condensation shock effects. The angle-of-attack range was from about -4° to 22° at angles of sideslip of 0° and 4°. A limited number of tests were also conducted over an angle-of-sideslip range of approximately $\pm 6^\circ$ at angles of attack of about 0° and 17°. Transition strips, 0.32 cm wide and composed of No. 120 carborundum grains, were applied at the following locations (measured streamwise): 3.18 cm aft of the nose stagnation point; 1.14 cm aft of the leading edge of the wing, vertical tail, and engine cowling; and 1.14 cm inside the leading edges of the scramjet engine.

Corrections and Accuracy

Because of the slotted test section, no corrections to the free-stream Mach number and dynamic pressure for the effects of model and wake blockage are necessary. Also, no results are presented for supersonic Mach numbers where boundary-reflected disturbances would be expected to have an effect.

The drag data have been corrected to the condition of free-stream static pressure acting on the fuselage balance cavity and base. Typical measured base-pressure coefficients are presented in figure 5. No correction was made to the drag data for flow through the scramjet engine.

The angles of attack and sideslip have been corrected for the deflection of the balance and sting due to aerodynamic load. The angles of attack were also corrected for tunnel flow angularity.

The data presented at $M_\infty = 0.33$ should be used with caution since these data were acquired for a low free-stream dynamic pressure condition and also because the method suggested in reference 14 indicates that a larger grit size is needed to insure fully turbulent flow for this test condition.

RESULTS AND DISCUSSION

Static Longitudinal Characteristics

Configuration buildup and basic data.- The longitudinal aerodynamic characteristics for the configuration buildup are presented in appendix A. For convenience in assessing Mach number effects, the untrimmed aerodynamic characteristics for the configurations with and without the six-module scramjet engine are presented in figures 6 and 7. Note the pitch instability and simultaneous decrease in C_{L_α} at $M_\infty = 0.95$, $\alpha \approx 6^\circ$ for BWV_{CS}, and the subsequent resumption of stability and increasing C_{L_α} at higher angles of attack. This behavior is probably caused by interference from the vertical tail (see appendix A). Such behavior has been previously observed on the delta wing, center vertical tail F-102 configuration (ref. 15). Note also the nonlinearity in the lift and pitching-moment curves, particularly at the lower free-stream Mach numbers. The nonlinearity probably occurs because the flow about this clipped delta wing concept is mainly potential at $\alpha \leq 7^\circ$. At this point, vortex flow from the wing probably becomes significant because of the rather large tip chord (refs. 16 and 17).

The drag penalty of adding the engine package was assessed by studying the increments in $C_{D,o}$ for configurations with and without the six-module engine as a function of Mach number. (See fig. 8.) These increments were obtained by plotting C_D against C_L^2 and linearly extrapolating to $C_L = 0$. The addition of the engine increases $C_{D,o}$ by approximately 50 percent at Mach 0.80, but the incremental increase in $C_{D,o}$ through the transonic regime is roughly the same (0.025) both with and without the scramjet engine installed.

Trim characteristics.- The effect of elevon deflection on the longitudinal characteristics of the configurations with and without the six-module engine is presented in appendix B. These effects were used to determine the trimmed characteristics for each configuration. These characteristics for BWV_{CS} and $BWV_{CS}E_6$ are presented in figures 9 and 10, respectively. Except for the BWV_{CS} configuration at $M_\infty = 0.95$, the plots have been extrapolated where necessary to establish the Mach number history for the anticipated trimmed angle of attack ranging from $\alpha_t \approx 17^\circ$ to 4° during ascent and descent, respectively, through the transonic speed regime. Extrapolation of the data for the BWV_{CS} configuration indicates that multiple trim points occur for $\delta_e \geq 9^\circ$ (or $\alpha_t = 7.5^\circ$); therefore, the trimmed characteristics for $\delta_e \geq 9^\circ$ cannot be clearly defined. The usual performance parameters ($(L/D)_{maximum}$, etc.) are not discussed for this off-design speed regime. The Mach number histories of primary parameters of interest at transonic speeds are presented in figure 11 for BWV_{CS} and $BWV_{CS}E_6$ at $\alpha_t \approx 4^\circ$ and 17°. The curve of elevon power $\partial C_m/\partial \delta_e$ plotted against Mach number was taken for the untrimmed C_L at $\alpha_t \approx 4^\circ$ and 17° and the slope of the C_m plotted against the δ_e curve was read at $\delta_e = 0^\circ$. Figure 11 indicates that the basic configuration is unstable at $\alpha_t \approx 4^\circ$, $0.925 \leq M_\infty \leq 0.96$ but that the concept in general has large static longitudinal stability at all other transonic flight conditions. The low elevon control power exhibited at transonic speeds indicates that large elevon deflections are required to trim the vehicle, especially at $0.95 \leq M_\infty \leq 1.25$. The implied elevon deflections for the

extrapolations presented in this paper could promote separation and alter these results; however, to meet the present mission study projections, the best estimates of the trimmed characteristics at the required trimmed angles of attack are presented in figures 9, 10, and 11. These trim characteristics together with the roll-yaw characteristics presented later indicate that the design concept discussed in this paper may be improved by enlarging the elevons. Also, the local pitch instability may be alleviated by geometric alteration. Preliminary mission analyses using the data presented in this paper indicate that a slight adjustment in angle of attack to avoid the region of instability during transonic descent would not significantly affect the overall mission profile.

Theoretical comparisons.- The vortex lattice method of reference 18, with improvements in the leading-edge suction by John E. Lamar (as yet unpublished), was used to predict the aerodynamic characteristics of the fuselage and wing configuration only at $M_\infty = 0.80$. This is the highest Mach number at which the predictions were made since local shocks (which render the technique invalid) were noted on schlieren photographs for $0.90 \leqq M_\infty$. The prediction technique was used by assuming potential flow over the entire planform plus vortex flow over the wing leading edge and side edge (tip). The mean camber lines of the fuselage and the wing were used to determine local angle-of-attack input at each vortex panel. The comparison of theoretical prediction with experimental data is presented in figure 12; theory predicts the data quite well, especially at the lower lift coefficients.

Static Lateral-Directional Characteristics

Basic lateral aerodynamic characteristics are presented in appendix C. The static lateral-directional characteristics for the body buildup were evaluated at $\beta \approx 0^\circ$ and 4° and are presented in figure 13. The body alone is unstable both laterally and directionally at all free-stream Mach numbers. The addition of the wing provides positive effective dihedral at most positive angles of attack, but as expected, there is very little gain in directional stability. The center vertical tail provides directional stability up to a minimum of about 12° angle of attack at $M_\infty = 1.10$ and to as high as 14° at $M_\infty = 0.98$. The loss of tail effectiveness at high angles of attack is due in part to adverse effects from the fuselage forebody. In general, the center vertical tail provides a slight improvement in lateral stability. Addition of the six-module engine has a stabilizing influence on the directional stability based on the model moment reference which represents the center of gravity of the basic BWV_{CS} configuration. Therefore, the magnitude of this improvement in stability may be diminished if the center of gravity of the flight vehicle experiences a significant rearward shift with the addition of the flight engine. The six-module engine does not prevent the loss of stability at high angles of attack even at the test moment reference. The lateral stability is slightly improved by the six-module engine at the lower α range but decreases at the higher α range. The directional stability characteristics are insufficient to provide a stable ascent through transonic speeds with or without the engine. The effect of this instability on vehicle transonic performance will depend on simulation studies and the effect of flight vehicle inertias on $C_{n_{\beta_{dyn}}}$.

Lateral and Directional Control

The roll control which was investigated for the $BWV_{CS}E_6$ configuration only is presented in figure 14. These data were obtained by deflecting the left elevon 10° and the right elevon -10°. The yawing moment due to roll control is adverse but is not considered a serious problem.

The yaw control for this same configuration is presented in figure 15. These data were obtained by deflecting the rudder 15.6°. The rolling moment due to yaw control $C_{l_{\delta_v}}$ is negligible; however, effective control reversal was encountered at $M_{\infty} = 0.90$, 0.95, and 0.98 as evidenced by the negative values of $C_{l_{\delta_v}}$ and positive values of $C_{n_{\delta_v}}$. The effective reversal is probably caused by separation on the wing toward which the rudder was deflected.

CONCLUSIONS

An analysis of the data from an experimental investigation of a model of a wing-body concept for the proposed National Hypersonic Flight Research Facility at transonic speeds and over a Reynolds number per meter range of 4.8×10^6 to 10.4×10^6 indicates that the requirements at transonic flight could be met. The following conclusions, resulting directly from that analysis, are also considered noteworthy in the overall evaluation of this concept.

1. The basic configuration (i.e., without engine installed) experienced a local pitch instability at an angle of attack of about 6° and free-stream Mach number of 0.95, but the concept with or without engine generally showed large amounts of static longitudinal stability.

2. Yaw control was investigated only for the configuration with scramjet engine attached; effective control reversal occurred at free-stream Mach numbers of 0.90, 0.95, and 0.98.

The remaining conclusions apply to the concept with or without the scramjet engine installed.

3. Positive effective dihedral was exhibited at positive angles of attack.

4. Low elevon control power was exhibited which resulted in large deflections required for trimmed flight at transonic speeds.

5. Static directional stability was limited to angles of attack of 12° or less; therefore, configuration modifications are required for stable ascent through transonic speeds.

Langley Research Center
National Aeronautics and Space Administration
Hampton, VA 23665
October 21, 1977

APPENDIX A

CONFIGURATION BUILDUP

The untrimmed longitudinal aerodynamic characteristics for the configuration buildup are presented in figure 16. The addition of the wing to the body significantly altered the lift, drag, and pitching-moment curves with C_{L_α} becoming much more positive and C_{m_α} shifting from positive to negative. The addition of the center vertical tail to the body-wing configuration produced drag and pitching-moment increments which generally increase with increasing Mach number. The vertical tail also produced a break in the C_L plotted against α curve and a pitch instability at $M_\infty = 0.95$ and $4^o \leq \alpha \leq 7^o$ at which point C_{L_α} and C_{m_α} resume their expected trends. As noted in the main body of the paper, this behavior is probably due to partial wing separation caused by the vertical tail with subsequent reattachment and has been previously observed on a model of the F-102 which had a delta wing and a center vertical tail (ref. 15).

The addition of the flow-through engine modules generally increases the lift, with the six-module engine (E_6) effecting a larger increase than the three-module engine (E_3). The drag increase is also greater for E_6 than for E_3; however, the drag increment between BWV_{CS} and $BWV_{CS}E_3$ is somewhat larger than the drag increment between $BWV_{CS}E_3$ and $BWV_{CS}E_6$. The addition of either engine package generally results in a nose-down pitching-moment increment with the E_6 having more effect than the E_3. The addition of the base fairing to the $BWV_{CS}E_6$ configuration slightly increases the lift and drag, but slightly decreases the pitching moment. Therefore, the base fairing did not have a significant effect on the aerodynamic characteristics at transonic speeds with E_6 installed.

APPENDIX B

EFFECT OF ELEVON DEFLECTION

The effect of elevon deflection on the longitudinal characteristics of the configurations with and without the six-module scramjet engine is presented in figures 17 and 18, respectively. These data were used to determine longitudinal aerodynamic characteristics without the engine. Pitch instability occurred at $M_\infty = 0.95$ and $0 \leq C_L \leq 0.5$ for the basic configuration at each elevon deflection whereas the configuration with the scramjet engine did not exhibit the same instability. The engine may be compensating for the apparent separation noted on the basic configuration.

APPENDIX C

BASIC LATERAL AERODYNAMIC CHARACTERISTICS

Basic lateral aerodynamic characteristics of the $BWV_{CS}E_6$ configuration are presented in figure 19 at 0° and 17° angles of attack. These data were obtained to determine the linearity of the lateral aerodynamic characteristics. The linearity is good at both angles of attack with the exception of the yawing moment at $\alpha \approx 17^{\circ}$.

REFERENCES

1. Swihart, J. M: NASA Hypersonic Cruise Vehicles. NASA TM X-70361, 1960.

2. Marks, F. M.: Application of Airbreathing Propulsion to an Advanced Wide Area Defense Missile System. 1974 JANNAF Propulsion Meeting, vol. 2, pt. 1, CPIA-260-Vol-2-PT-1, Appl. Phys. Lab., Johns Hopkins Univ., Oct. 1974, pp. 171-187. (Available from DDC as AD C002 276.)

3. Altis, H. D.; and Crocker, W. D.: Advanced Air Defense Vehicle Study. Volume 1 - Summary. AFFDL-TR-70-61-Vol-1, U.S. Air Force, 1970. (Available from DDC as AD 509 825.)

4. Morris, R. E.; and Williams, N. B.: Study of Airbreathing Launch Vehicles With Cruise Capability. Volume I - Summary. NASA CR-73194, 1968.

5. Kirkham, F. S.; Jackson, L. Robert; and Weidner, John P.: Study of a High-Speed Research Airplane. J. Aircr., vol. 12, no. 11, Nov. 1975, pp. 857-863.

6. Hypersonic Research Facilities Study. Volume IV, Part 1, Phase 3: Final Studies Flight Research Facilities. NASA CR-114327, 1970.

7. Palchett, George L: Preliminary Design Evaluation of the Incremental Growth Vehicle Concept. AFFDL-TR-74-65, U.S. Air Force, June 1974.

8. Hearth, Donald P.; and Preyss, Albert E.: Hypersonic Technology - Approach to an Expanded Program. Astron. & Aeron., vol. 14, no. 12, Dec. 1976, pp. 20-37.

9. Kirkham, F. S.; Jones, R. A.; Buck, M. L.; and Zima, W. P.: Joint USAF/NASA Hypersonic Research Aircraft Study. AIAA Paper No. 75-1039, Aug. 1975.

10. Weidner, J. P.; Small, W. J.; and Penland, J. A.: Scramjet Integration on Hypersonic Research Airplane Concepts. AIAA Paper No. 76-755, July 1976.

11. Henry, John R.; and Anderson, Griffin Y.: Design Considerations for the Airframe-Integrated Scramjet. NASA TM X-2895, 1973.

12. Johnston, Patrick J.; Pittman, Jimmy L.; and Huffman, Jarrett K.: Effect of an Integrated Scramjet Installation on the Subsonic Performance of an Aircraft Designed for Mach 6 Cruise. AIAA Paper No. 77-1230, Aug. 1977.

13. Schaefer, William T., Jr.: Characteristics of the Major Active Wind Tunnels at the Langley Research Center. NASA TM X-1130, 1965.

14. Braslow, Albert L.; and Knox, Eugene C.: Simplified Method for Determination of Critical Height of Distributed Roughness Particles for Boundary-Layer Transition at Mach Numbers From 0 to 5. NACA TN 4363, 1958.

15. Osborne, Robert S.; and Wornom, Dewey E.: Aerodynamic Characteristics Including Effects of Wing Fixes of a 1/20-Scale Model of the Convair F-102 Airplane at Transonic Speeds. NACA RM SL54C23, U.S. Air Force, 1954.

16. Palmer, William E.: Effect of Reduction in Thickness From 6 to 22 Percent and Removal of the Pointed Tips on the Subsonic Static Longitudinal Stability Characteristics of a 60° Triangular Wing in Combination With a Fuselage. NACA RM L53F24, 1953.

17. Kirby, D. A.: Low-Speed Wind-Tunnel Measurements of the Lift, Drag and Pitching Moment of a Series of Cropped Delta Wings. R. & M. No. 3744, British A.R.C., Nov. 1972.

18. Lamar, John E.; and Gloss, Blair B.: Subsonic Aerodynamic Characteristics of Interacting Lifting Surfaces With Separated Flow Around Sharp Edges Predicted by a Vortex-Lattice Method. NASA TN D-7921, 1975.

TABLE I.- GEOMETRIC CHARACTERISTICS OF MODEL

Wing:	
Area (includes fuselage intercept), m^2 (in^2)	0.060 (92.63)
Area, exposed, m^2 (in^2)	0.030 (47.00)
Area, wetted, m^2 (in^2)	0.064 (98.98)
Span, m (in.)	0.244 (9.62)
Aspect ratio	0.999
Root chord (at fuselage center line), m (in.)	0.371 (14.59)
Tip chord, m (in.)	0.119 (4.7)
Taper ratio	0.322
Mean aerodynamic chord (includes fuselage intercept), m (in.)	0.294 (11.57)
Sweepback angles:	
Leading edge, deg	67.5
25-percent chord line, deg	61.1
Trailing edge, deg	0
Dihedral angle, deg	10
Incidence angle, deg	-2.1
Airfoil thickness ratio:	
Exposed root	0.051
Tip	0.078
Leading-edge radius (normal to leading edge), cm (in.)	0.064 (0.025)
Trailing-edge thickness, cm (in.)	0.064 (0.025)
Elevons:	
Tip chord, percent wing tip	36.6
Span, percent total span	59.8
Area, both, m^2 (in^2)	0.0064 (9.89)
Vertical tail:	
Area, exposed, m^2 (in^2)	0.007 (10.93)
Span, exposed, m (in.)	0.077 (3.06)
Aspect ratio of exposed area	0.857
Root chord at fuselage surface line, m (in.)	0.101 (3.99)
Tip chord, m (in.)	0.057 (2.256)
Taper ratio	0.565
Mean aerodynamic chord of exposed area, m (in.)	0.097 (3.804)
Sweepback angles:	
Leading edge, deg	49.9
Trailing edge, deg	18.5
Hinge line location, percent chord	68.7
A_{rudder}/A_{total}	0.295
Leading-edge radius, cm (in.)	0.064 (0.025)
Fuselage:	
Length, m (in.)	0.584 (23.0)
Nose radius, cm (in.)	0.159 (0.063)
Maximum height, m (in.)	0.076 (2.98)
Maximum width, m (in.)	0.097 (3.83)
Fineness ratio of equivalent round body	6.86
Planform area, m^2 (in^2)	0.042 (65.12)
Wetted area:	
Without components or base, m^2 (in^2)	0.122 (188.6)
With wing on, m^2 (in^2)	0.116 (179.4)
A_b, m^2 (in^2)	0.0023 (3.54)
Complete model:	
Planform area, m^2 (in^2)	0.072 (112.12)
Aspect ratio of planform	0.825

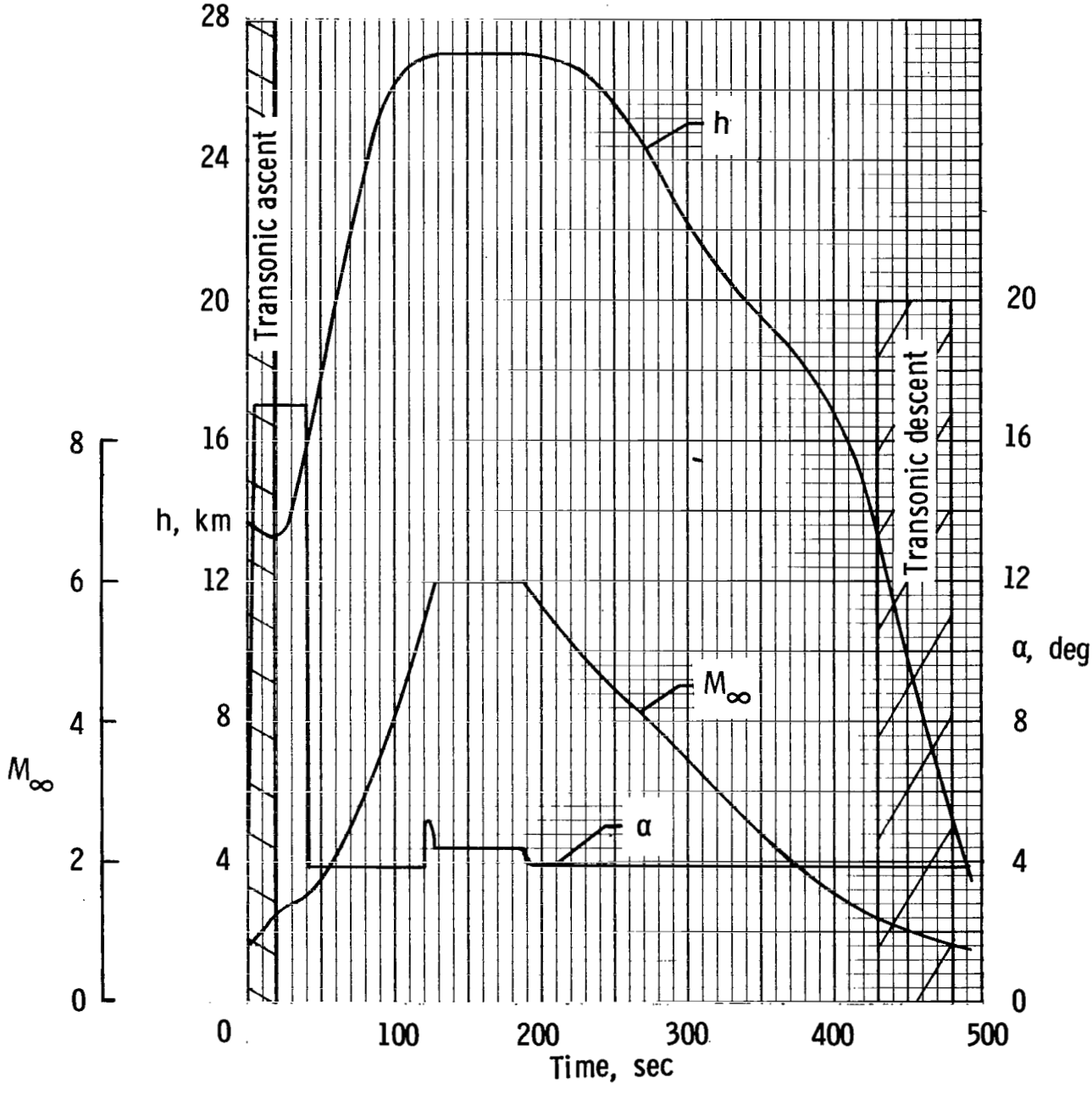


Figure 1.- Typical proposed mission profile for research vehicle.

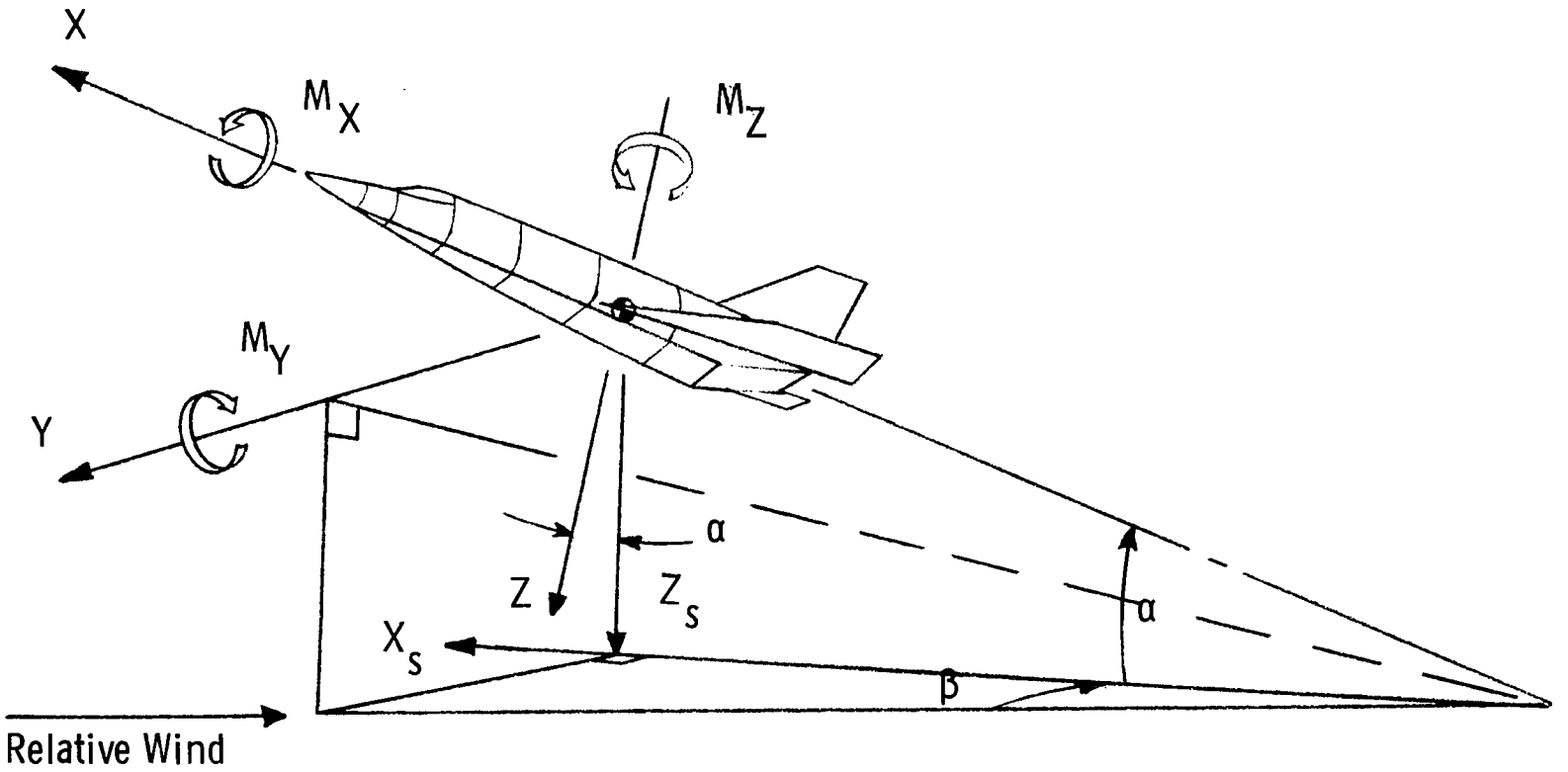
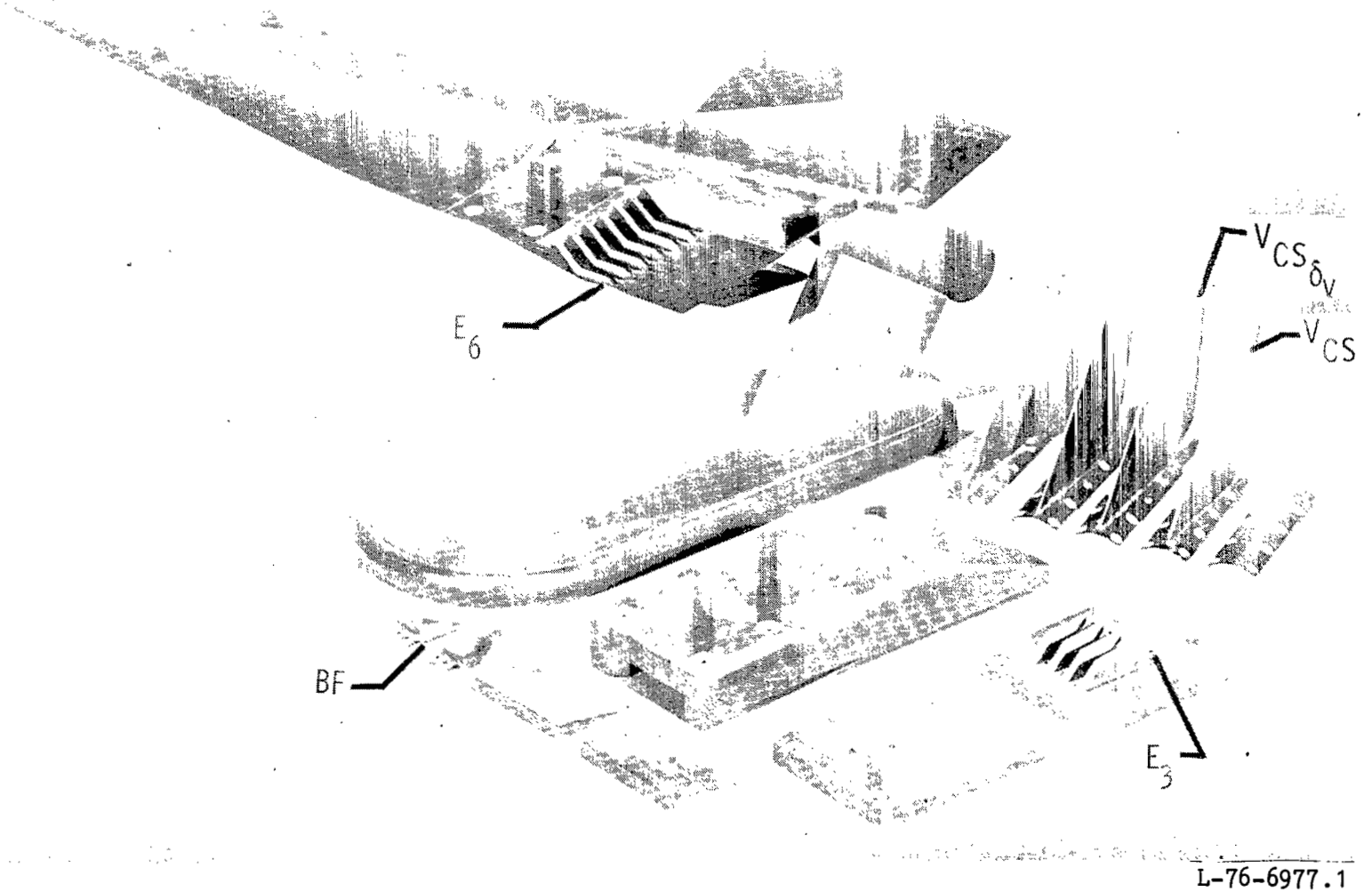
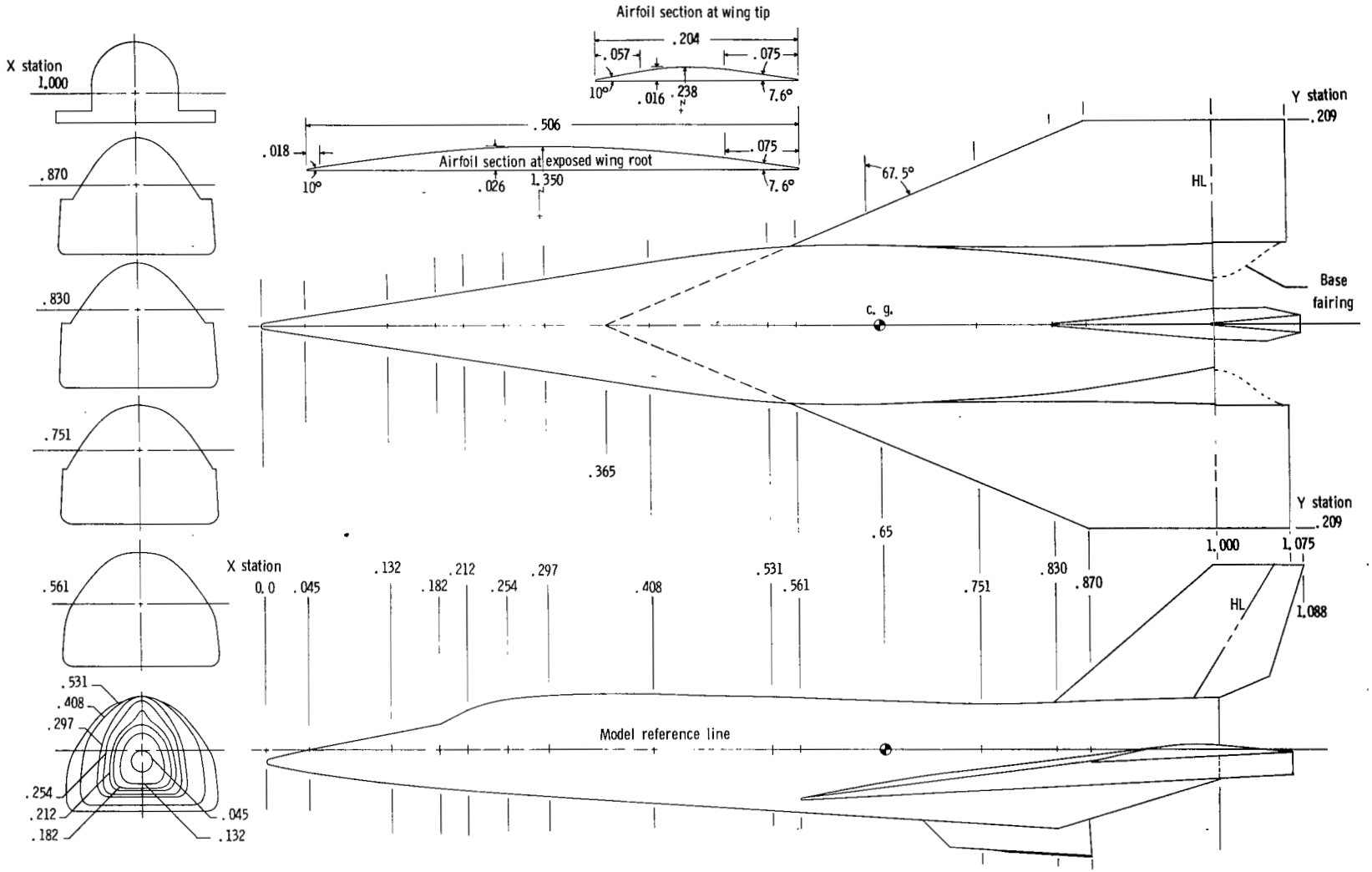


Figure 2.- System of reference axes. Arrows indicate positive directions.



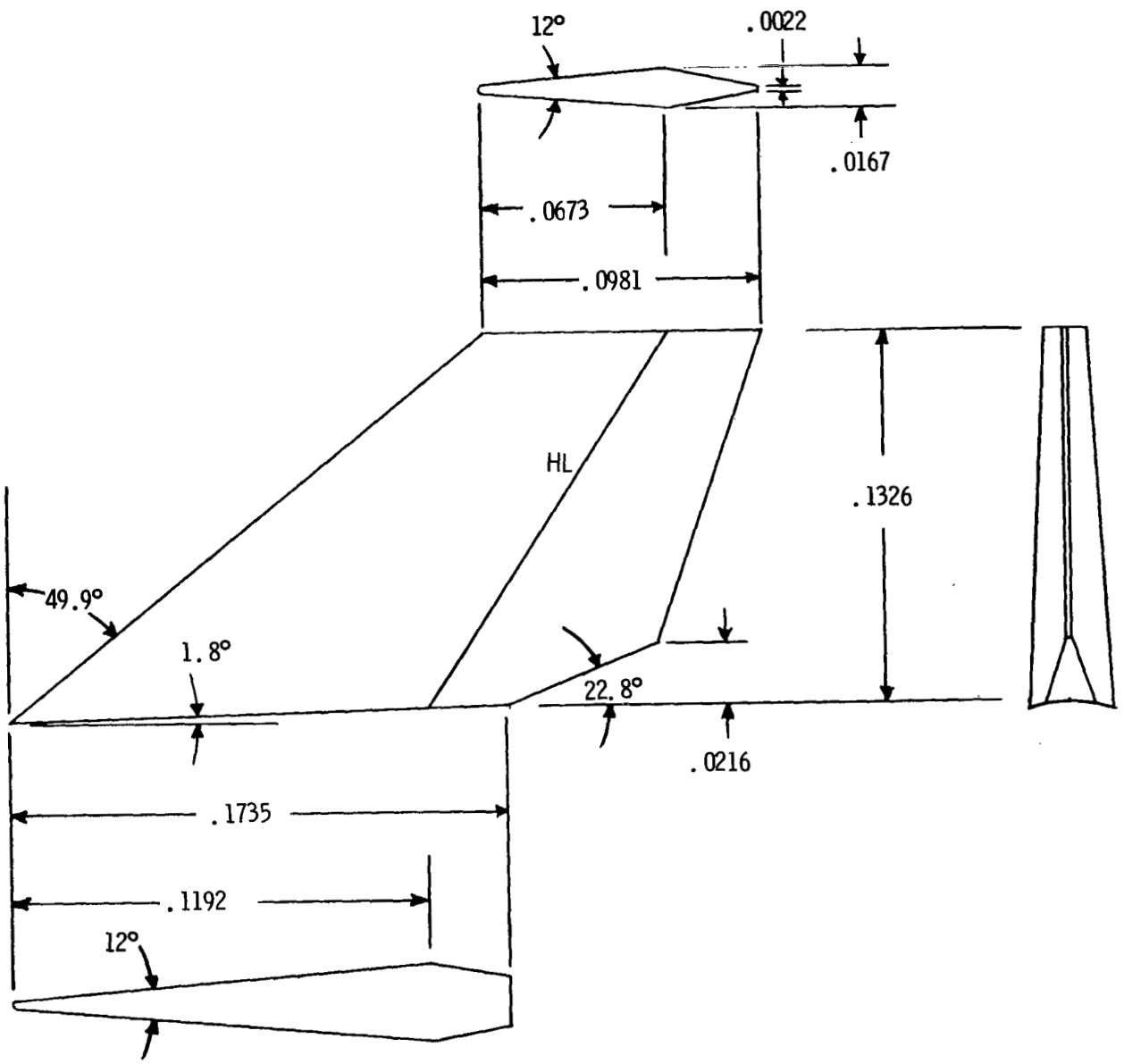
L-76-6977.1

Figure 3.- Photograph of cast model with interchangeable parts.



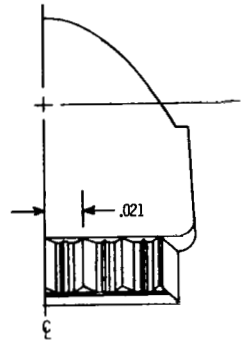
(a) Model details.

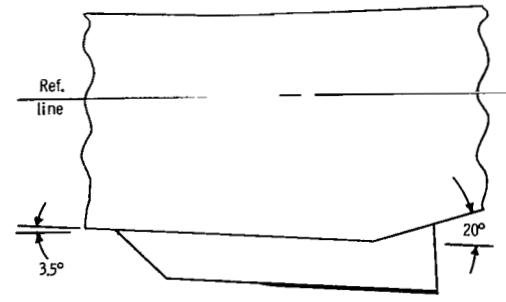
Figure 4.- Model general dimensions. All dimensions have been normalized by body length (ℓ = 0.584 m).

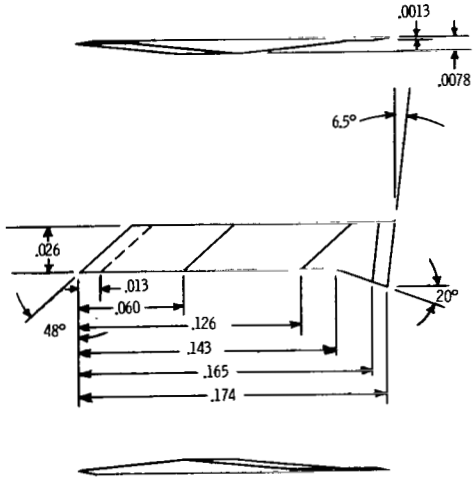


(b) Vertical tail subsonic airfoil.

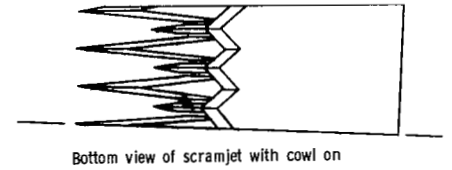
Figure 4.- Continued.



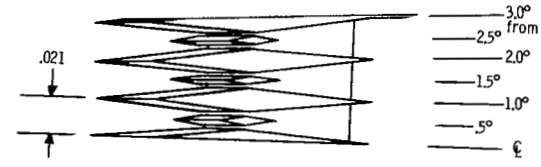




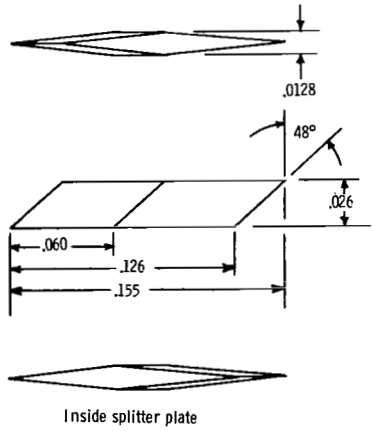
Left outside plate



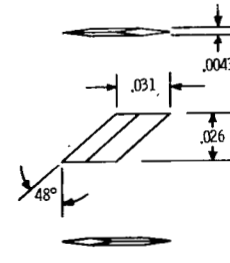
Bottom view of scramjet with cowl on



Bottom view of scramjet with cowl off



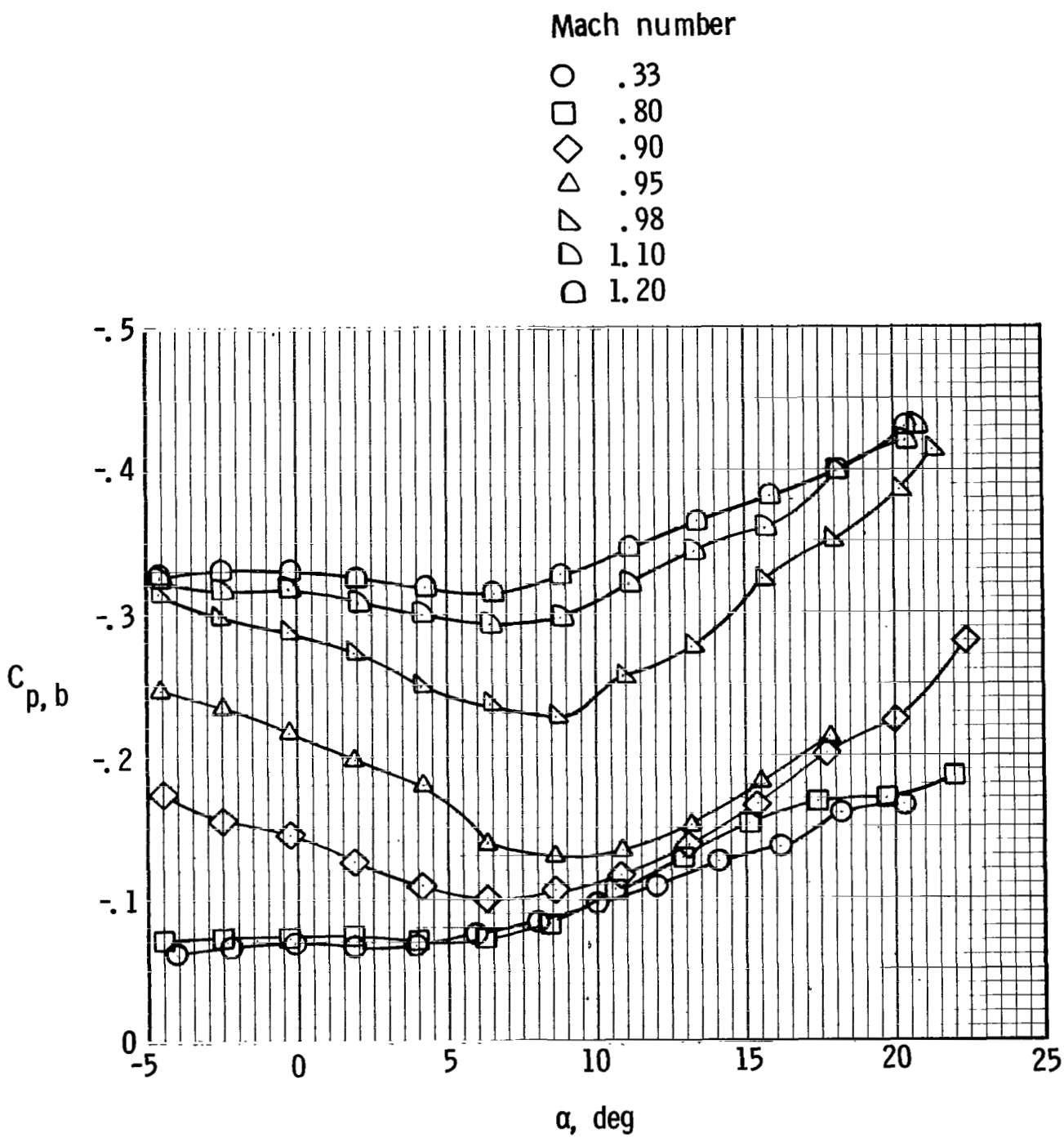
Inside splitter plate



Fuel strut

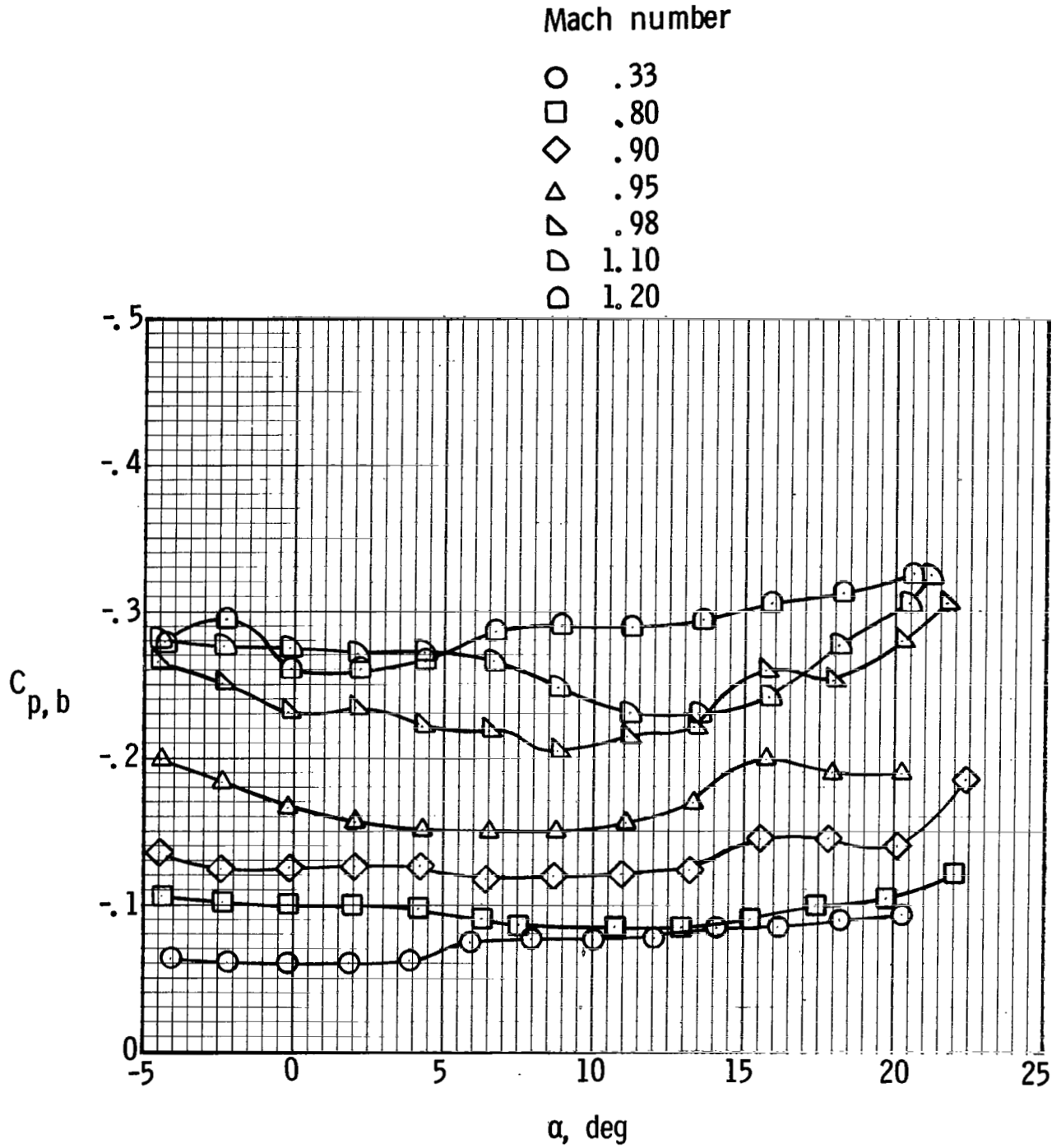
(c) Scramjet engine details.

Figure 4.- Concluded.



(a) BWV_{CS}.

Figure 5.- Variation of base-pressure coefficient with angle of attack. $\delta_e = 0^o$.



(b) $BWV_{CS}E_6$.

Figure 5.- Concluded.

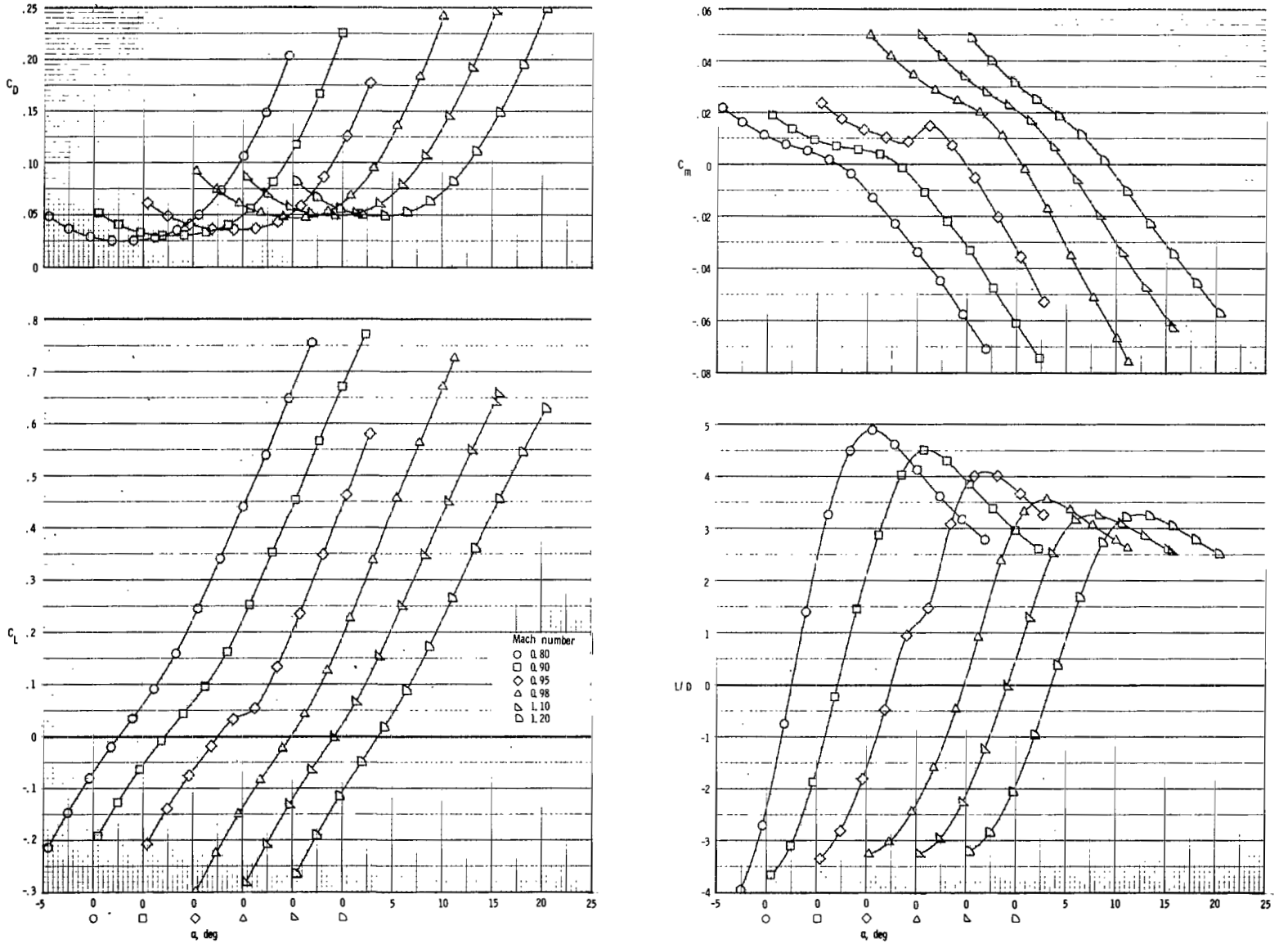


Figure 6.- Effect of Mach number on longitudinal characteristics of BWV_{CS} configuration.

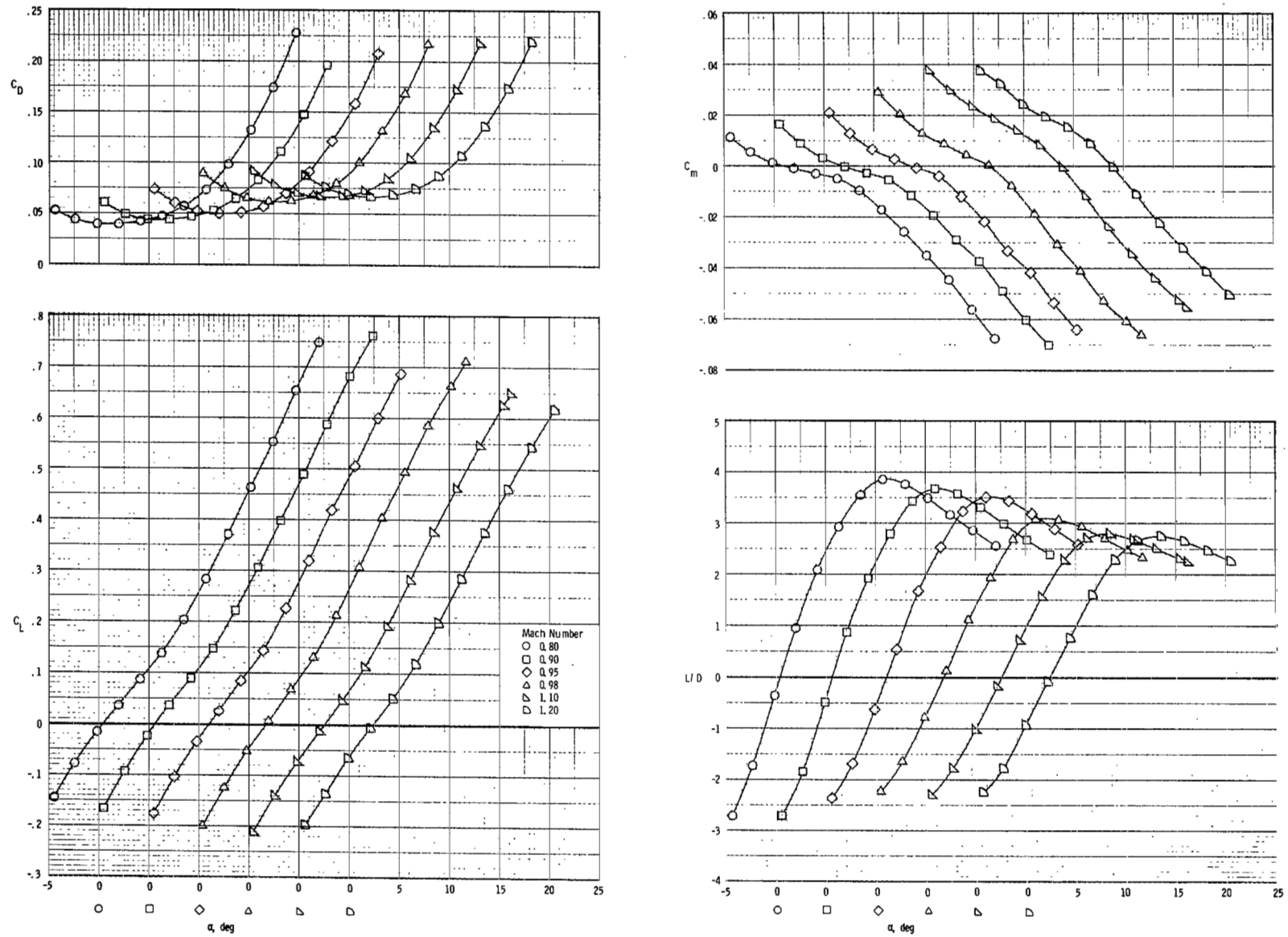


Figure 7.- Effect of Mach number on longitudinal characteristics of $BWV_{CS}E_6$ configuration.

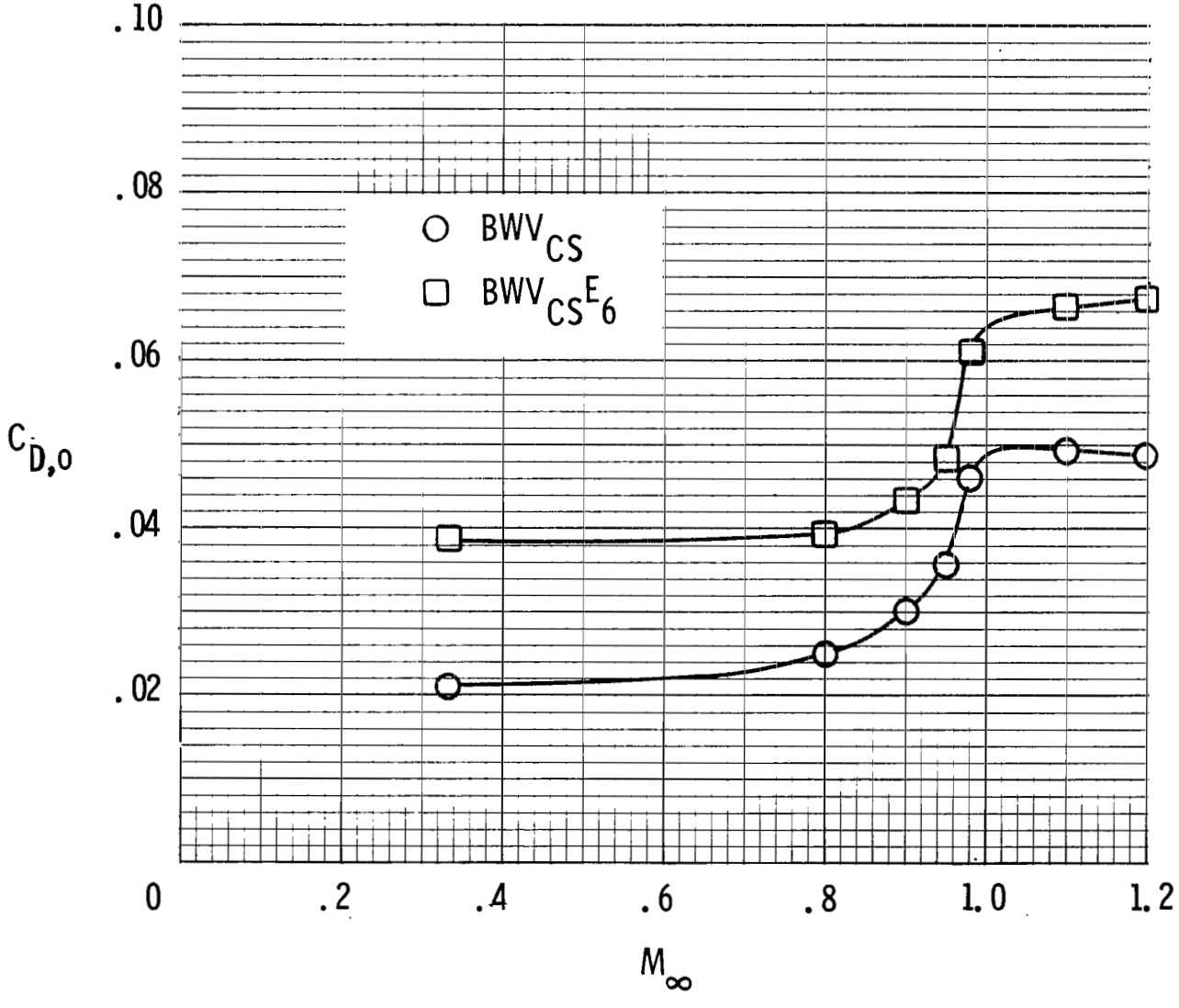
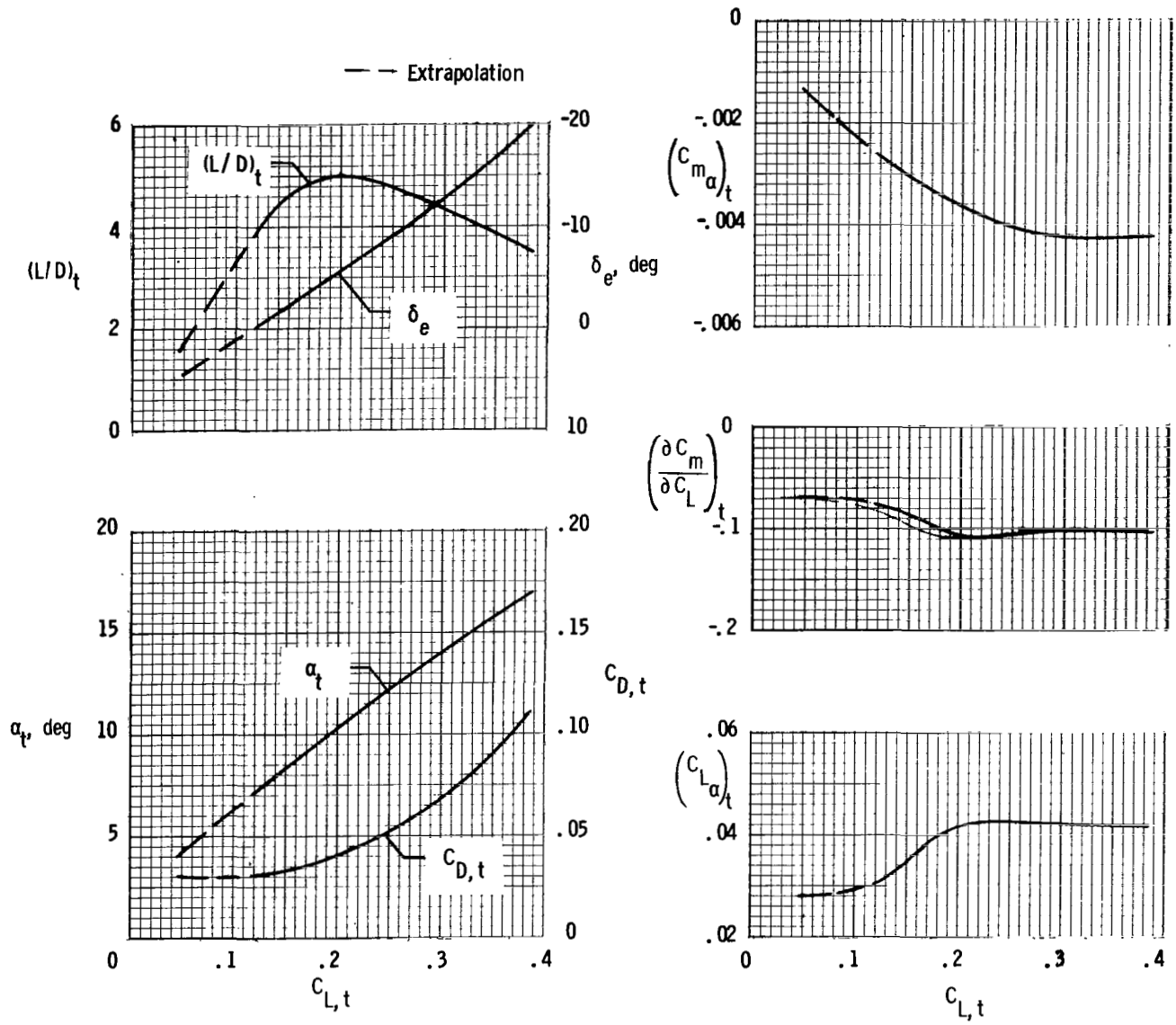
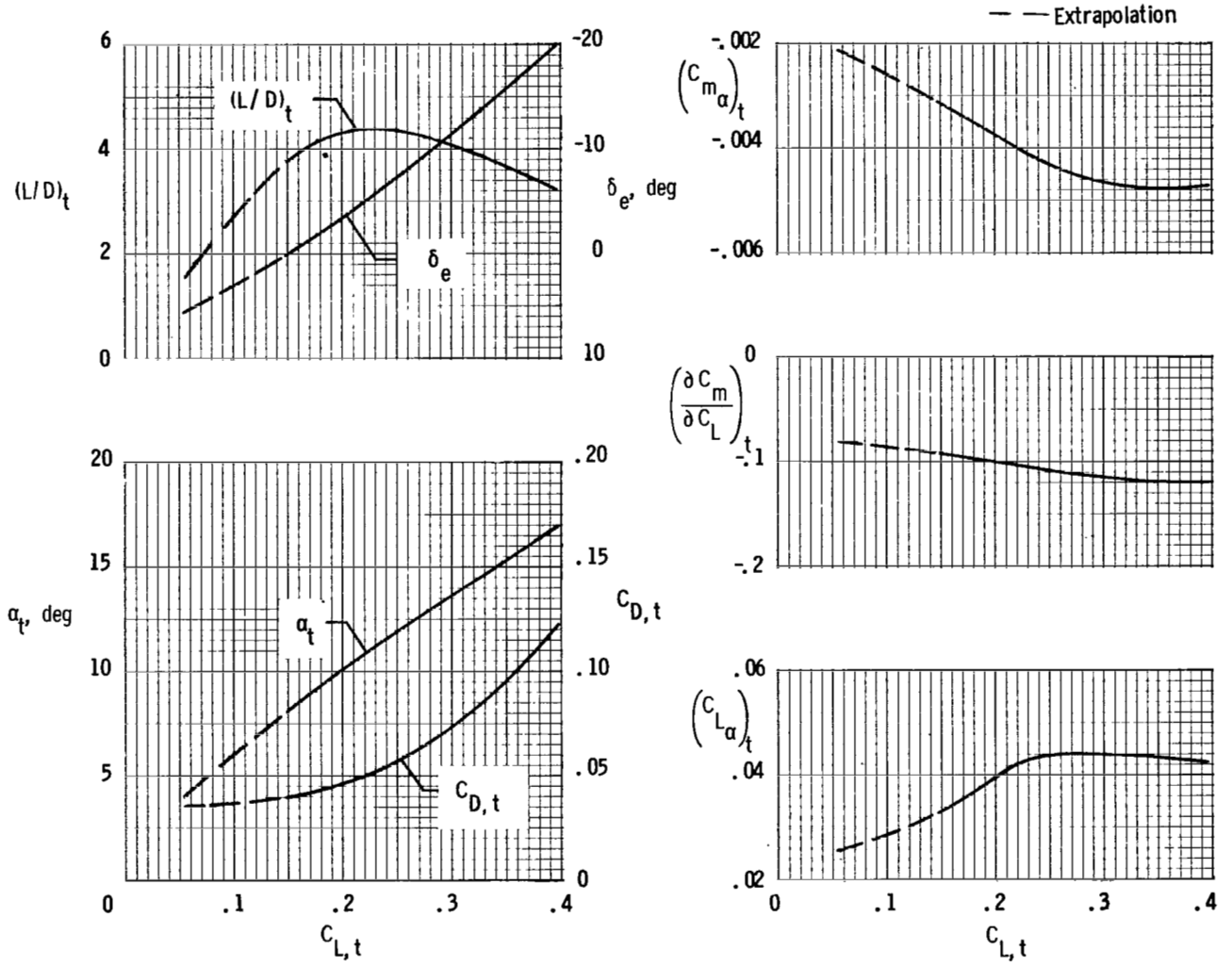


Figure 8.- Drag coefficient at zero lift as function of Mach number for BWV_{CS} and $BWV_{CS}E_6$ configurations.



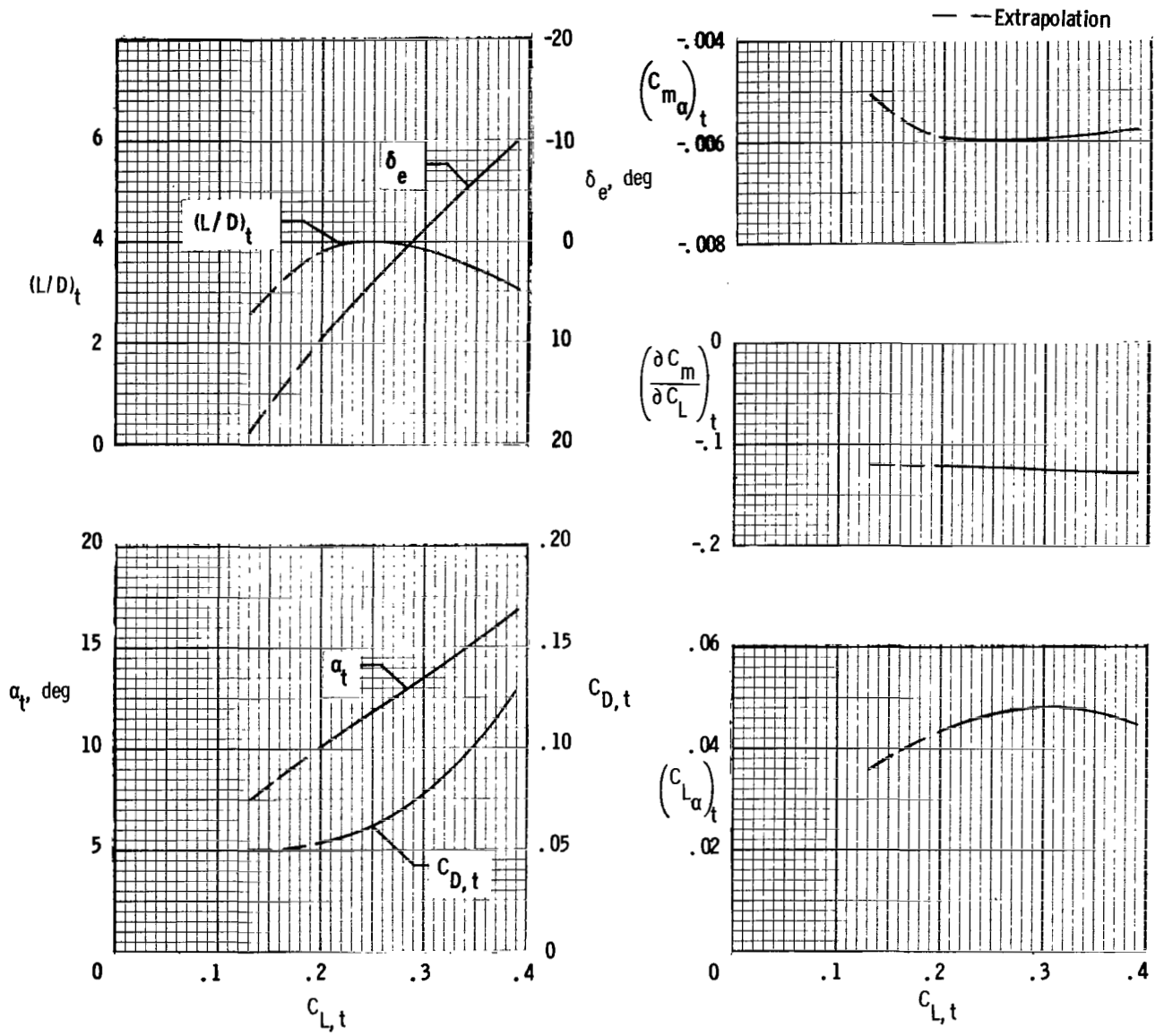
(a) $M_\infty = 0.80$.

Figure 9.- Longitudinal aerodynamic characteristics at trim of BWV_{CS} configuration.



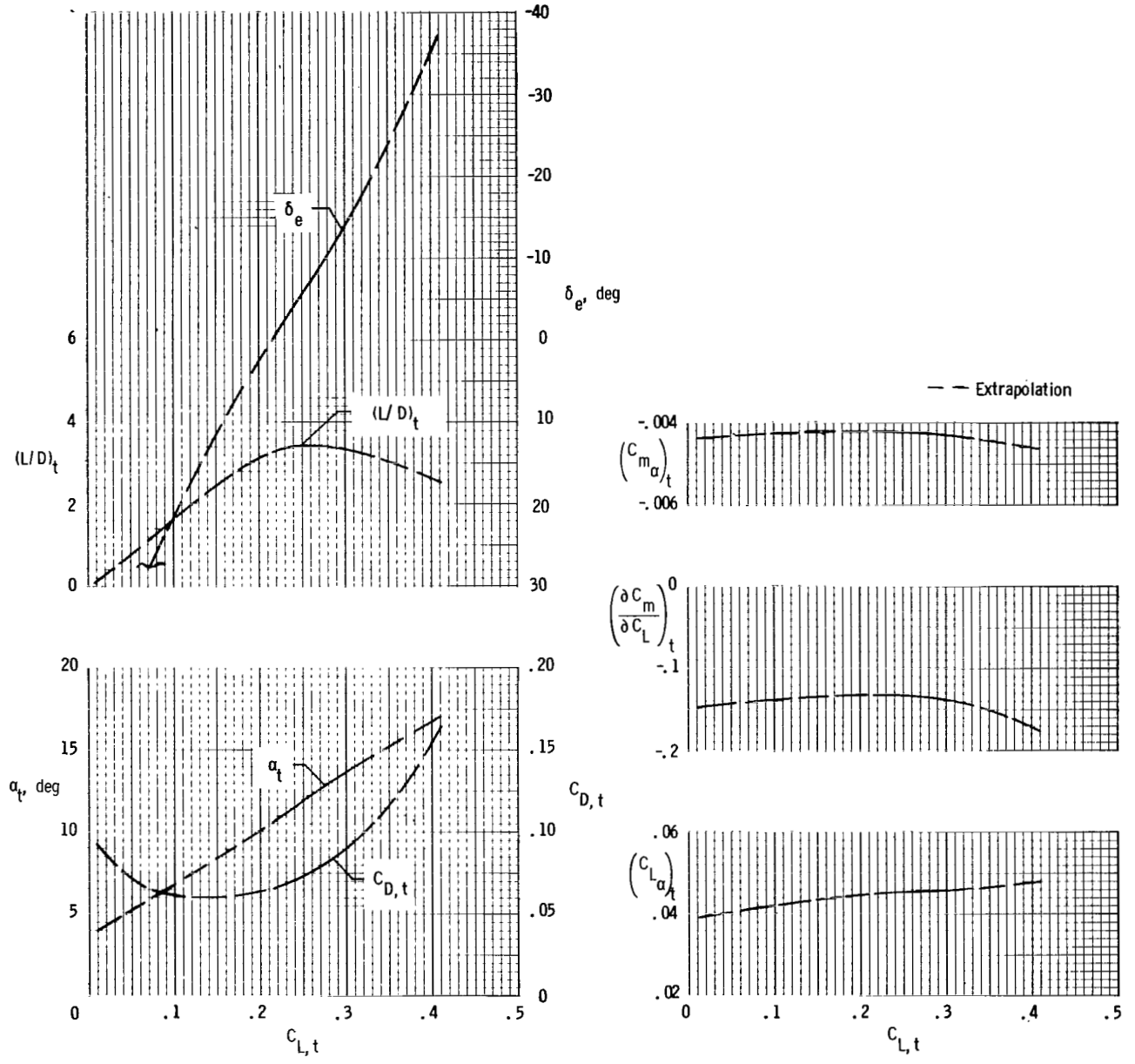
(b) $M_\infty = 0.90$.

Figure 9.- Continued.



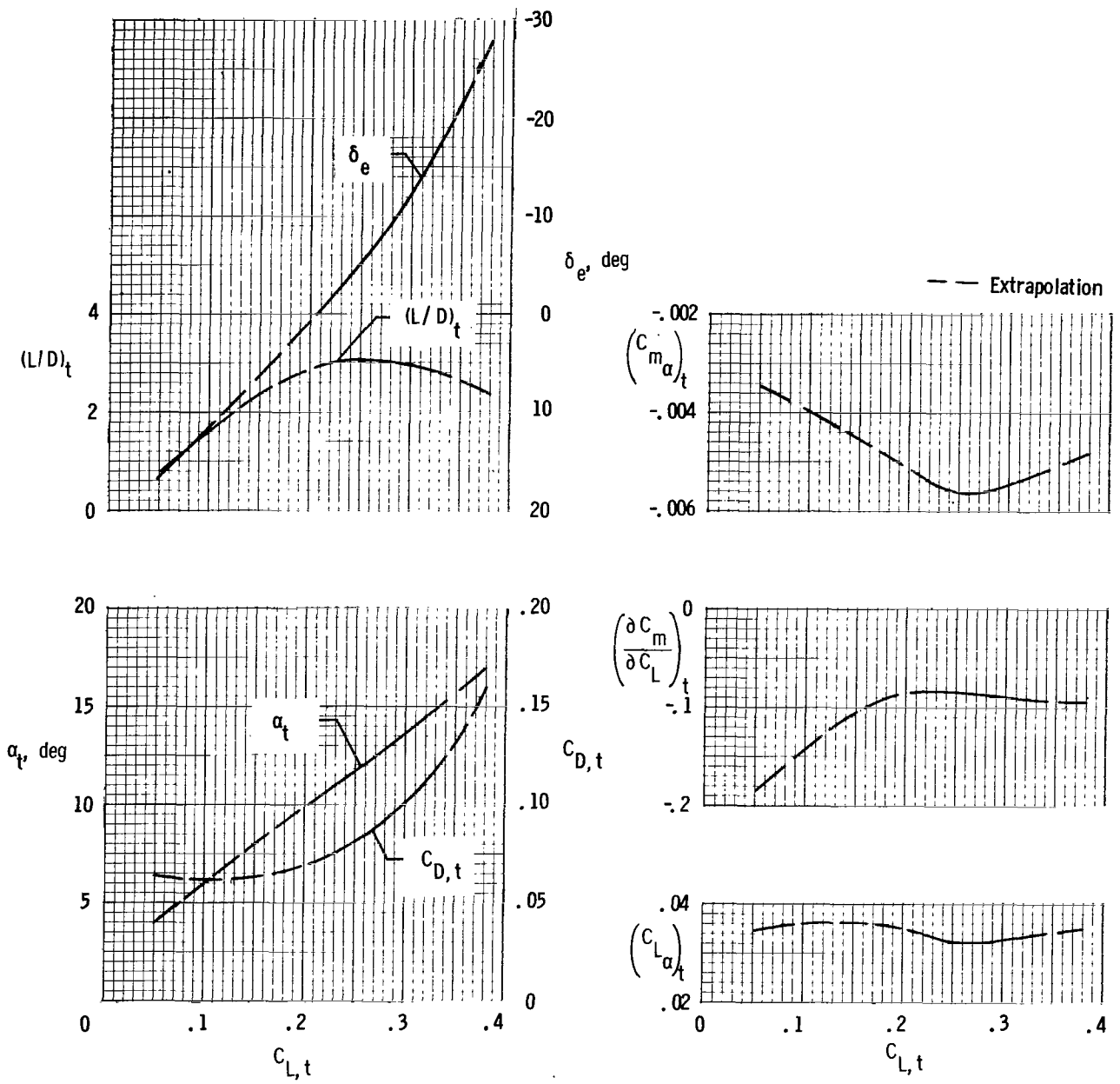
(c) $M_\infty = 0.95$.

Figure 9.- Continued.



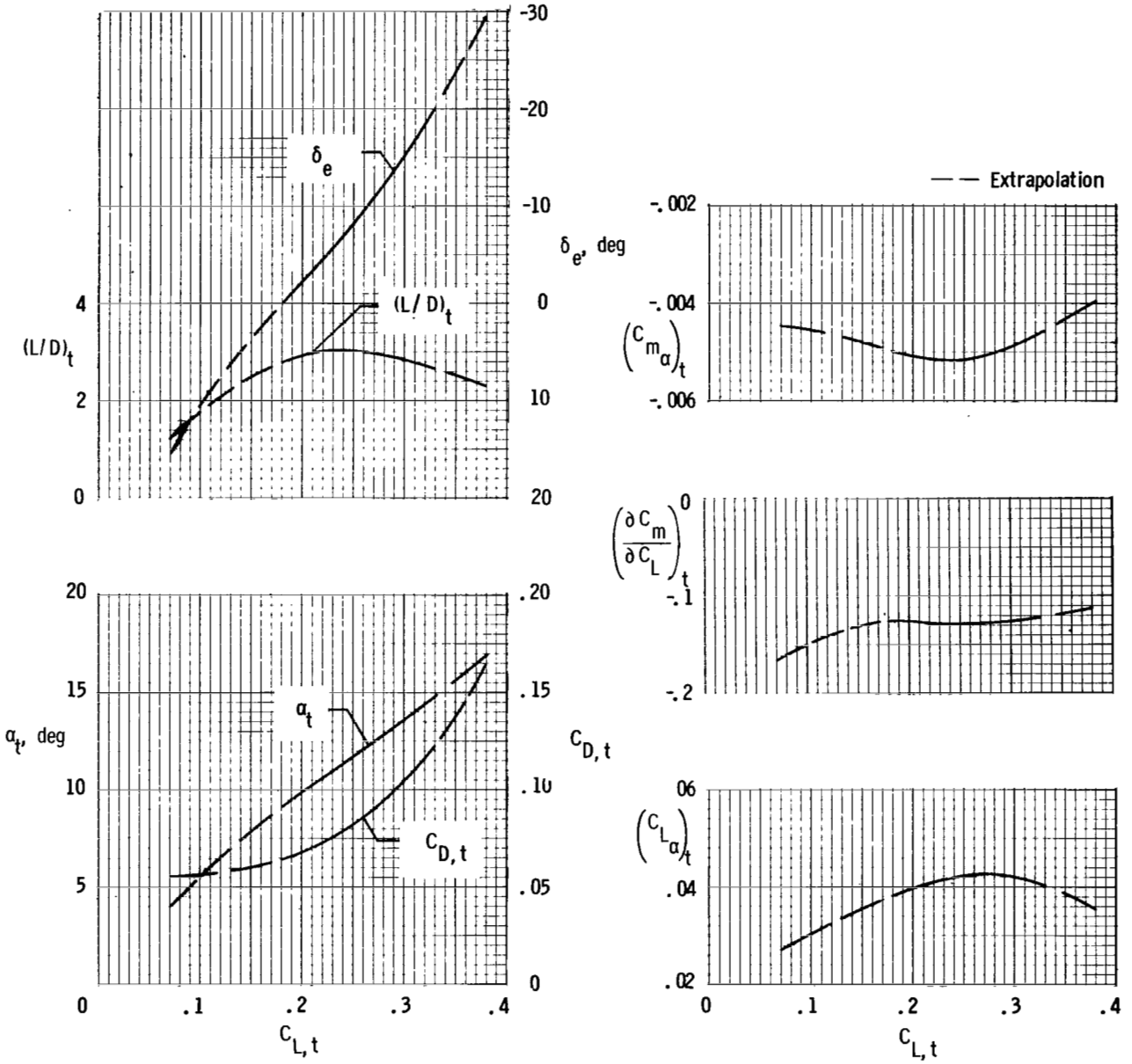
(d) $M_\infty = 0.98$.

Figure 9.- Continued.



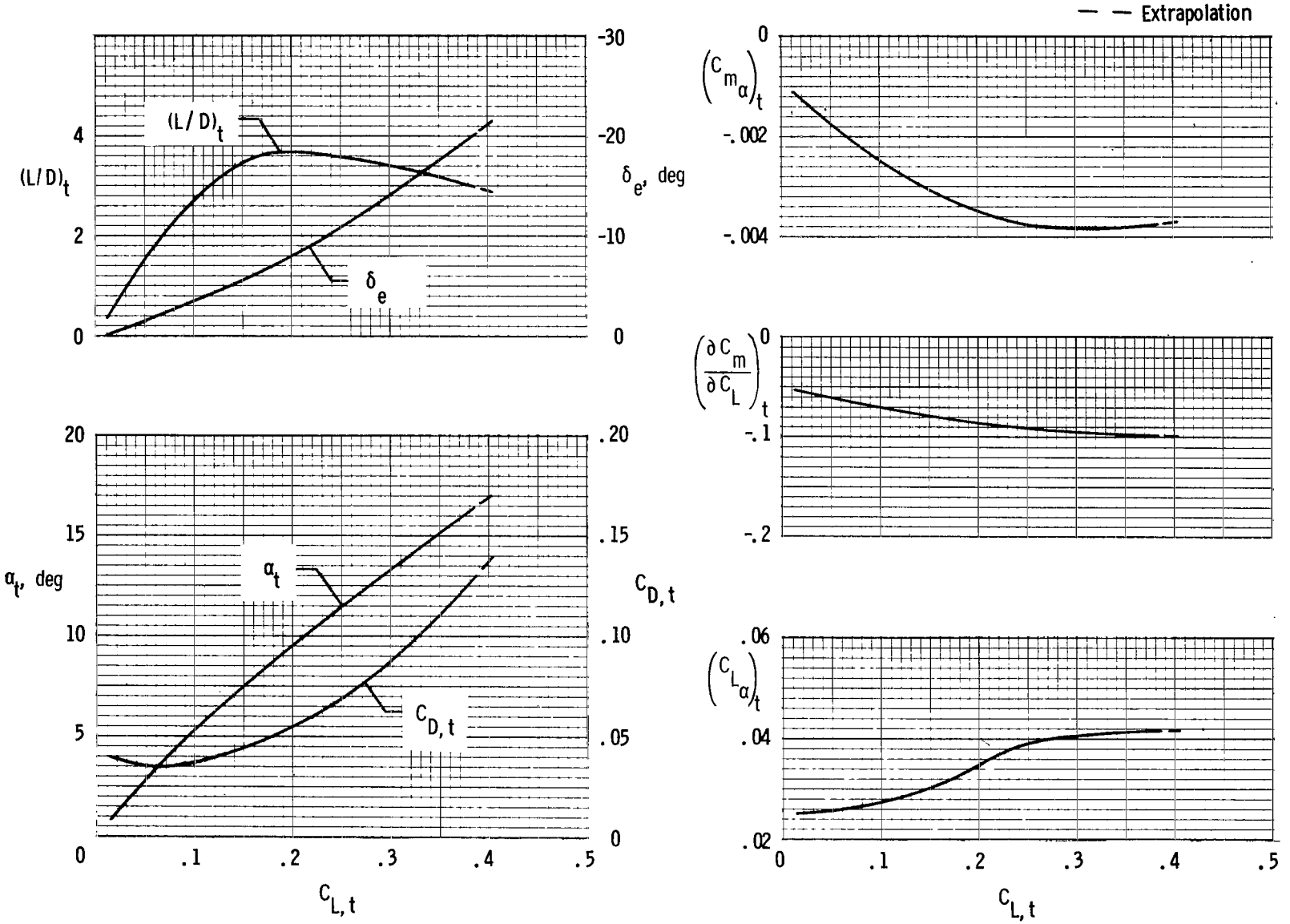
(e) $M_\infty = 1.10$.

Figure 9.- Continued.



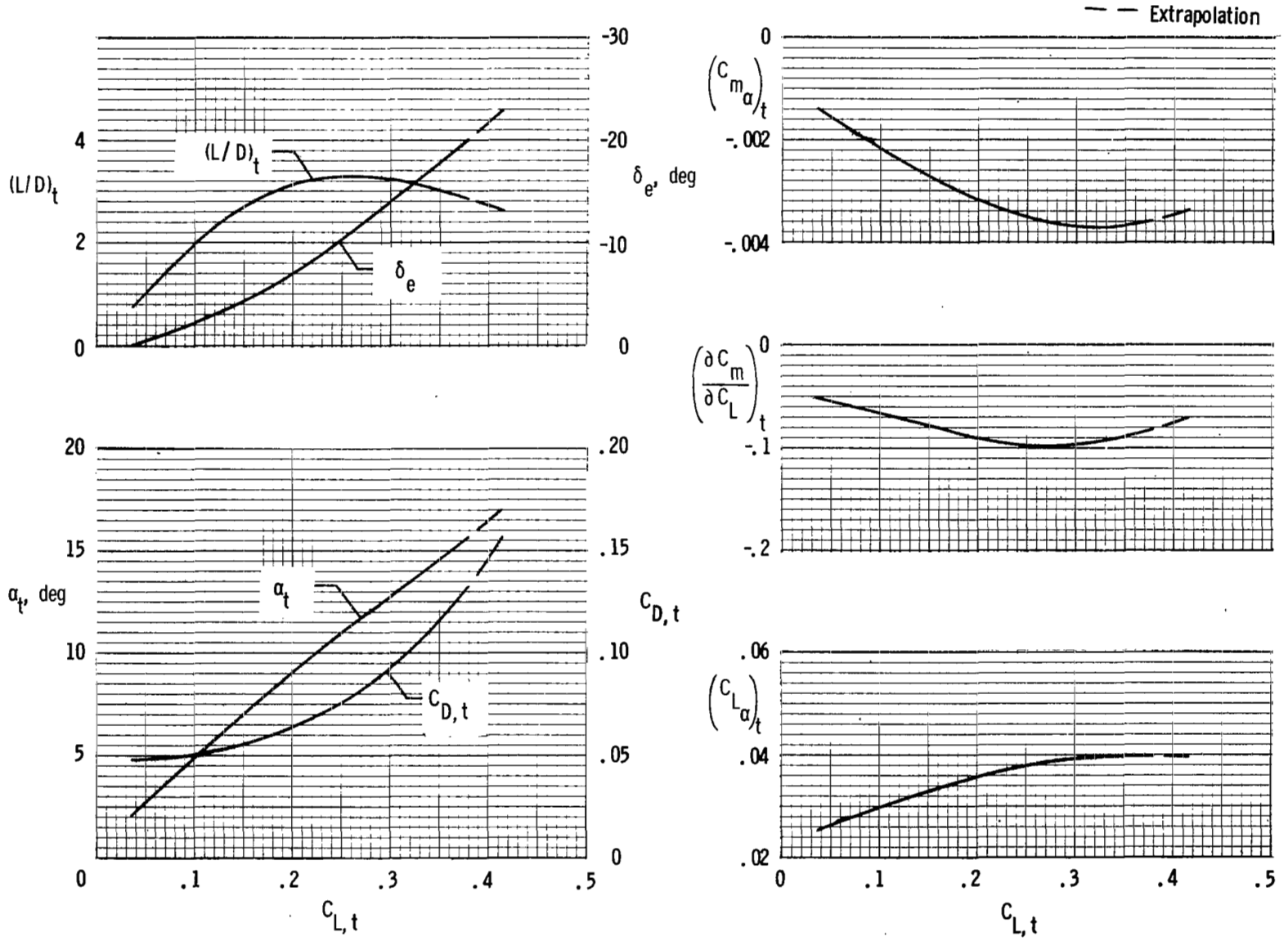
(f) $M_\infty = 1.20$.

Figure 9.- Concluded.



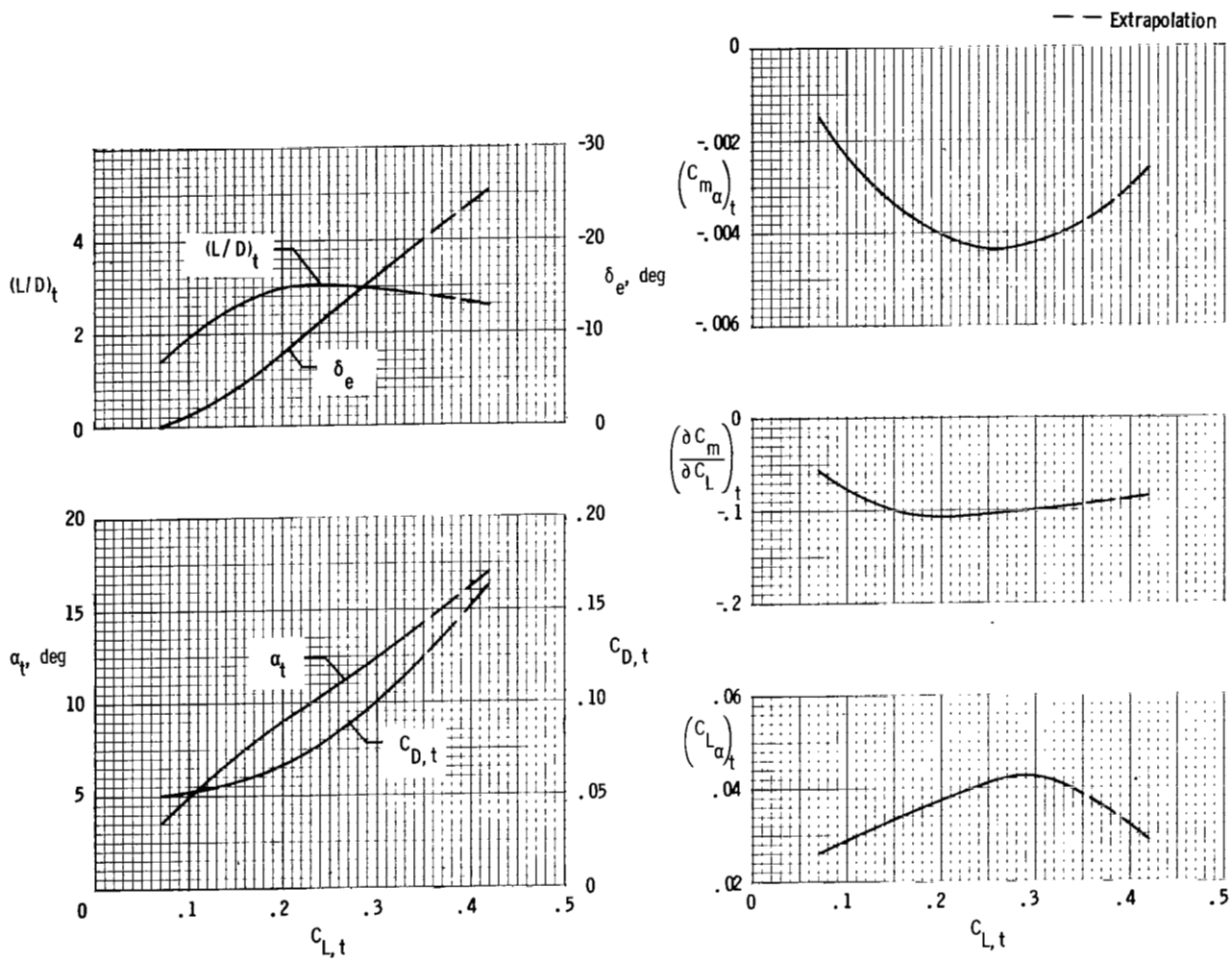
(a) $M_\infty = 0.80$.

Figure 10.- Longitudinal aerodynamic characteristics at trim of $BWV_{CS}E_6$ configuration.



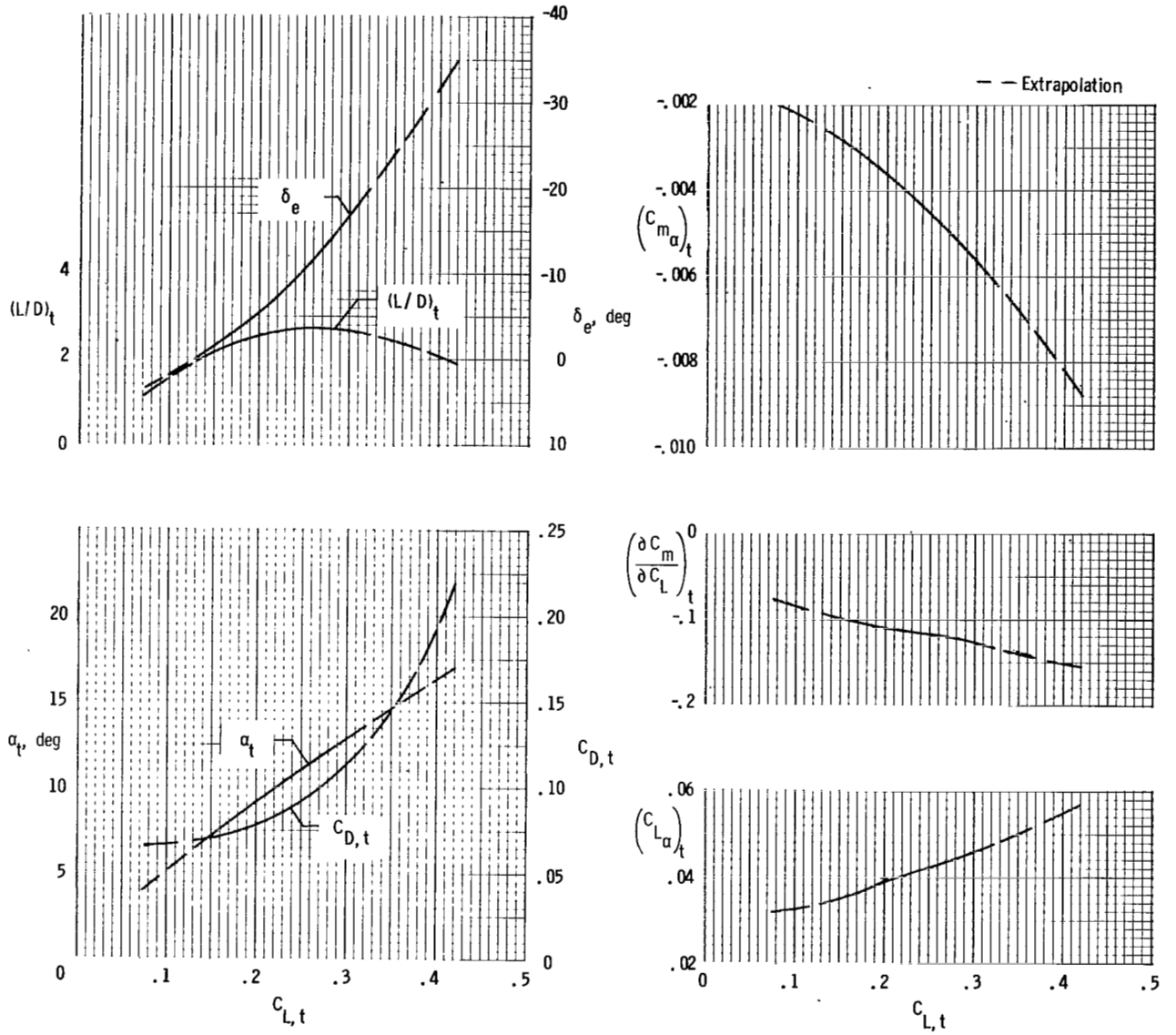
(b) $M_\infty = 0.90$.

Figure 10.- Continued.



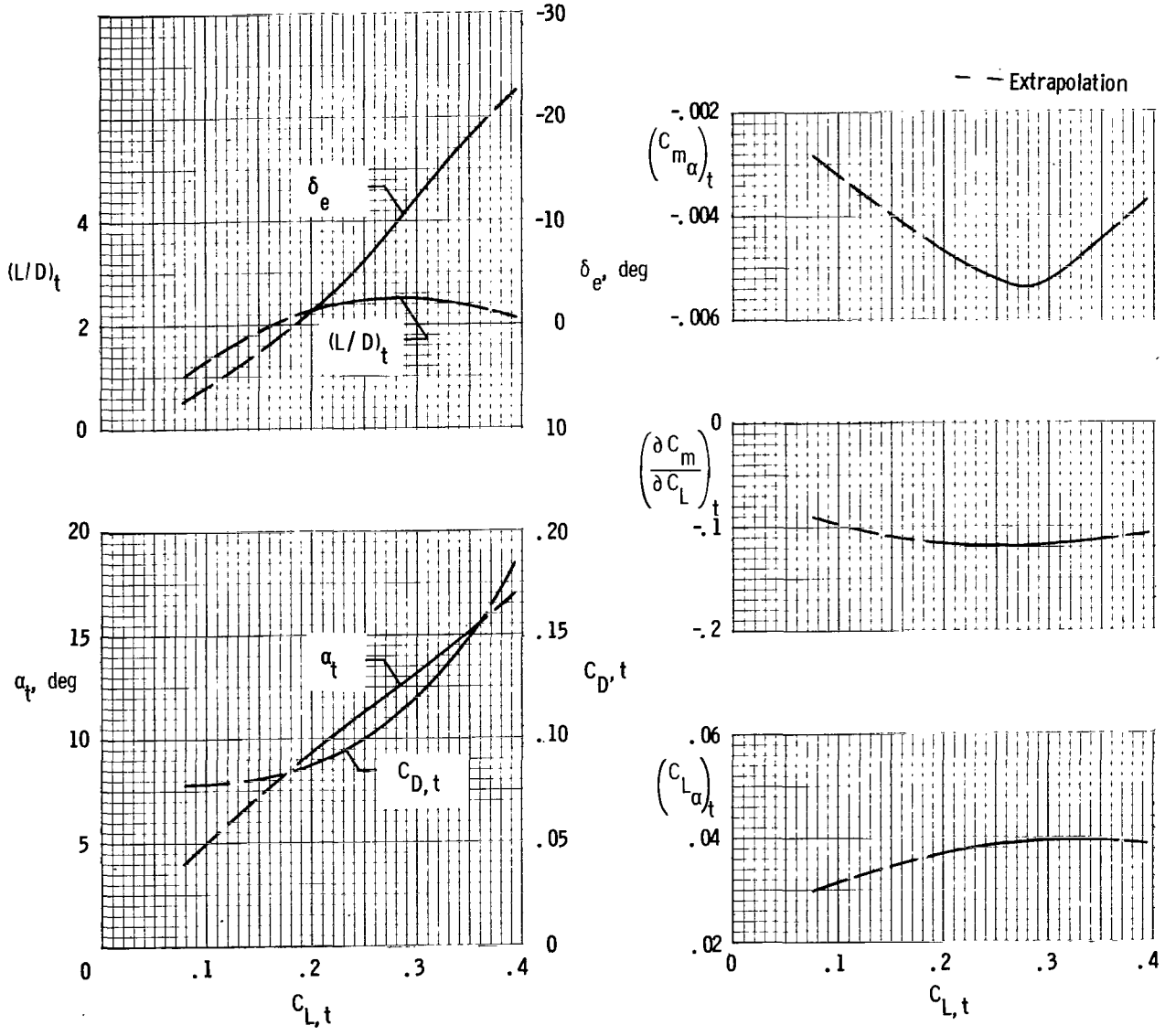
(c) $M_\infty = 0.95$.

Figure 10.- Continued.



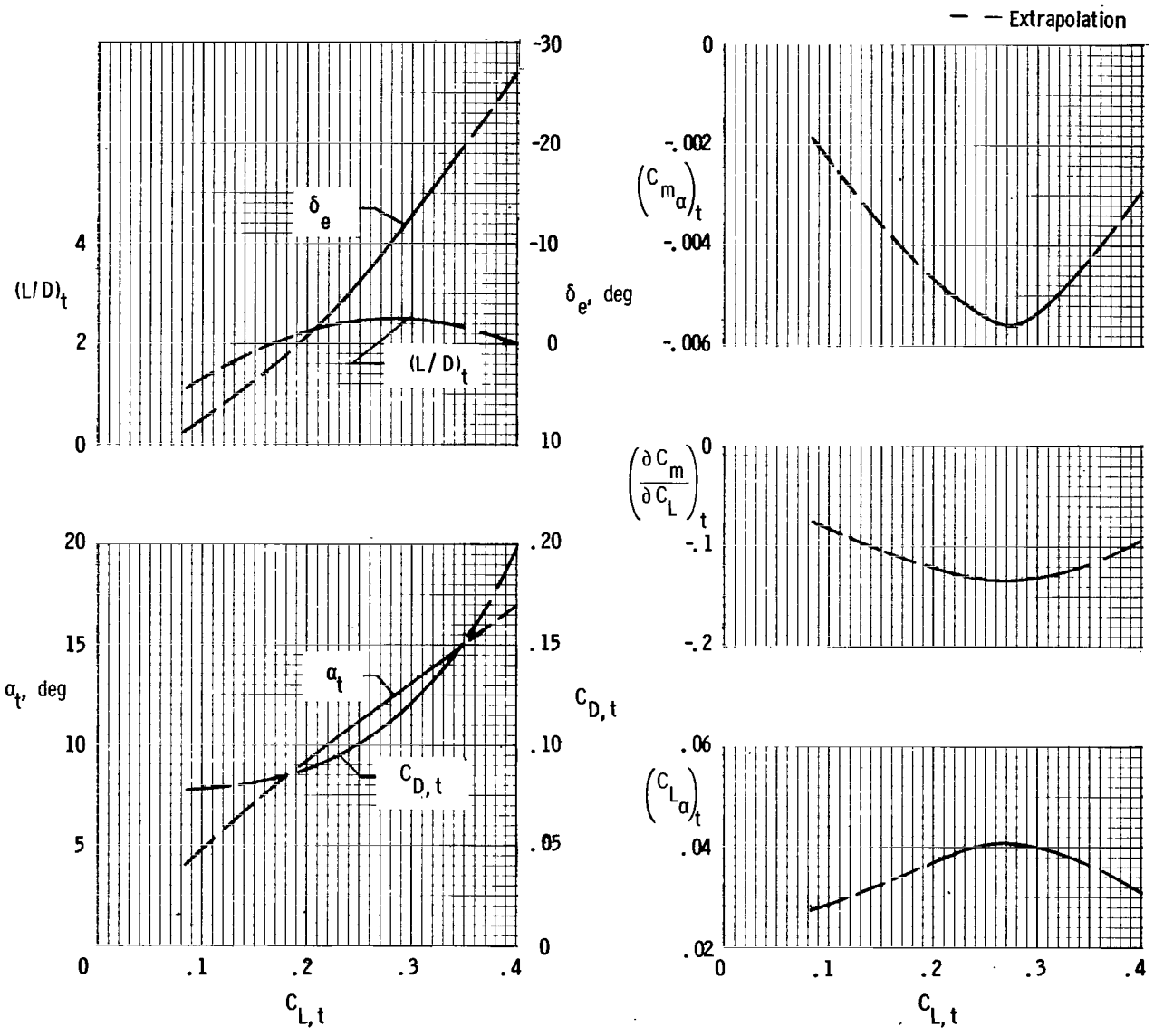
(d) $M_\infty = 0.98$.

Figure 10.- Continued.



(e) $M_\infty = 1.10$.

Figure 10.- Continued.



(f) $M_\infty = 1.20$.

Figure 10.- Concluded.

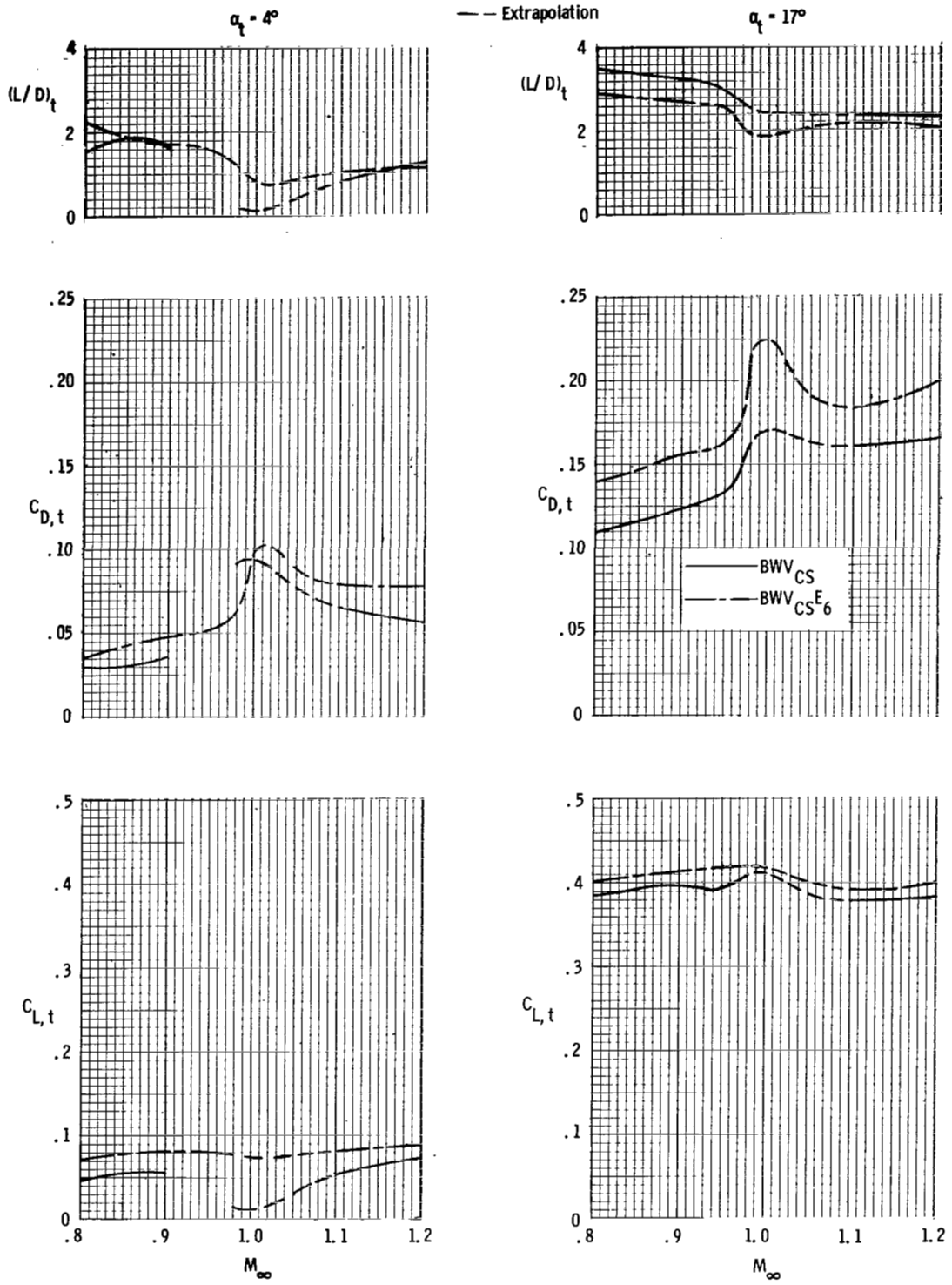


Figure 11.- Mach number history of several aerodynamic characteristics for BWV_{CS} and $BWV_{CS}E_6$ configurations at 4° and 17° trimmed angle of attack.

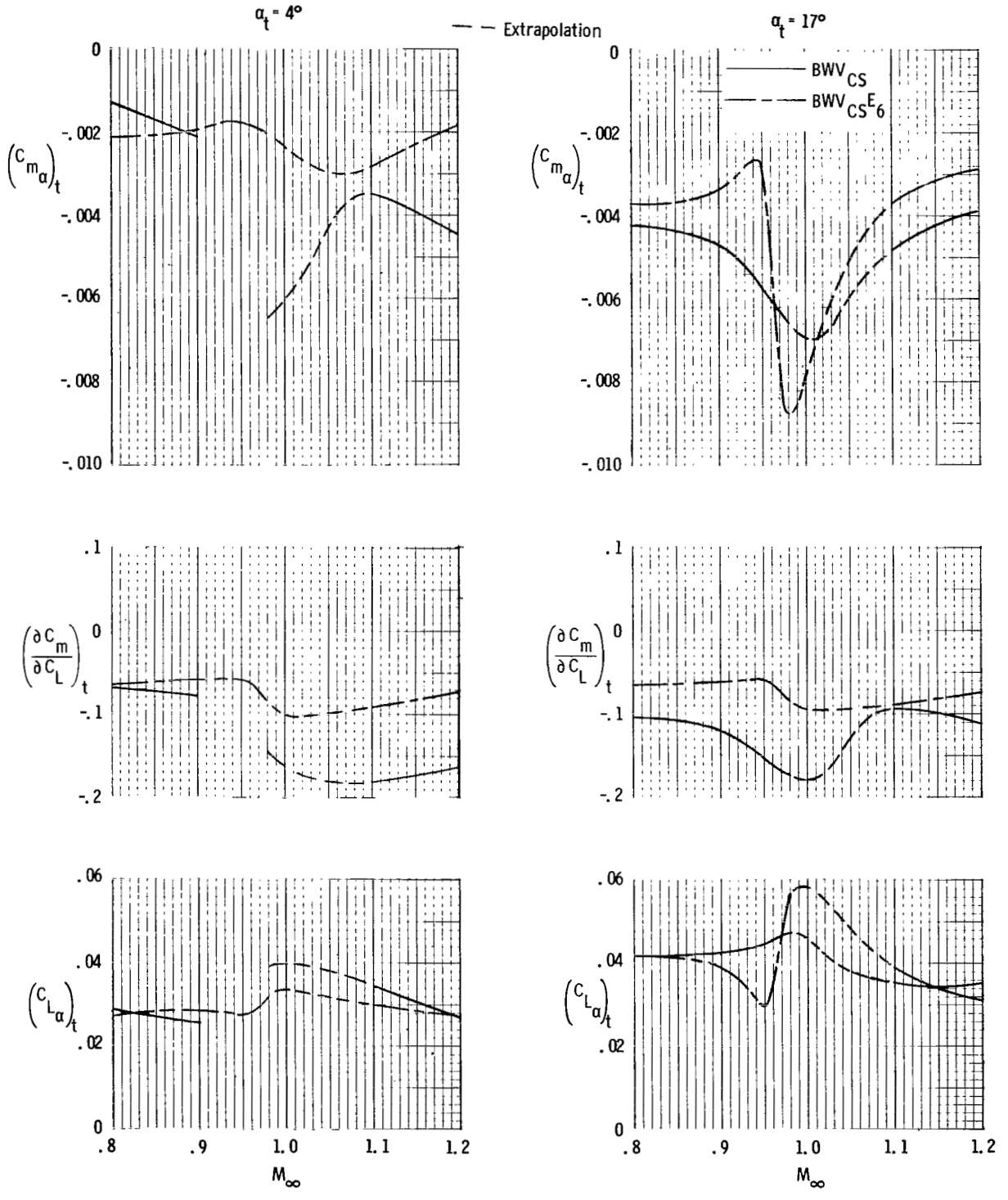


Figure 11.- Continued.

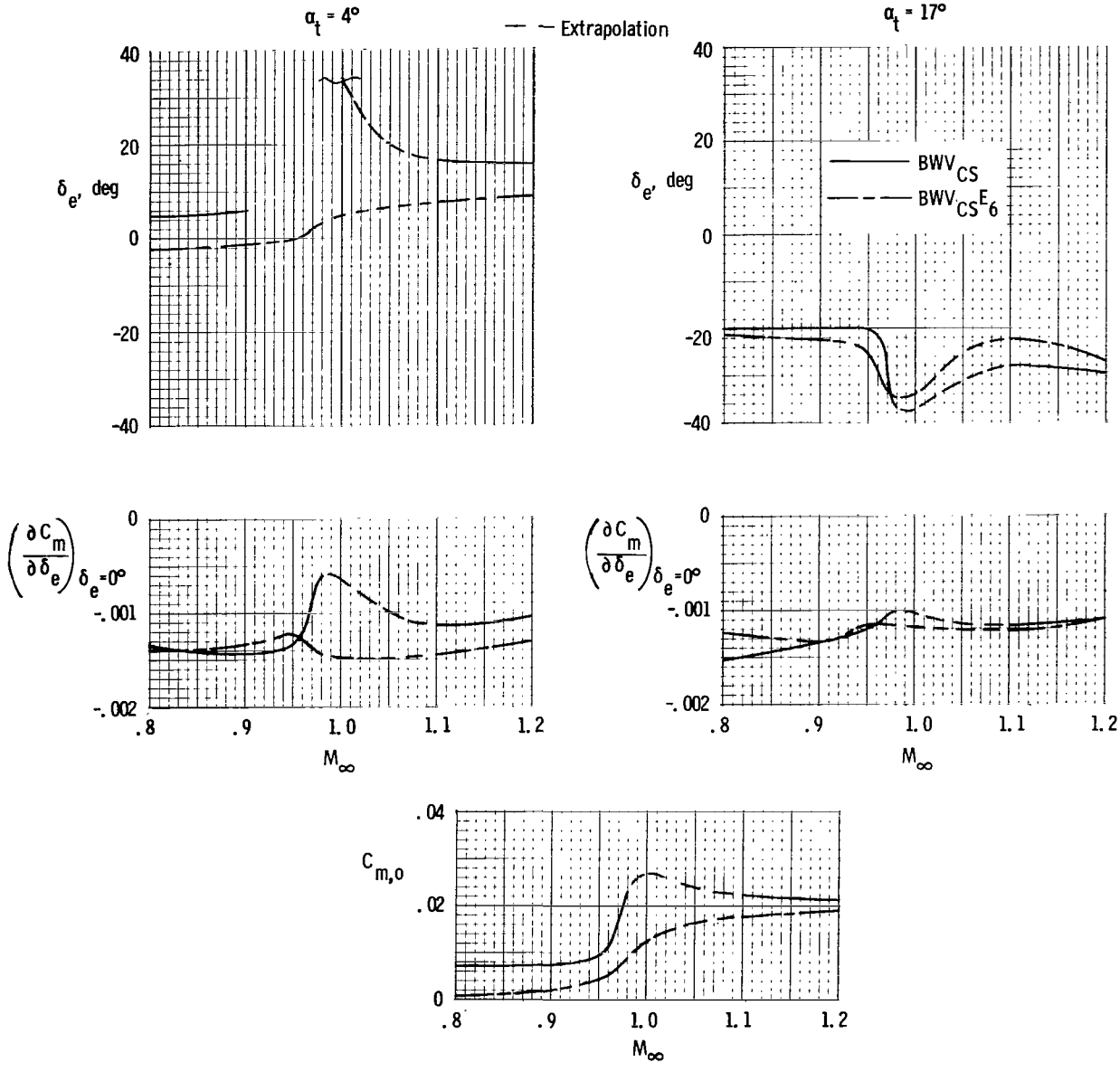


Figure 11.- Concluded.

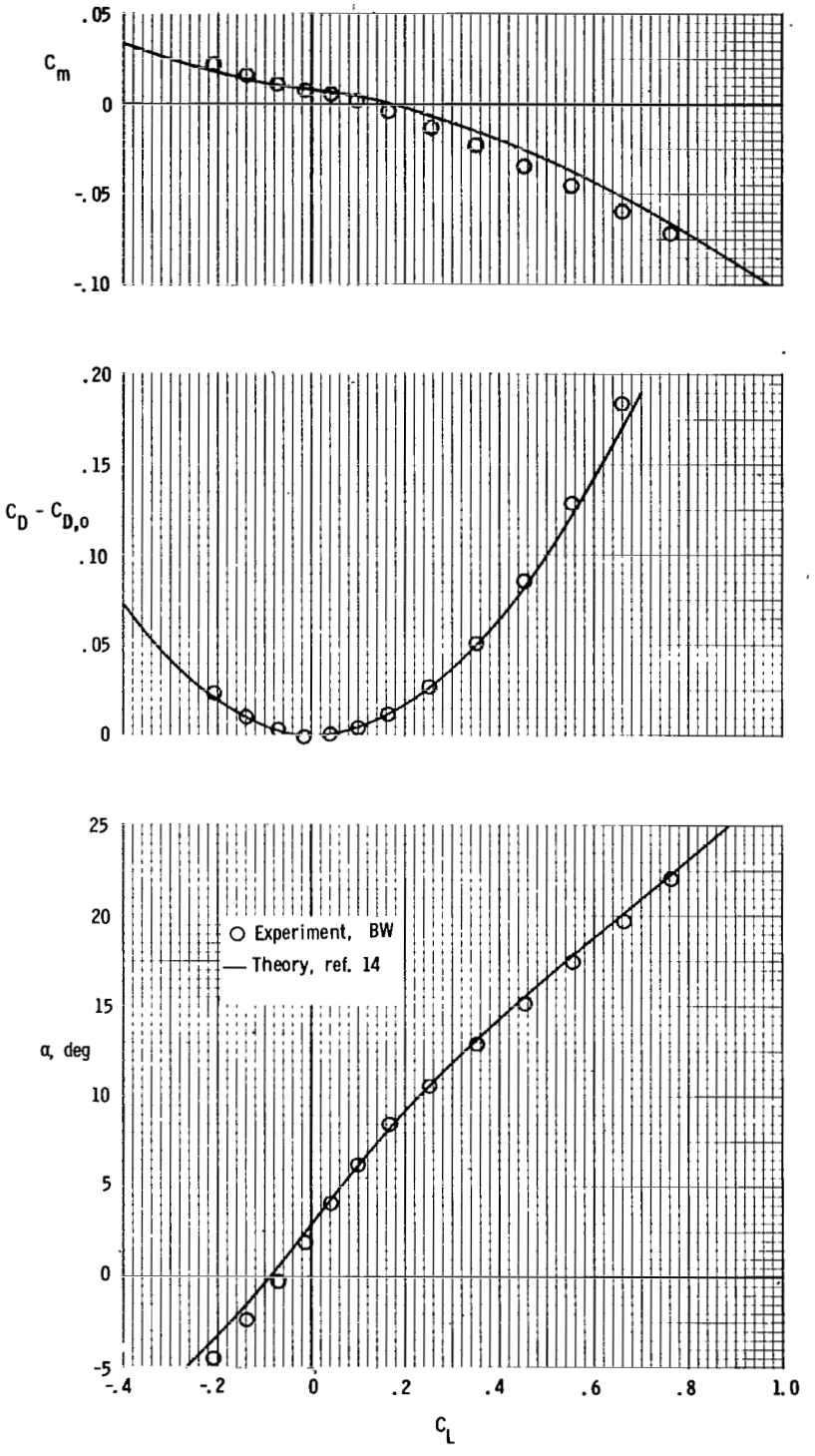
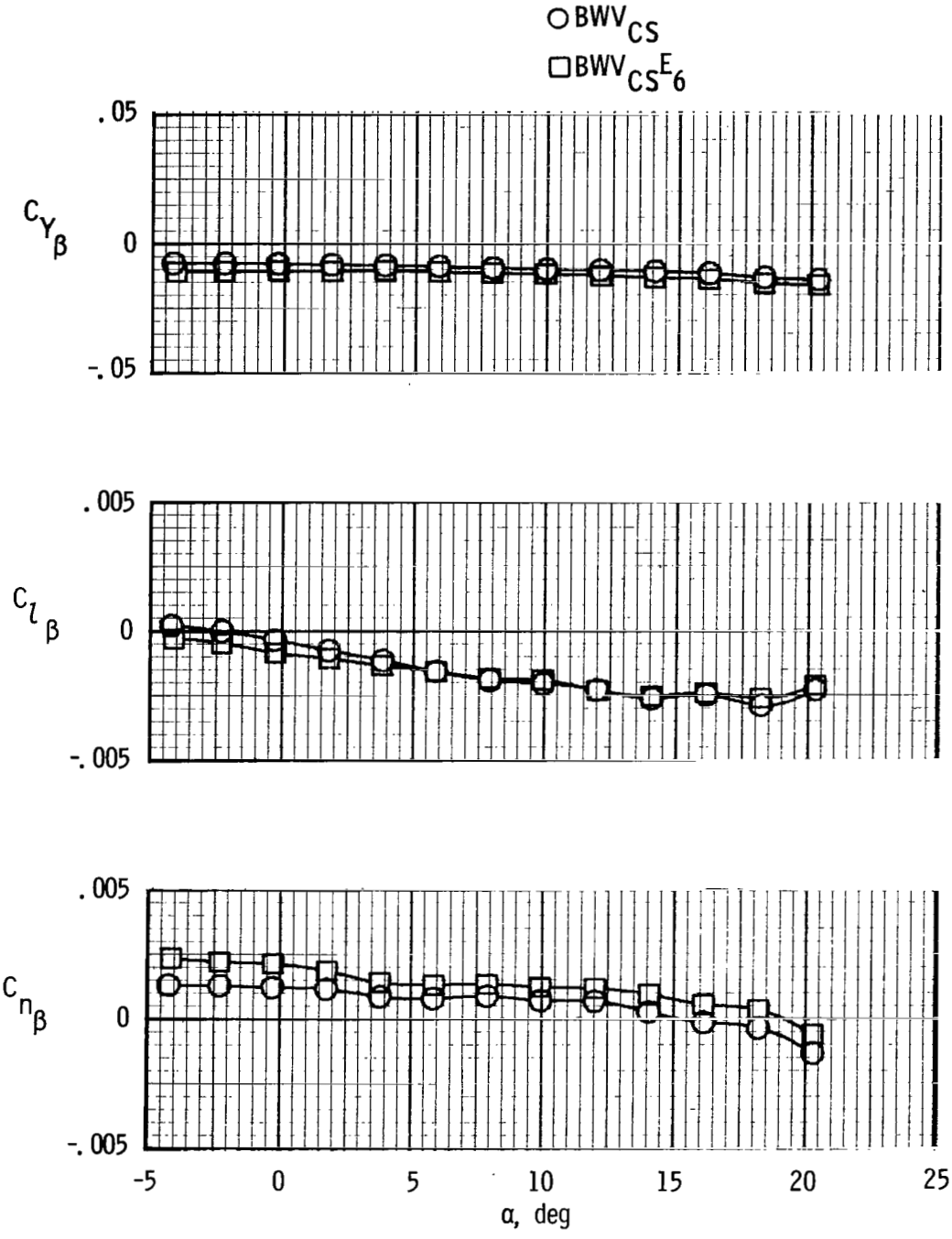
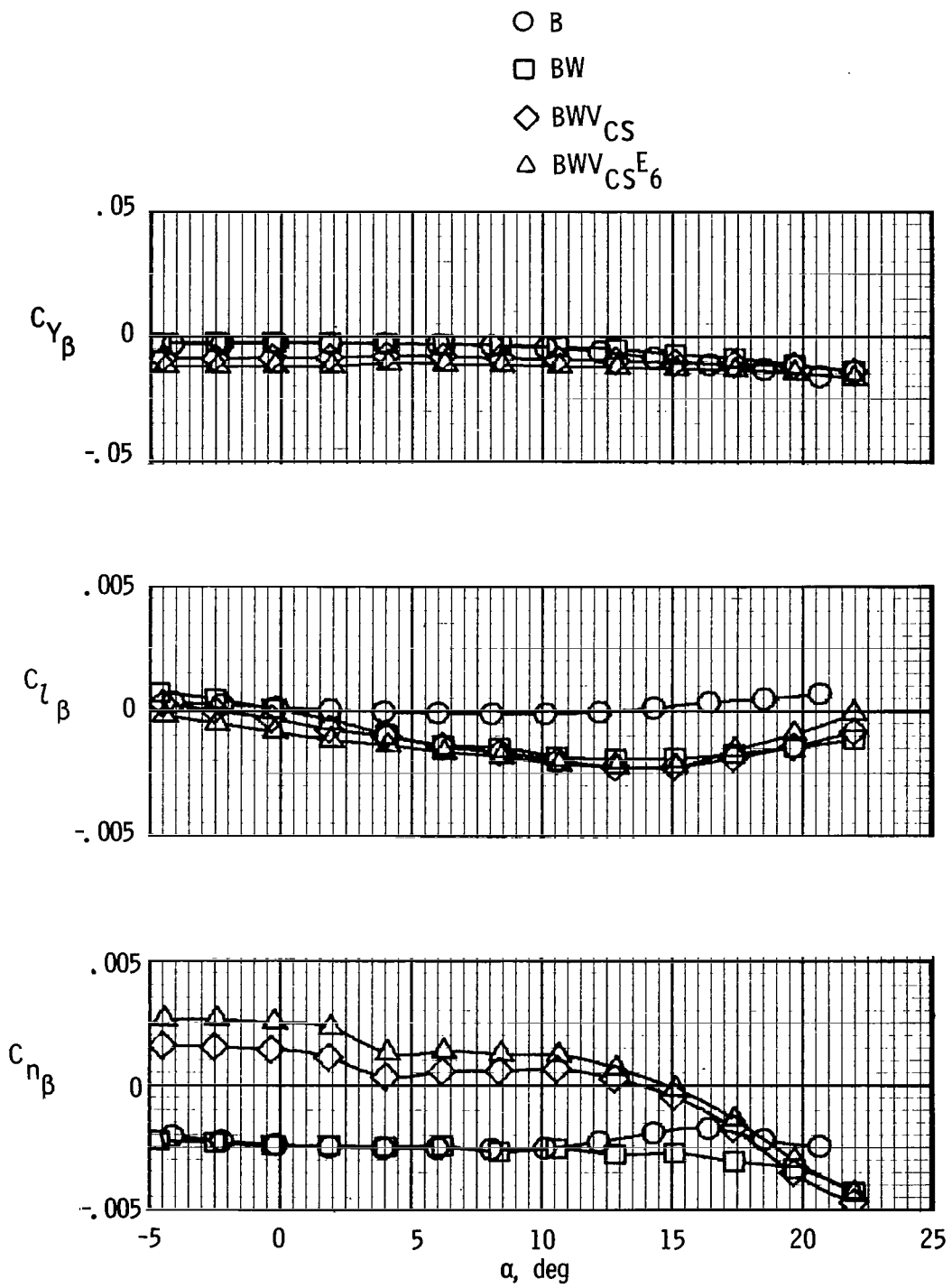


Figure 12.- Comparison of experiment with theory for body wing (BW) configuration only; M = 0.80.



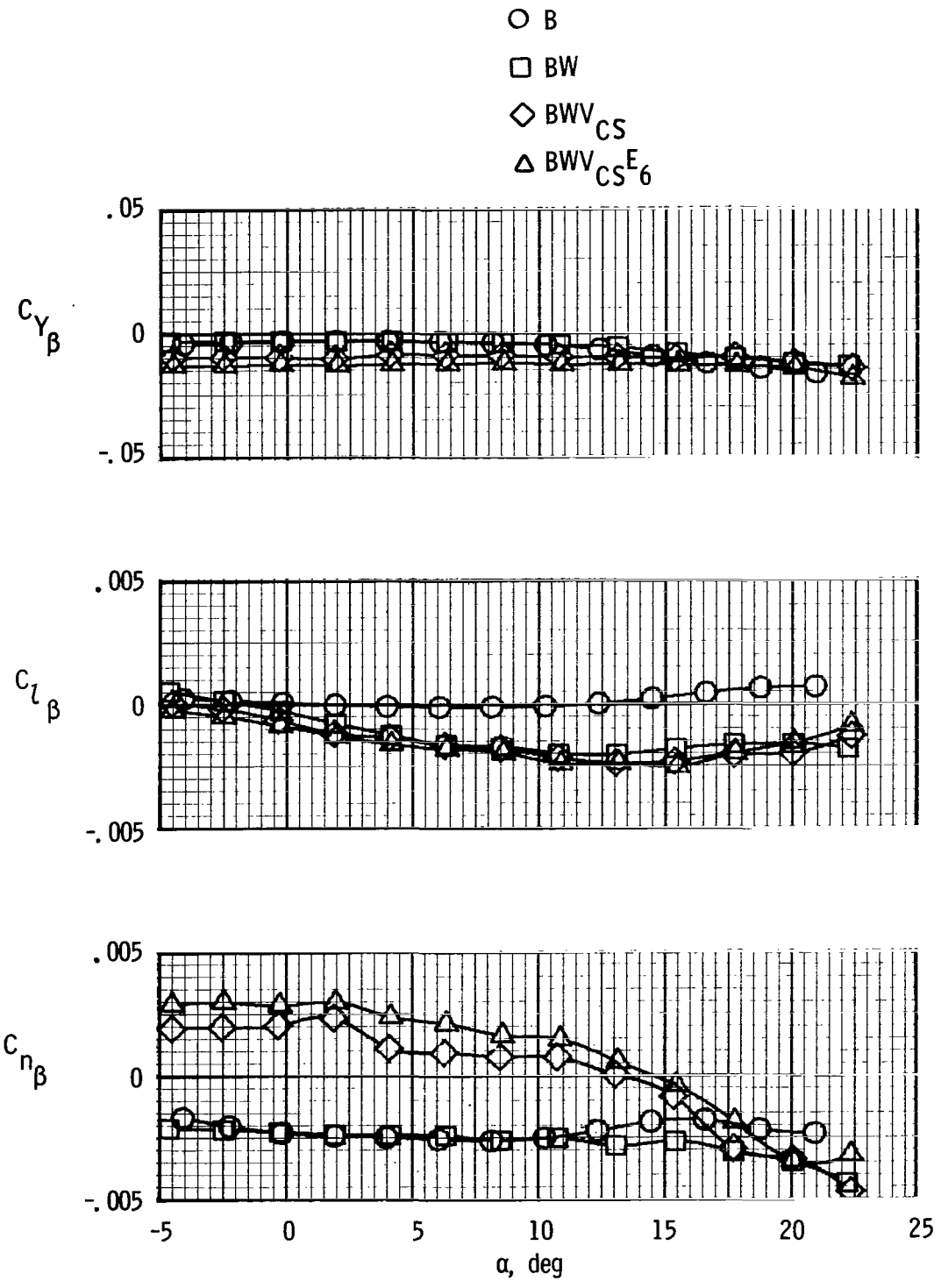
(a) $M_\infty \approx 0.33$.

Figure 13.- Effect of body buildup on static lateral-directional stability characteristics.



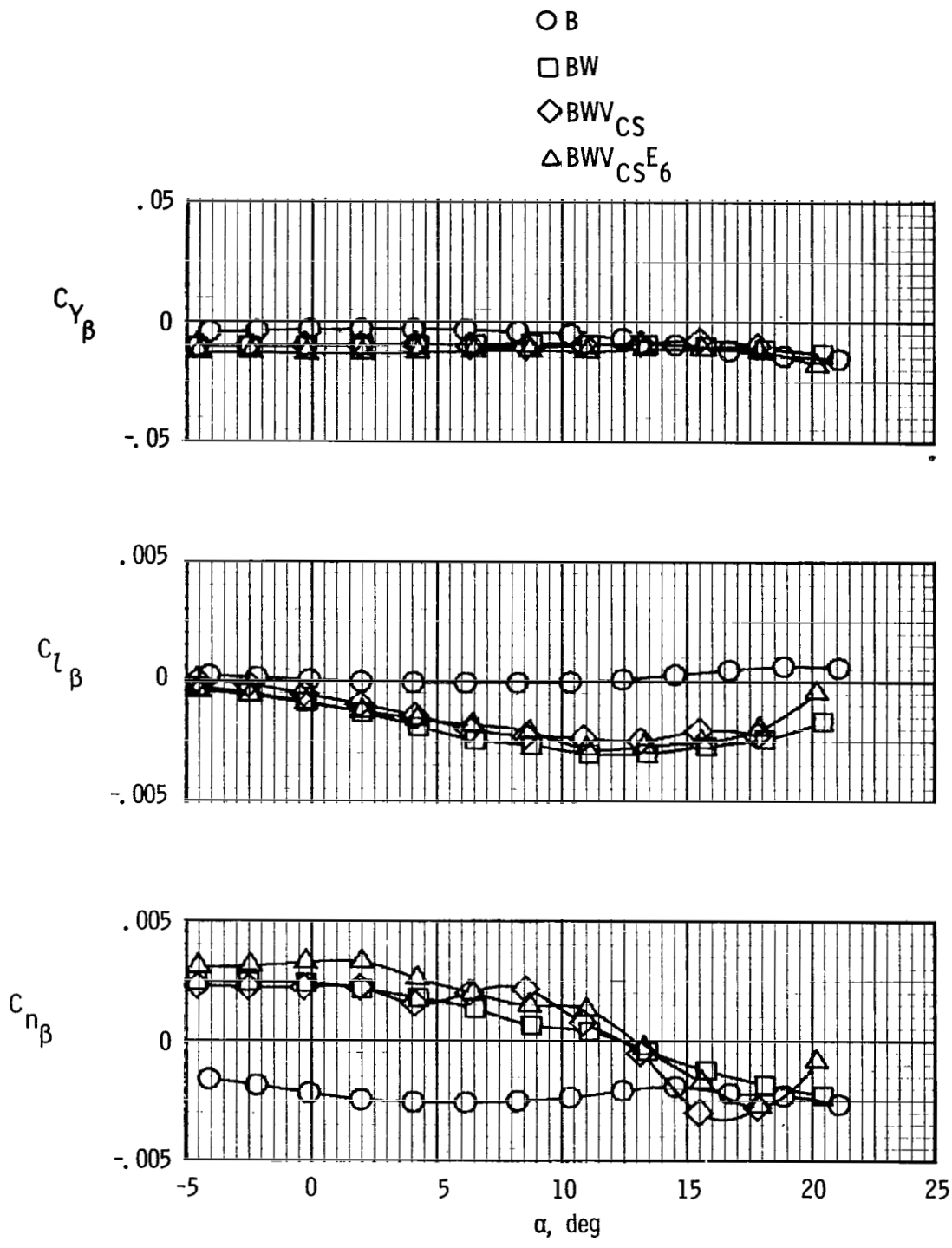
(b) M_∞ = 0.80.

Figure 13.- Continued.



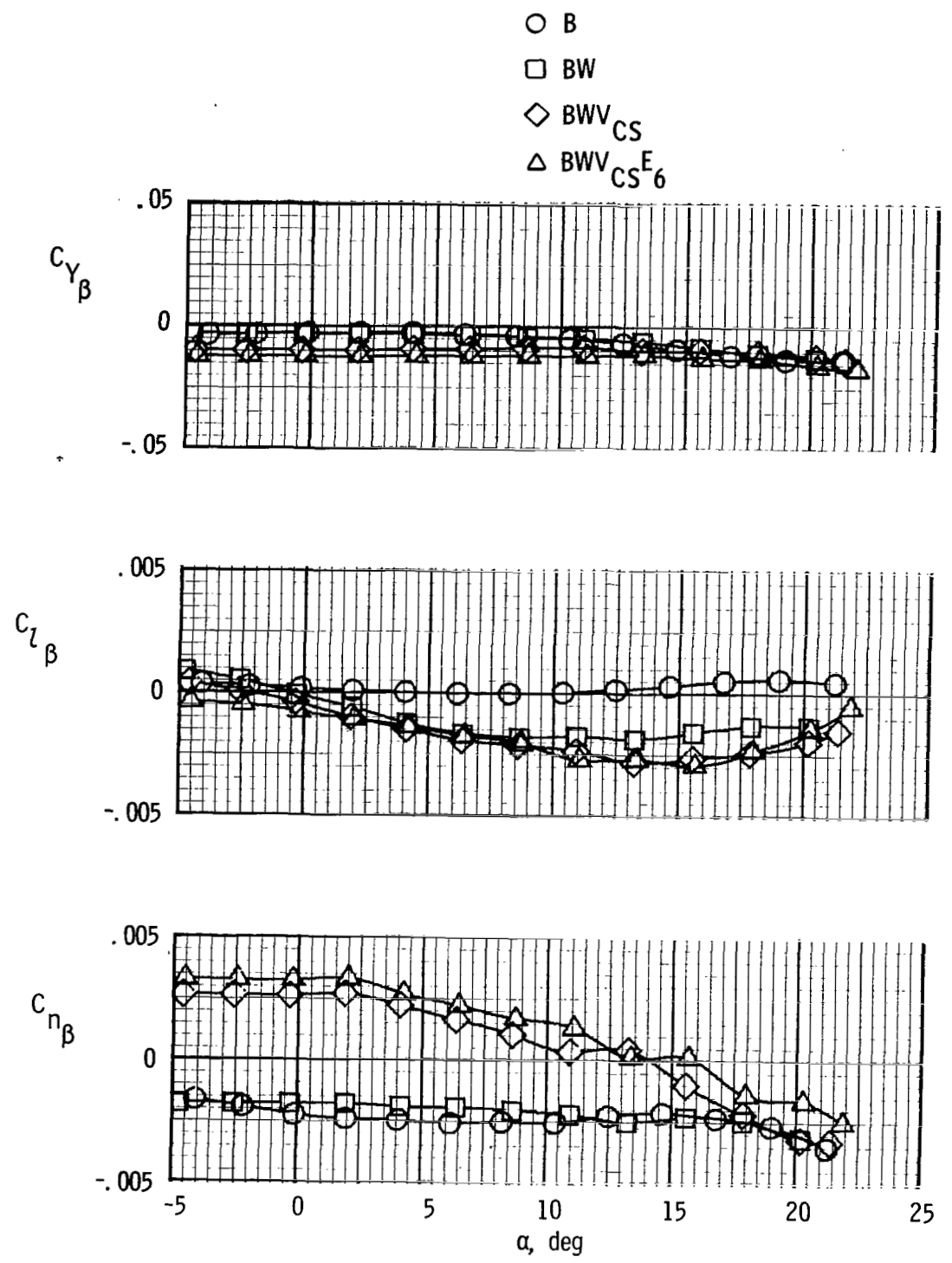
(c) $M_\infty = 0.90$.

Figure 13.- Continued.



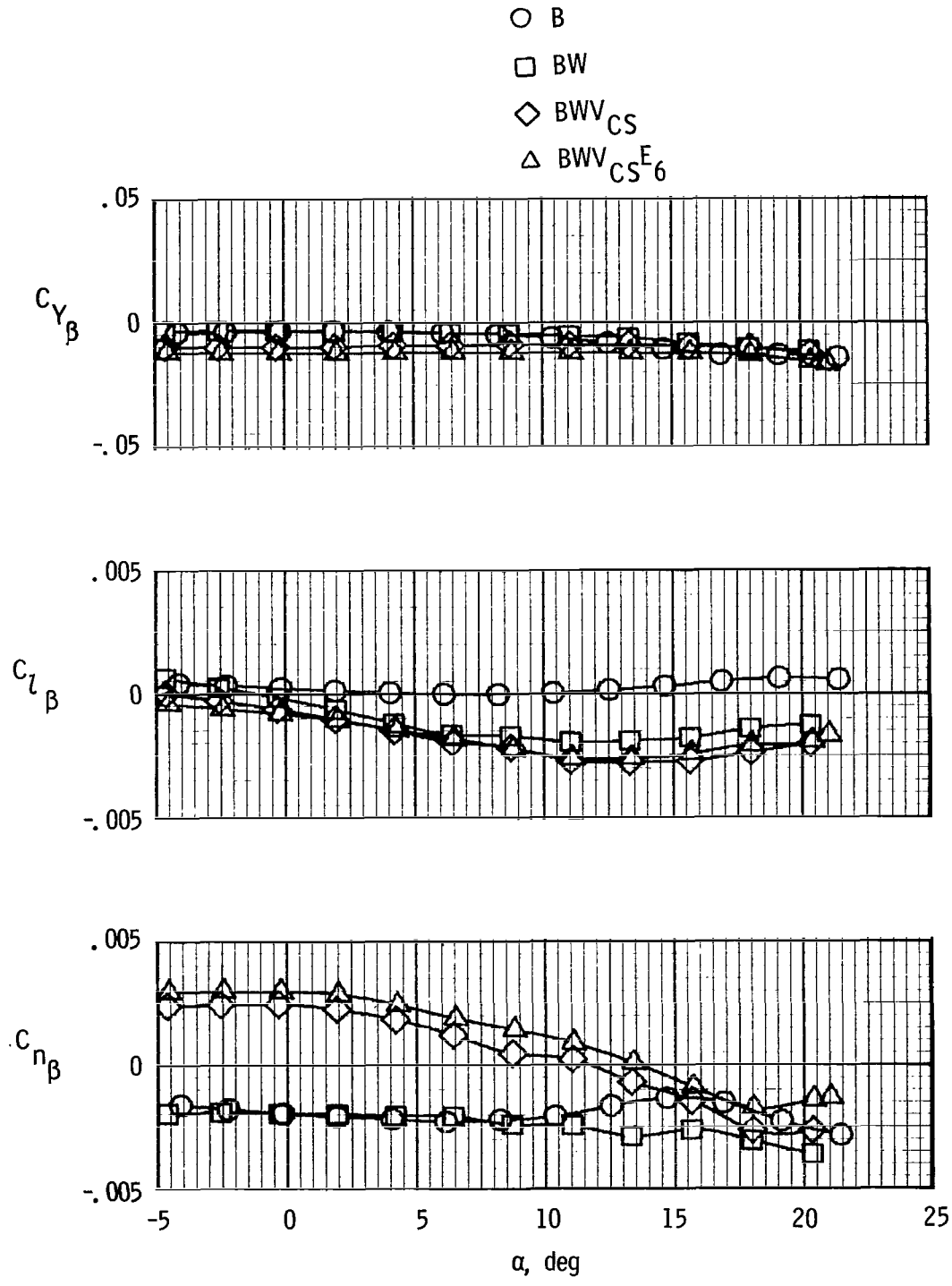
(d) $M_\infty = 0.95$.

Figure 13.- Continued.



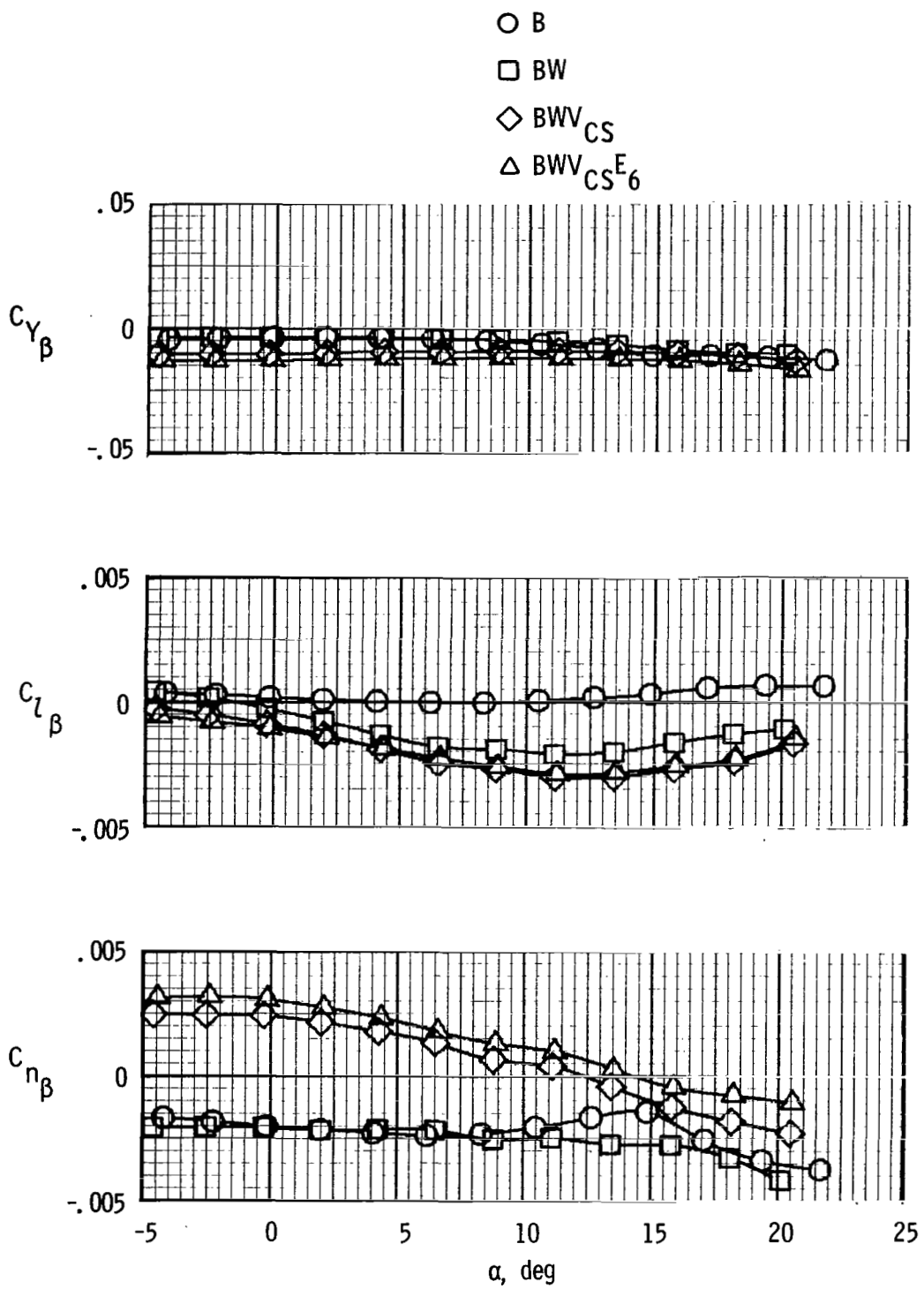
(e) $M_\infty = 0.98$.

Figure 13.- Continued.



(f) M_∞ = 1.10.

Figure 13.- Continued.



(g) M_∞ = 1.20.

Figure 13.- Concluded.

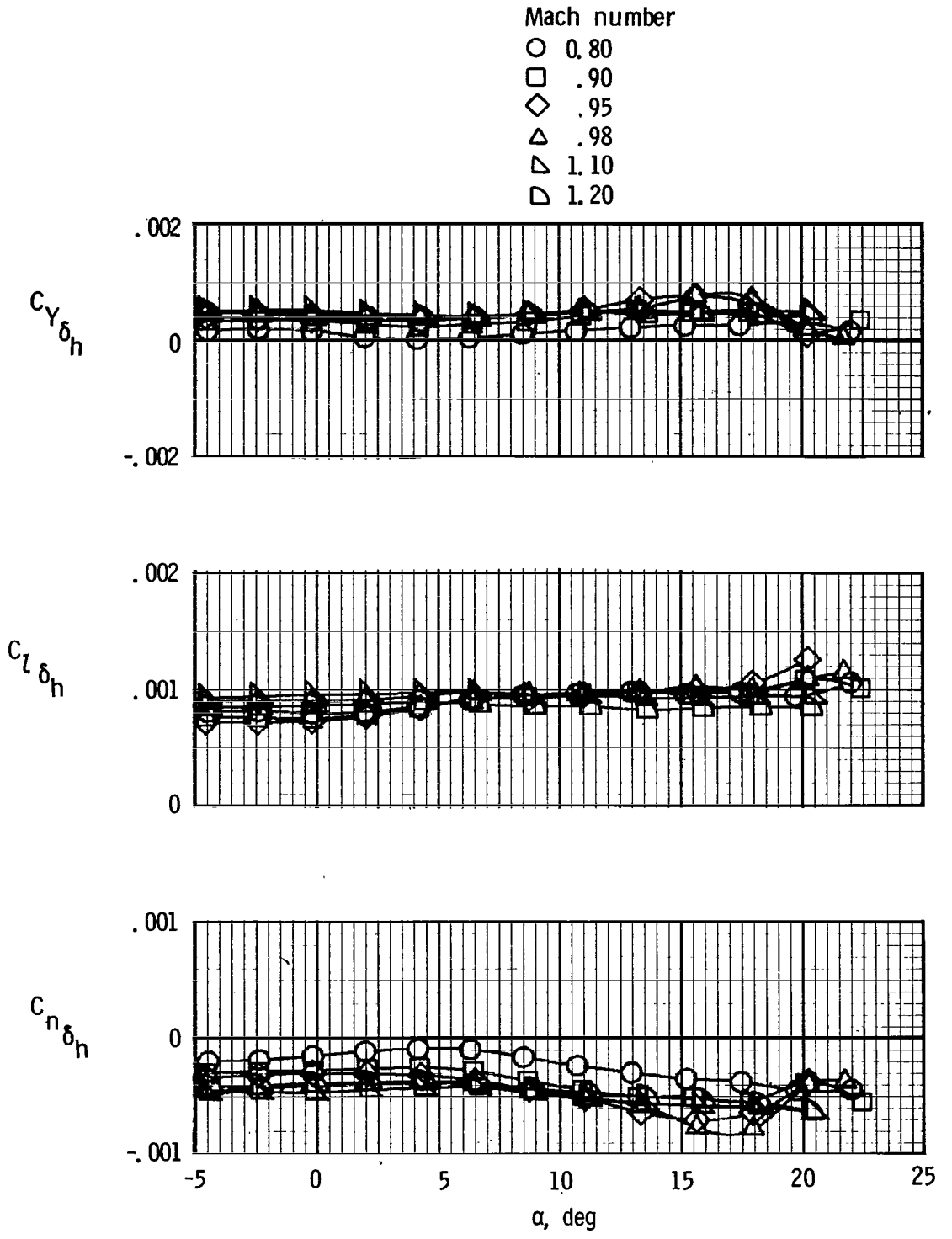


Figure 14.- Roll control characteristics for $BWV_{CS}E_6$ configuration.

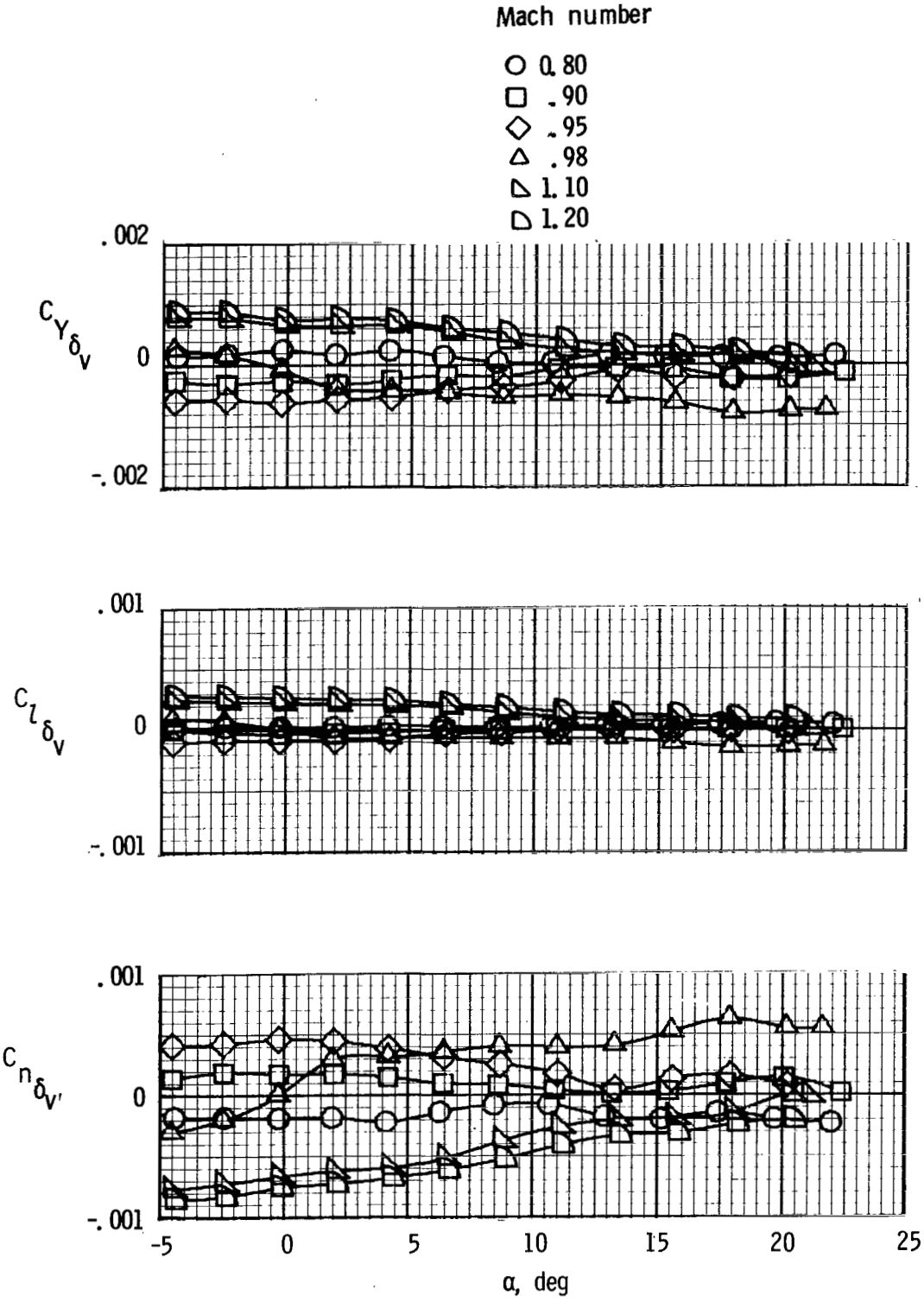
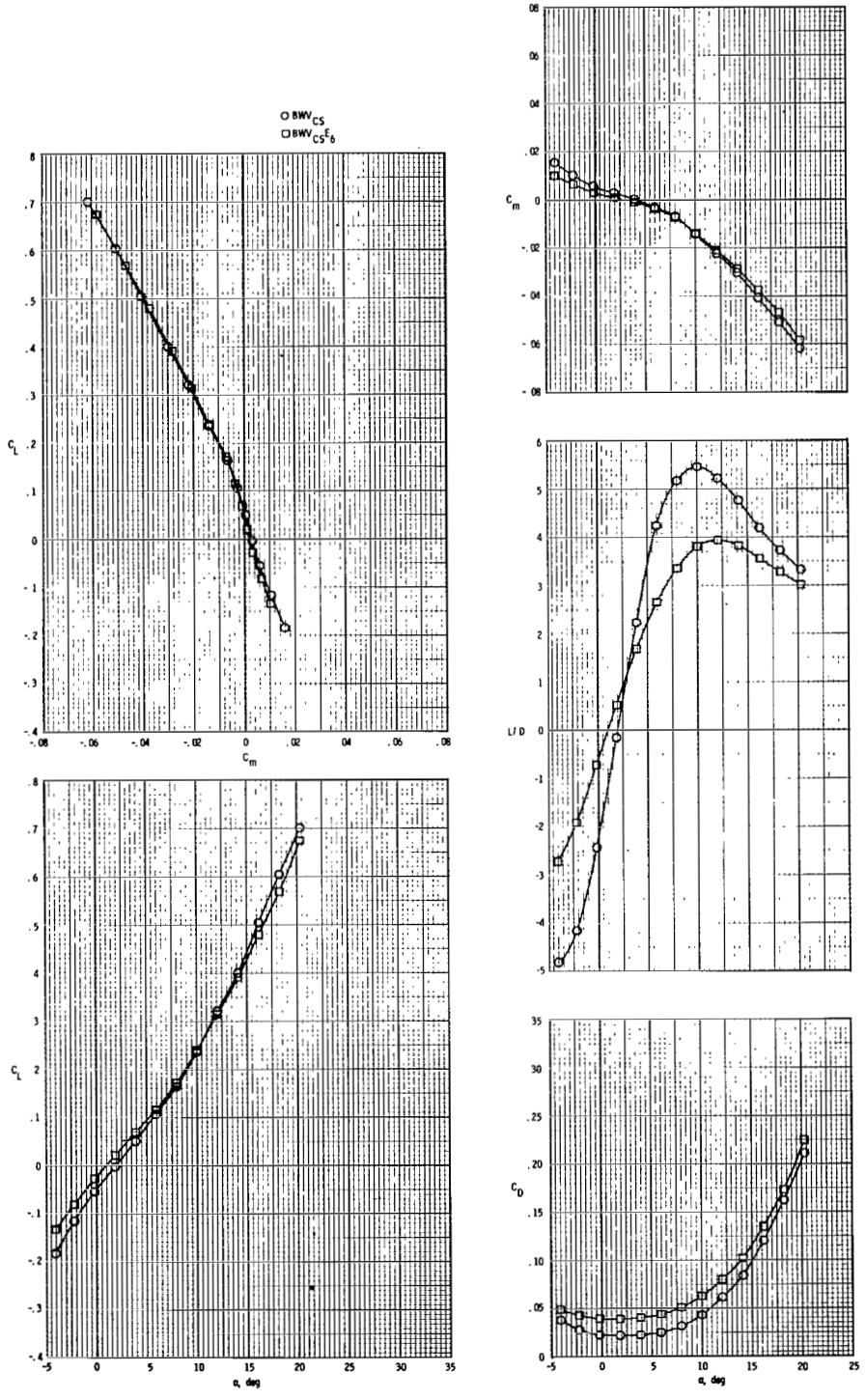
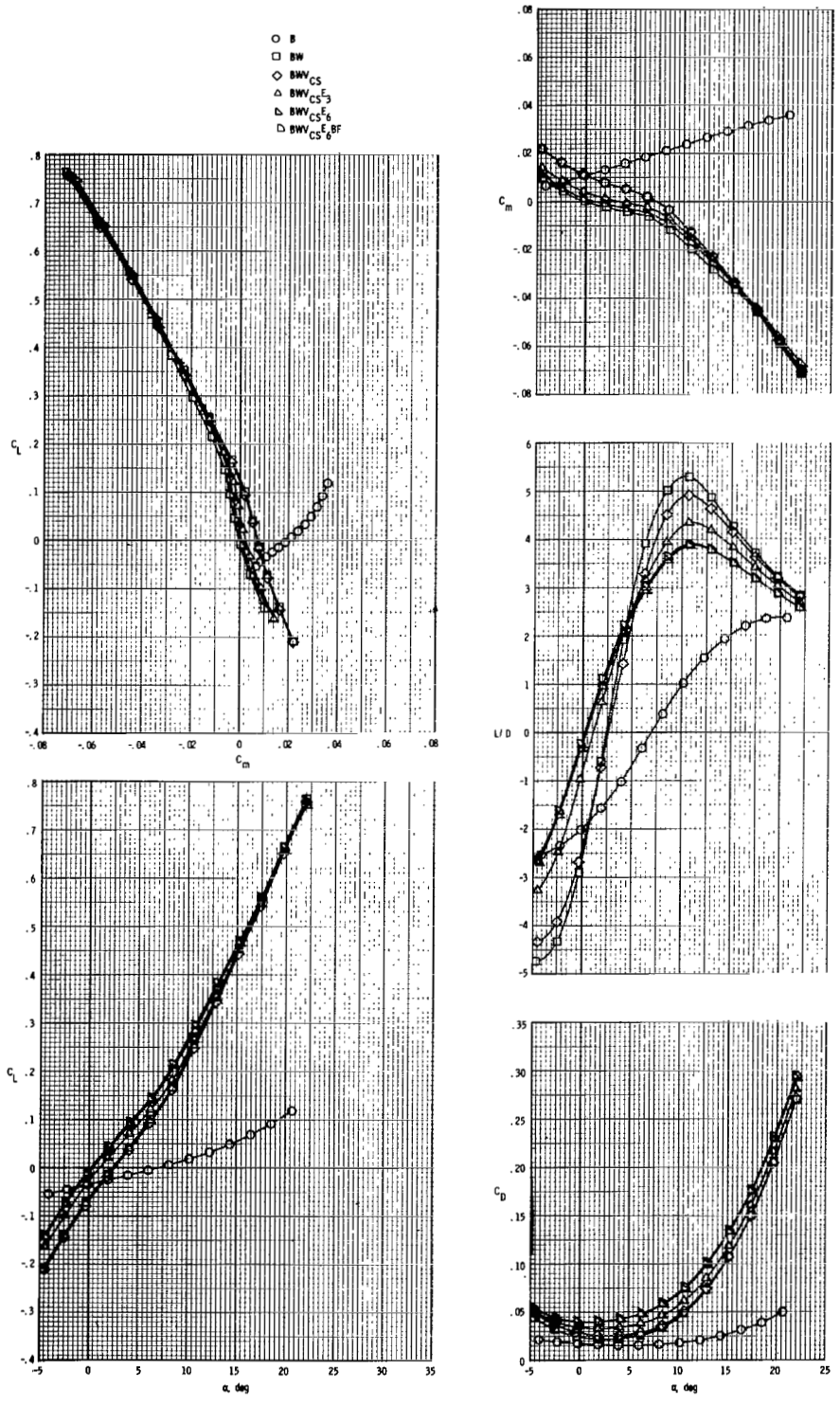


Figure 15.- Directional control characteristics for $BWV_{CS}E_6$ configuration.



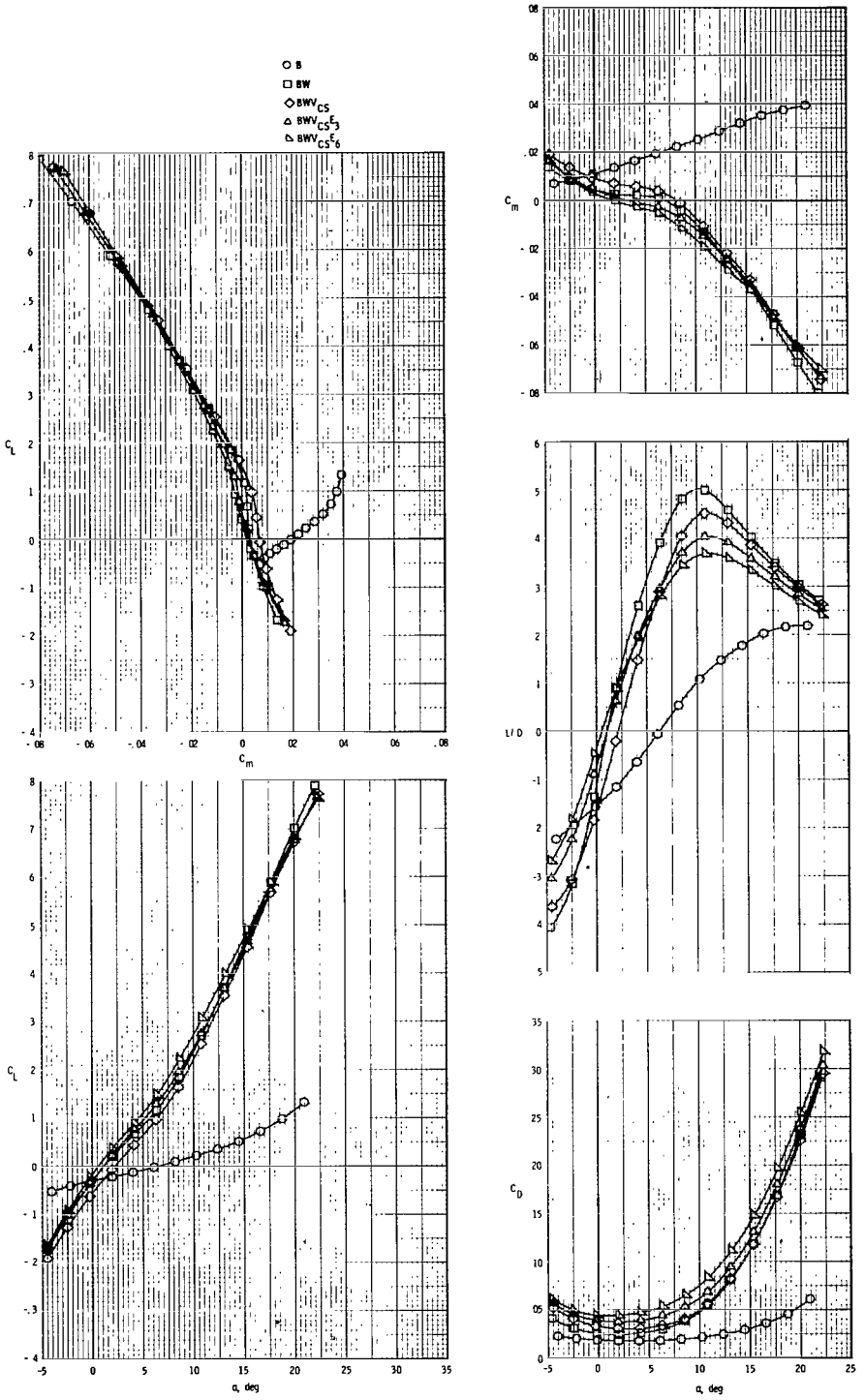
(a) $M_\infty = 0.33$.

Figure 16.- Effect of body buildup on untrimmed longitudinal aerodynamic characteristics.



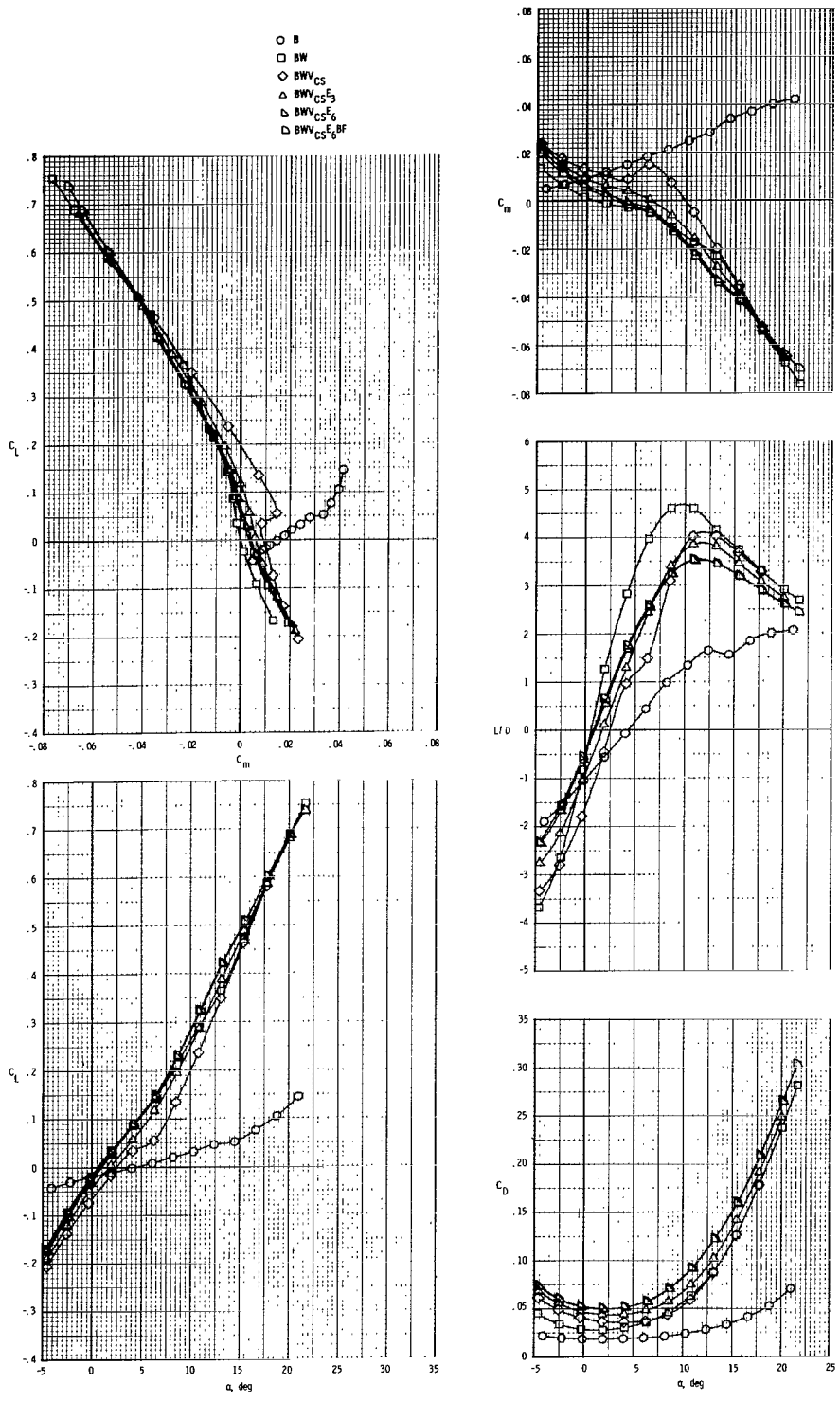
(b) $M_\infty = 0.80$.

Figure 16.- Continued.



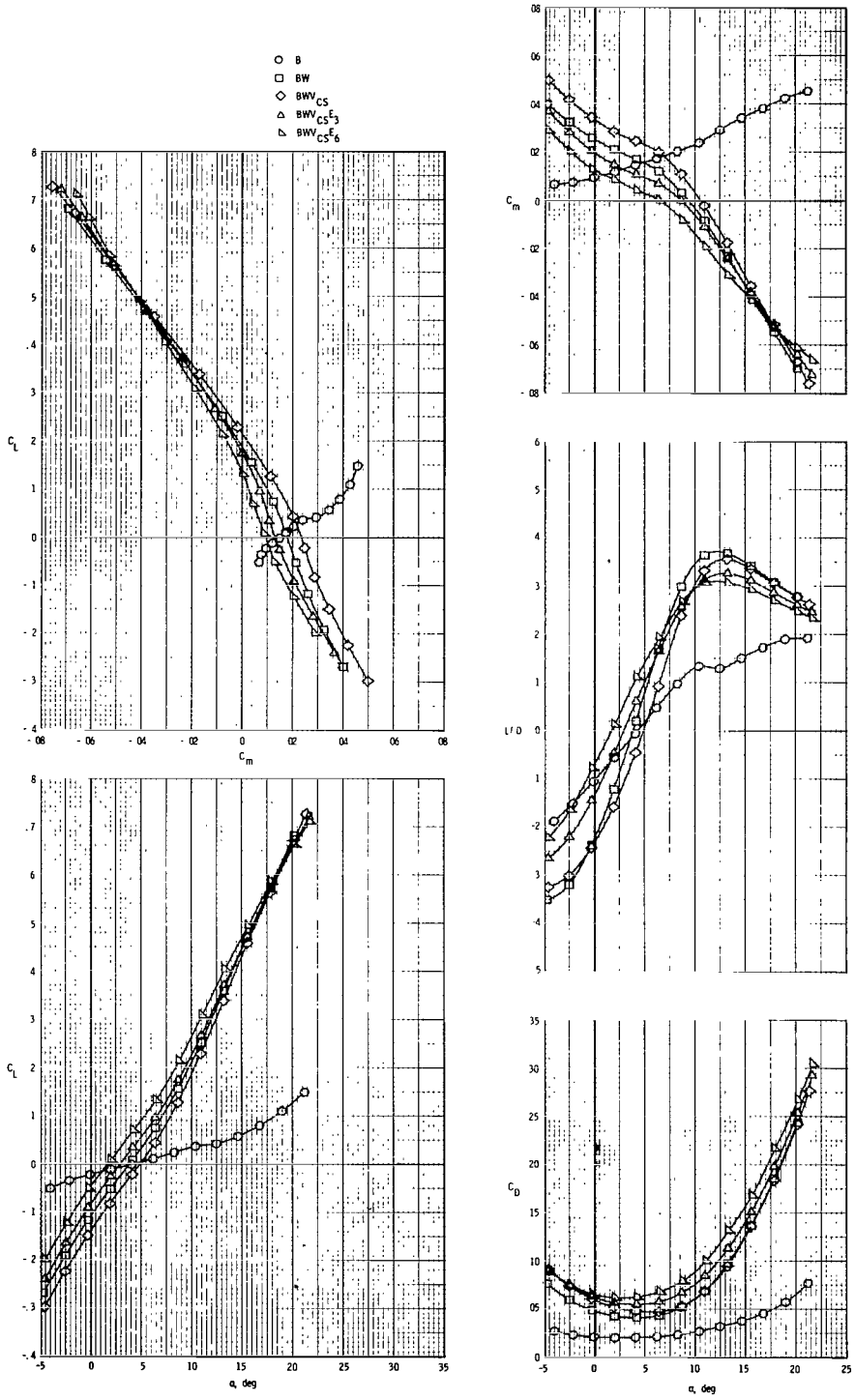
(c) M_∞ = 0.90.

Figure 16.- Continued.



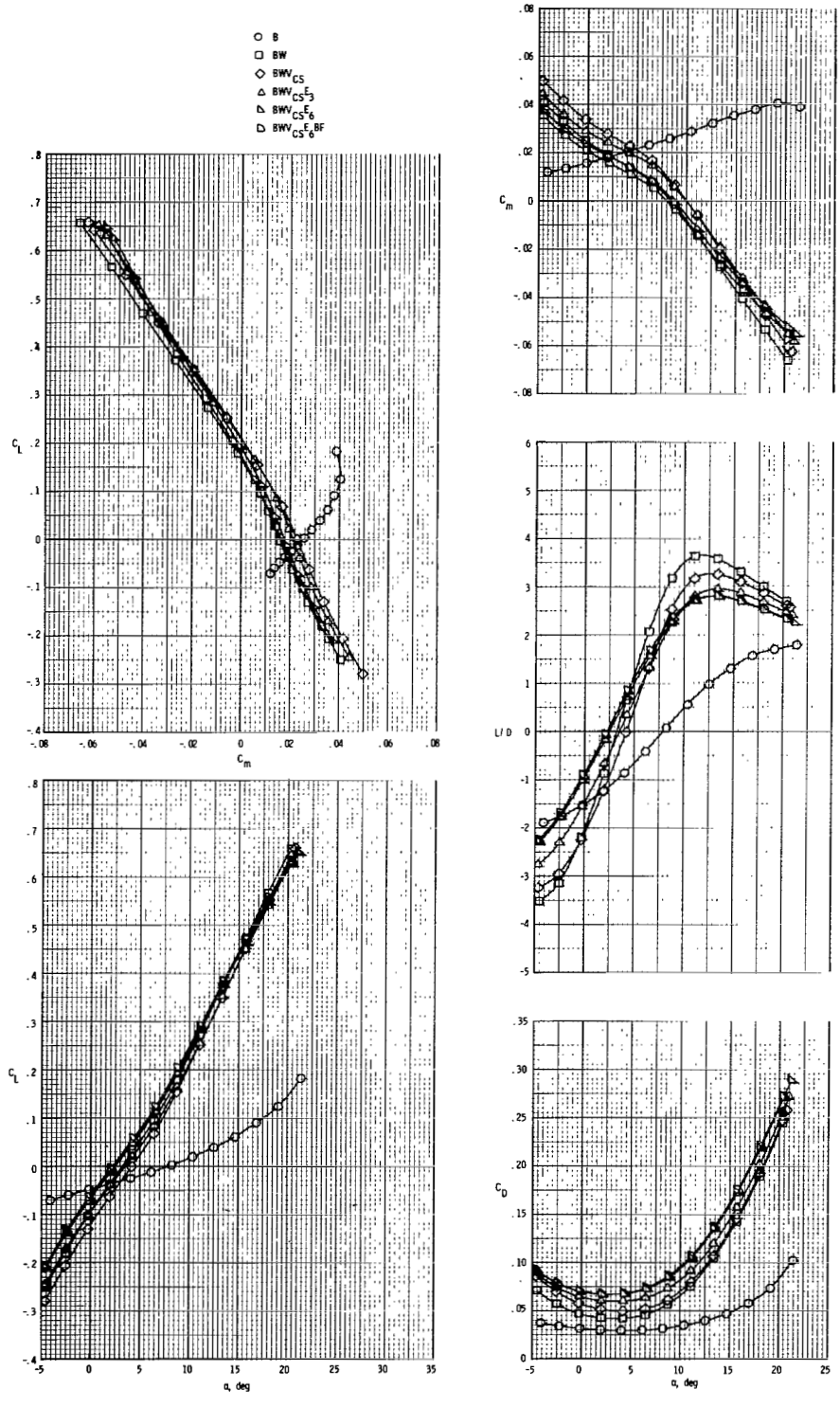
(d) M_∞ = 0.95.

Figure 16.- Continued.



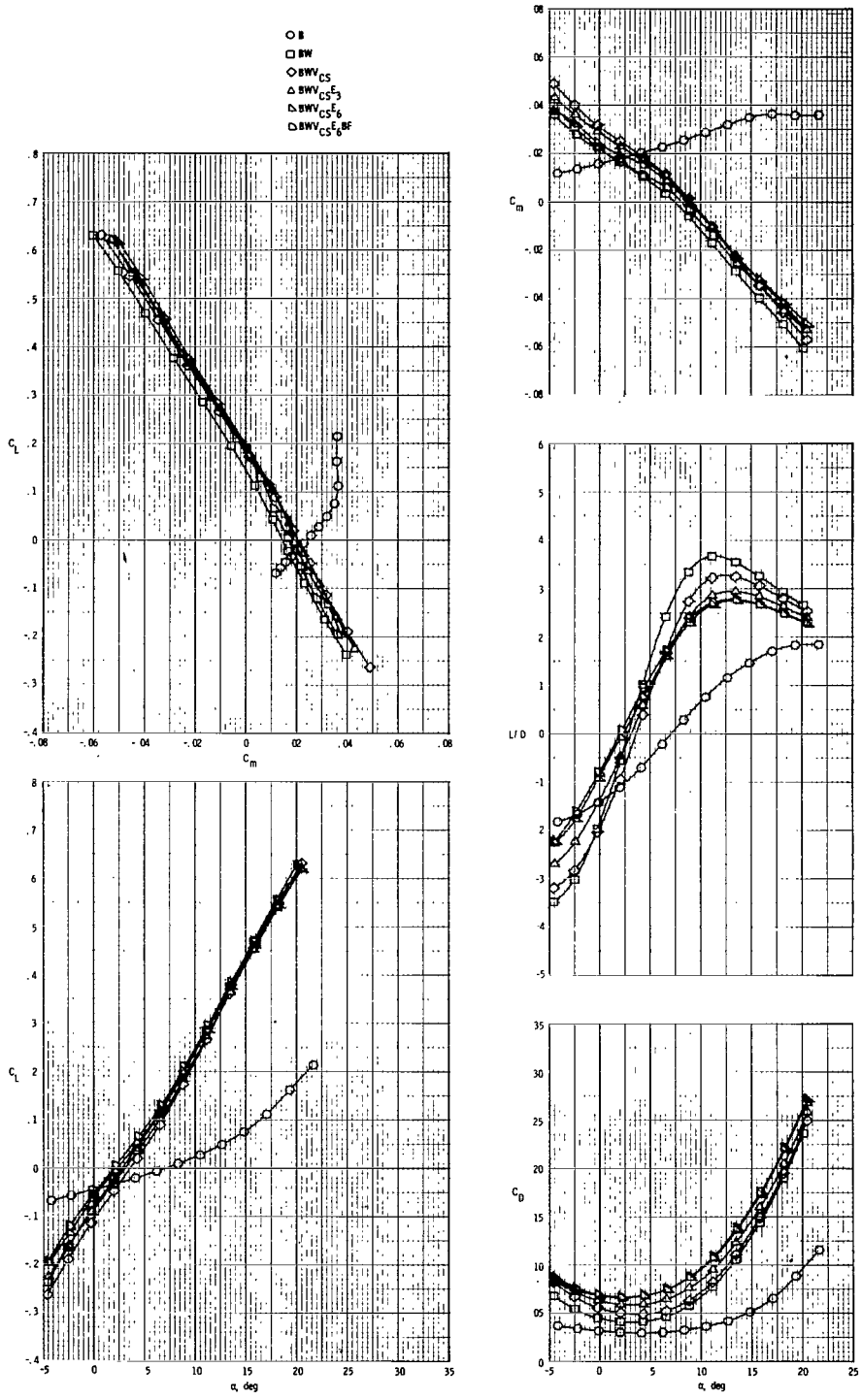
(e) $M_\infty = 0.98$.

Figure 16.- Continued.



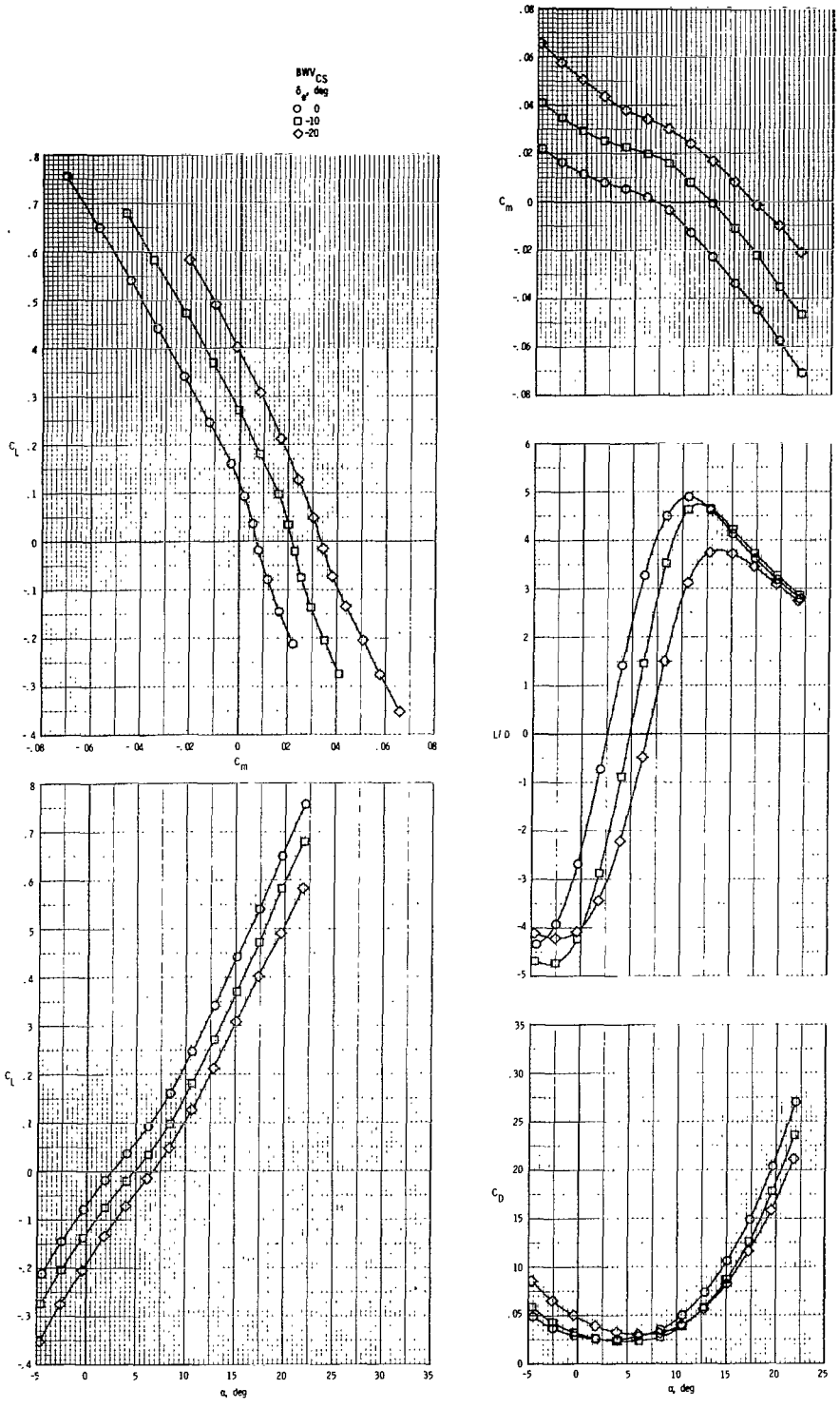
(f) M_∞ = 1.10.

Figure 16.- Continued.



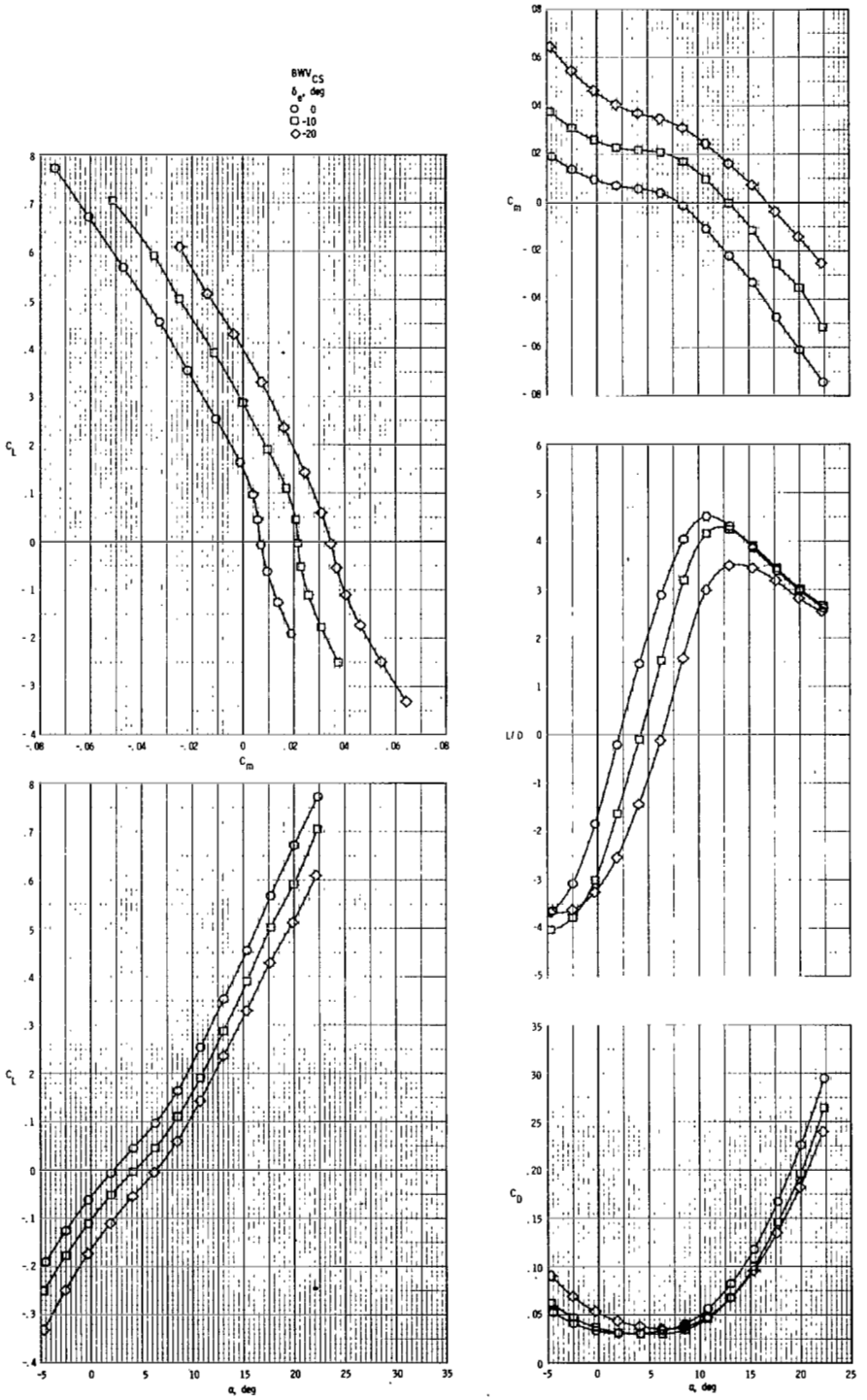
(g) M_∞ = 1.20.

Figure 16.- Concluded.



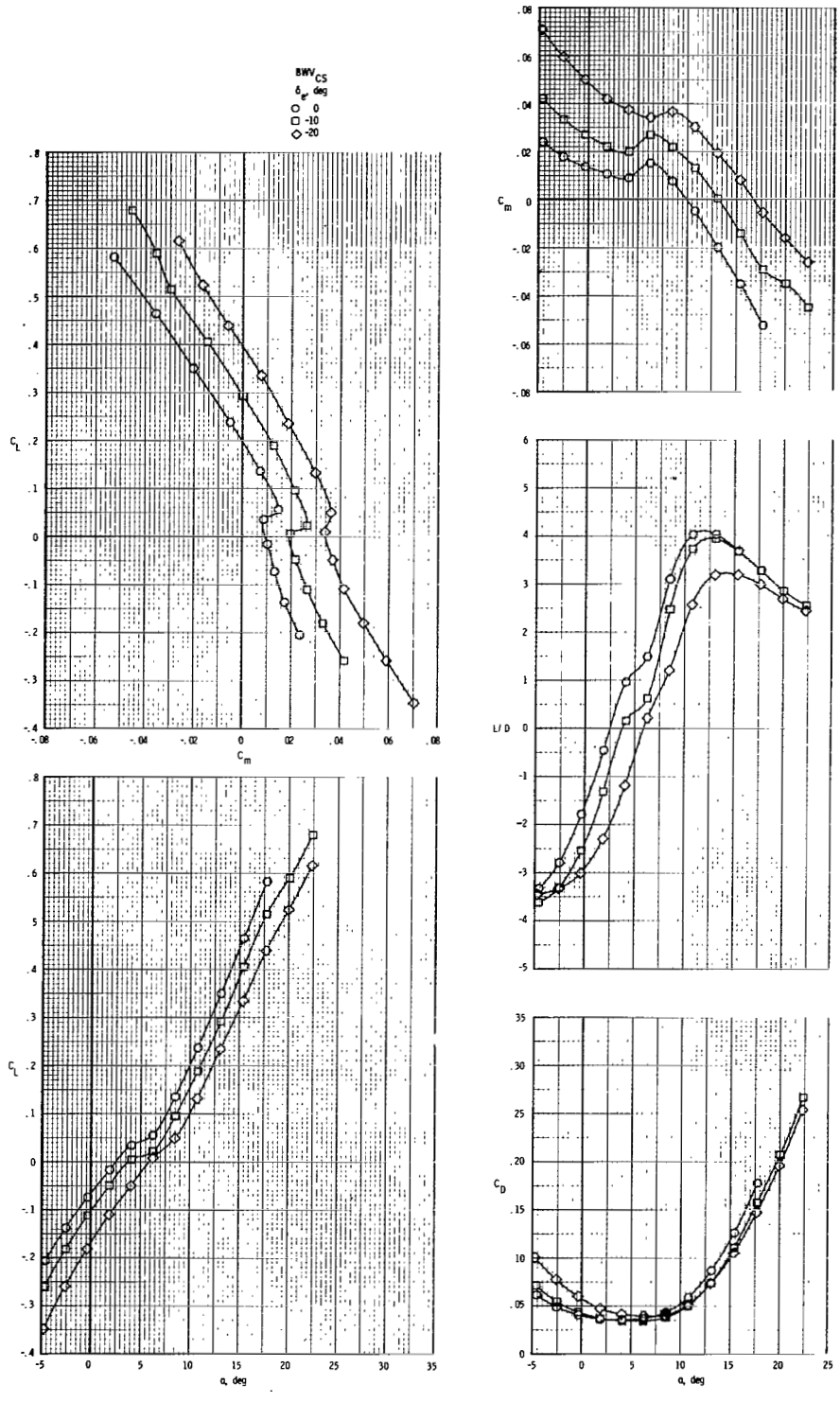
(a) $M_\infty = 0.80$.

Figure 17.- Effect of elevon deflection on longitudinal aerodynamic characteristics of BWV_{CS} configuration.



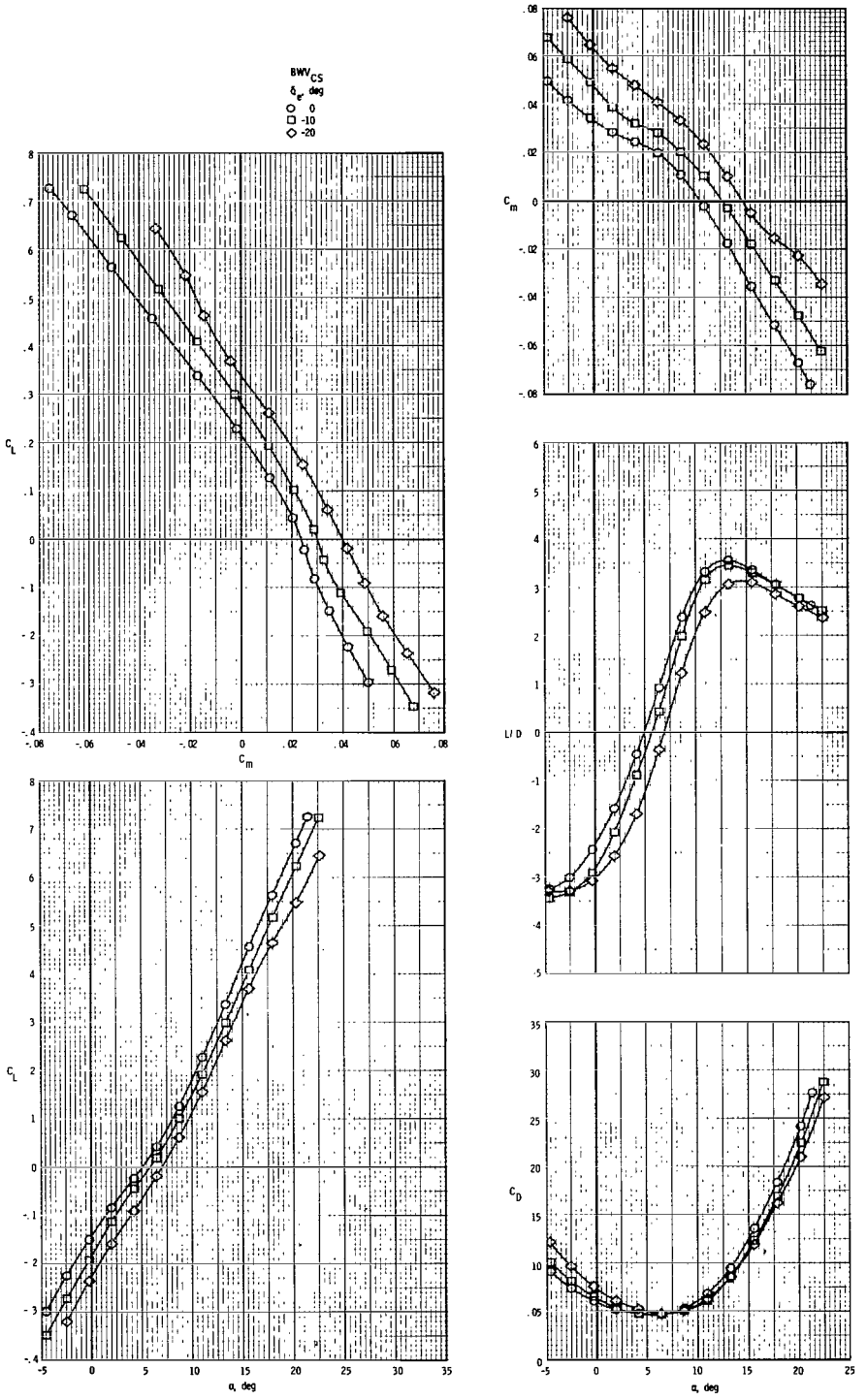
(b) $M_\infty = 0.90$.

Figure 17.- Continued.



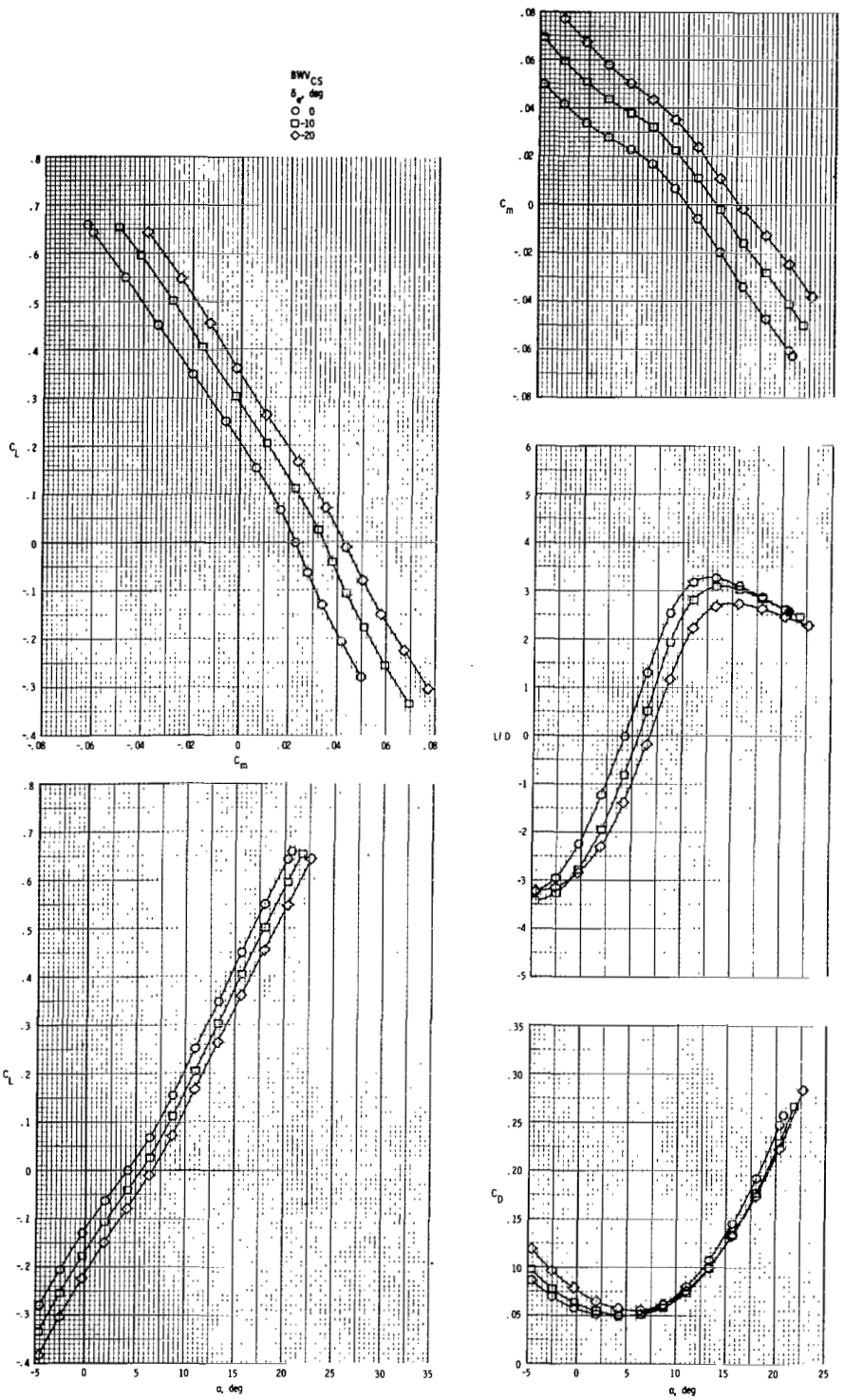
(c) $M_\infty = 0.95$.

Figure 17.- Continued.



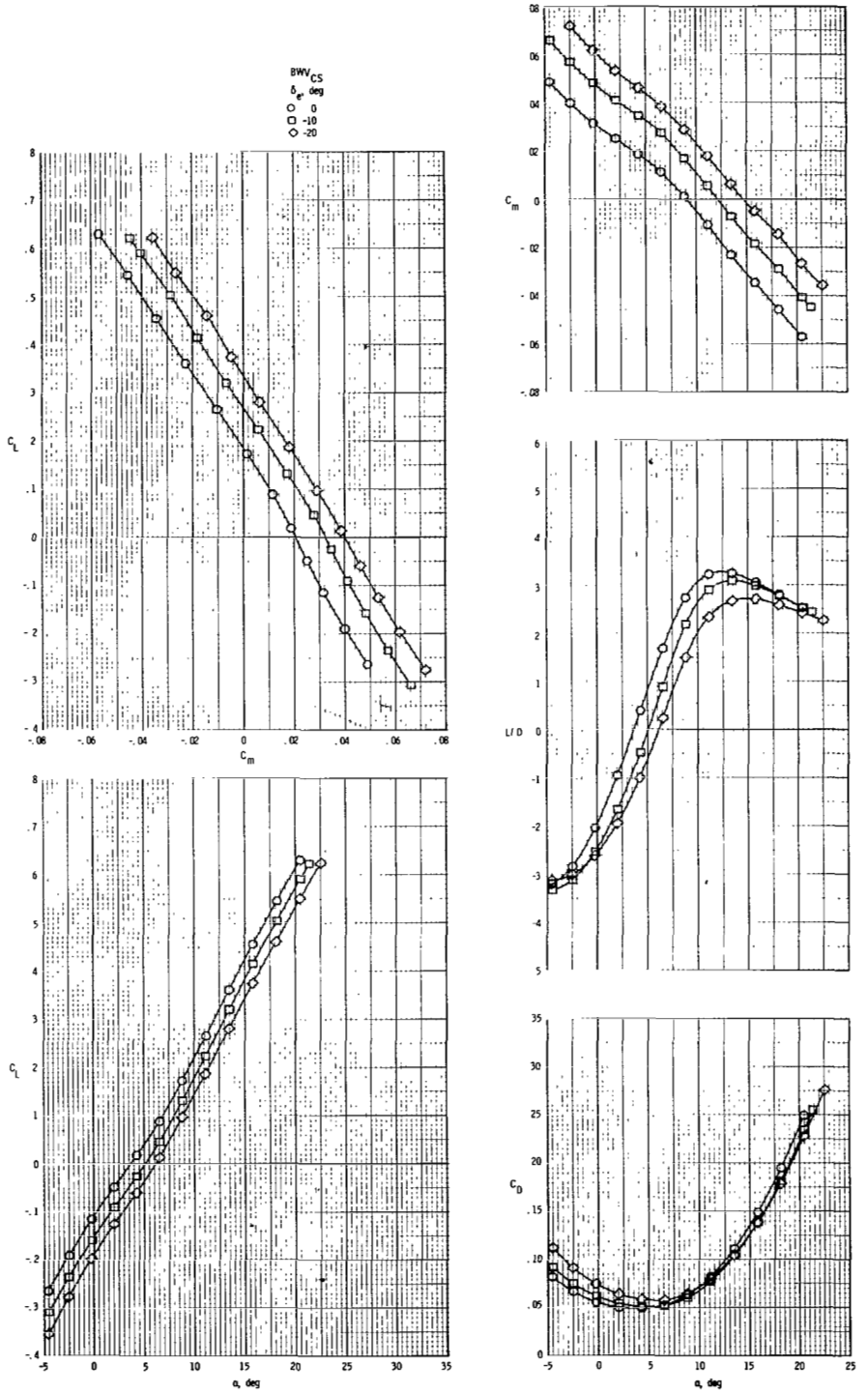
(d) $M_\infty = 0.98$.

Figure 17.- Continued.



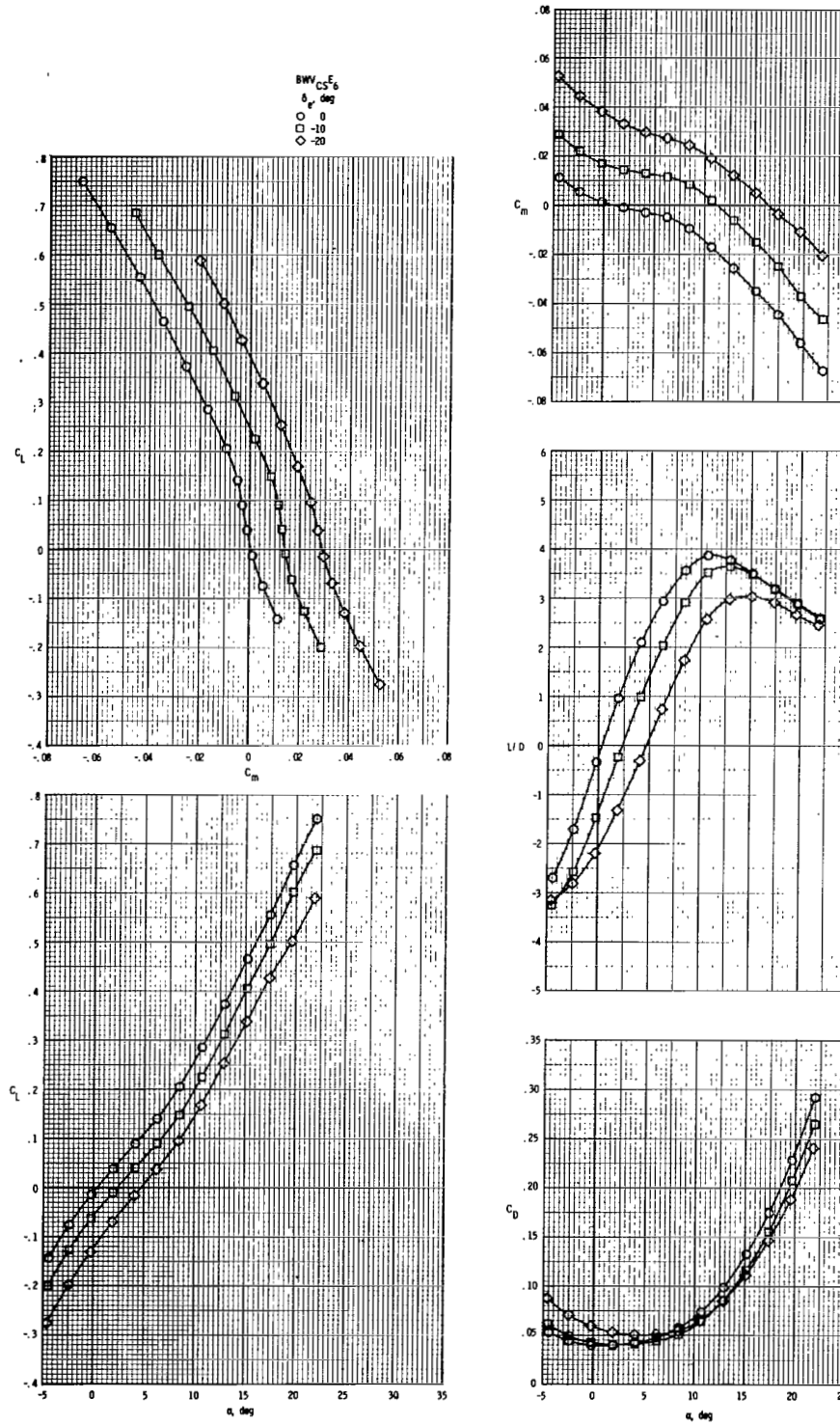
(e) M_∞ = 1.10.

Figure 17.- Continued.



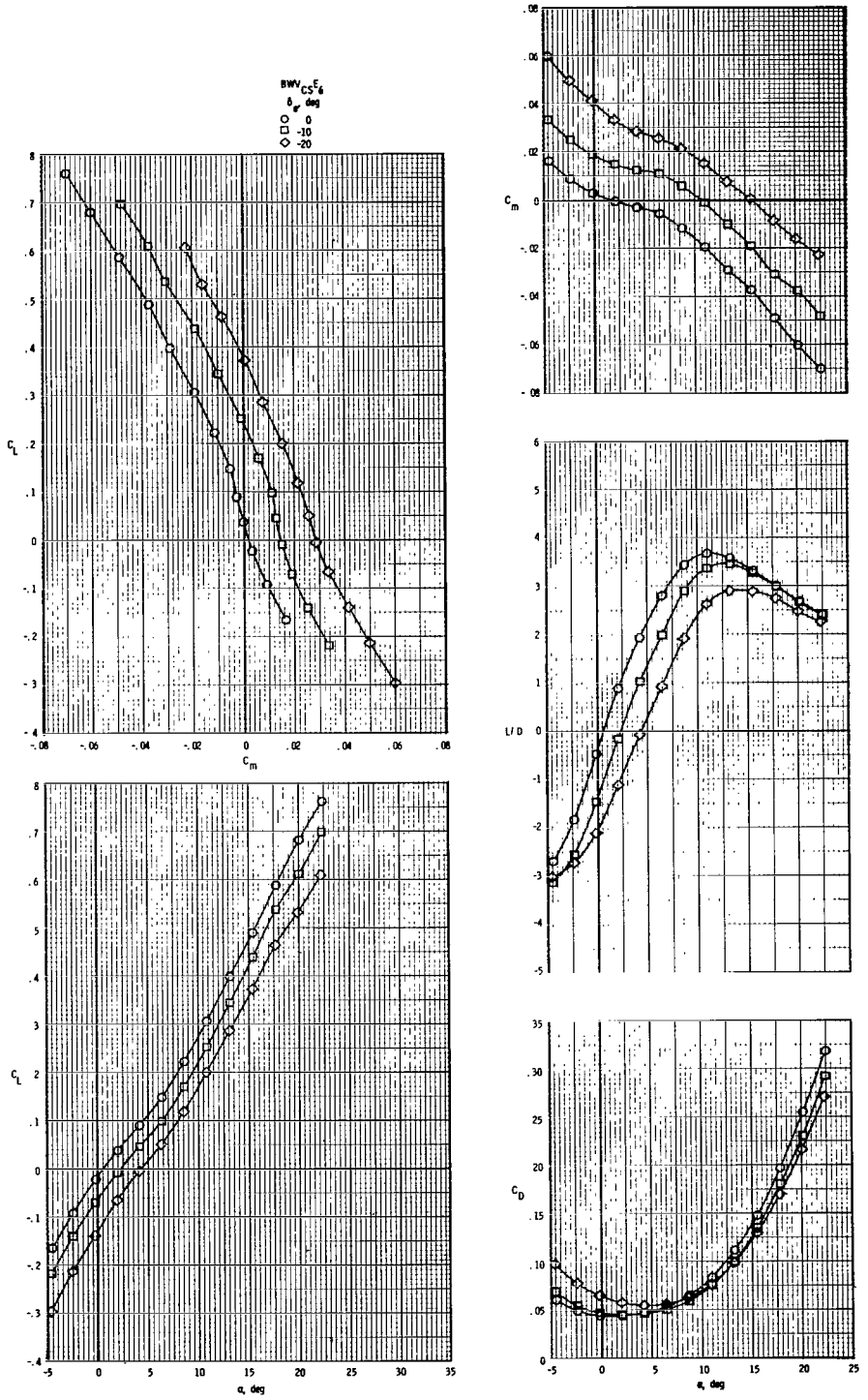
(f) M_∞ = 1.20.

Figure 17.- Concluded.



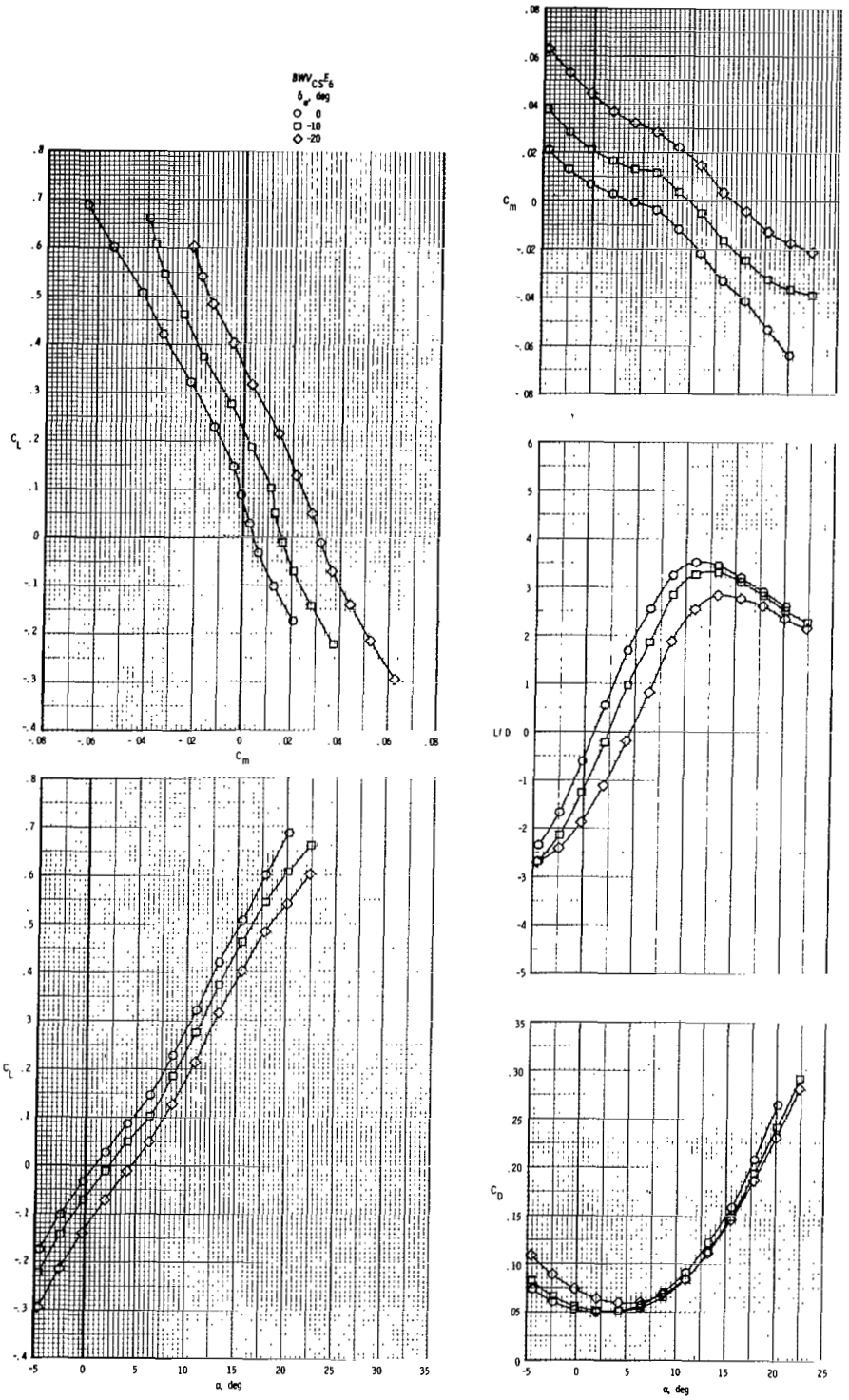
(a) M_∞ = 0.80.

Figure 18.- Effect of elevon deflection on longitudinal aerodynamic characteristics of $BWV_{CS}E_6$ configuration.



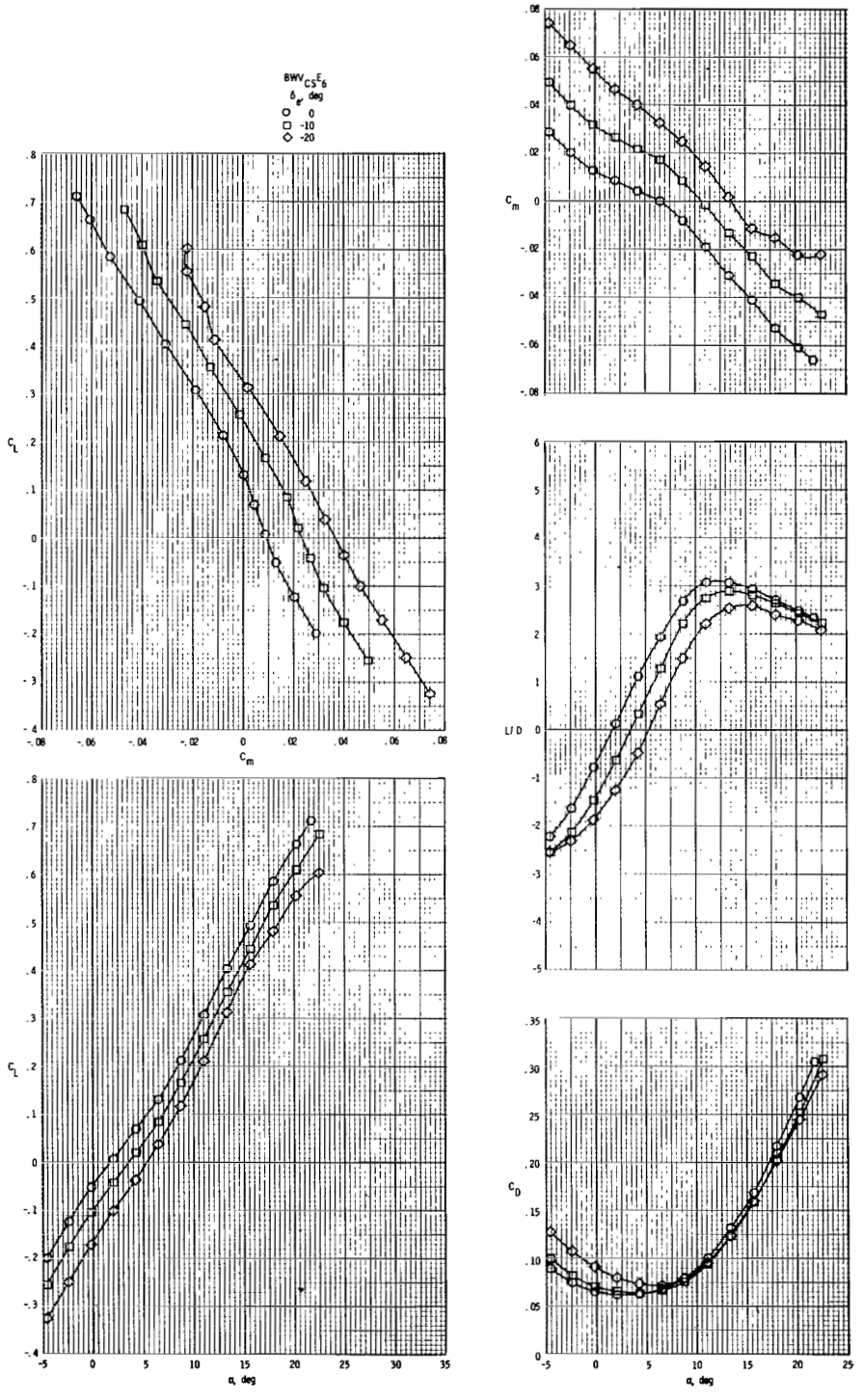
(b) M_∞ = 0.90.

Figure 18.- Continued.



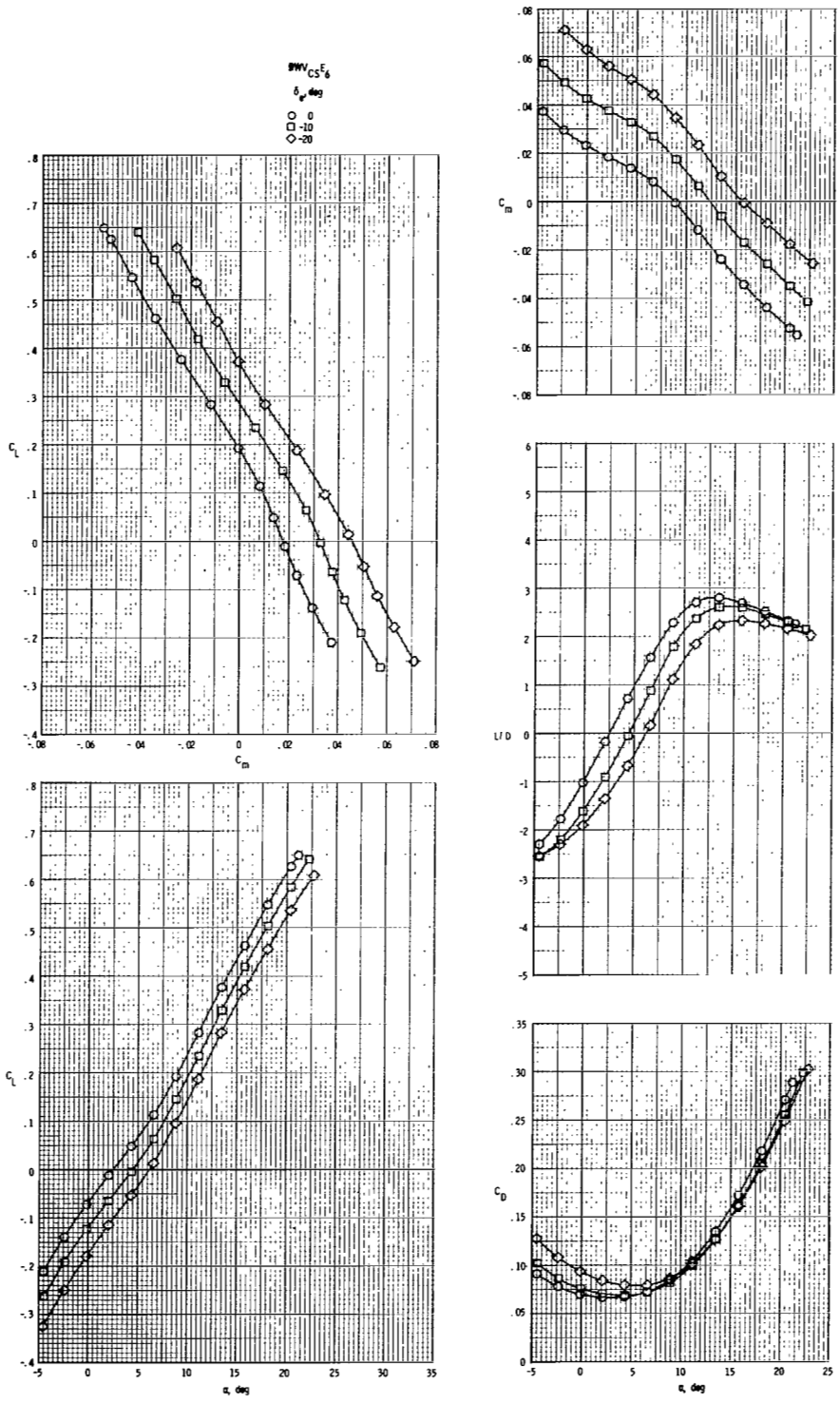
(c) $M_\infty = 0.95$.

Figure 18.- Continued.



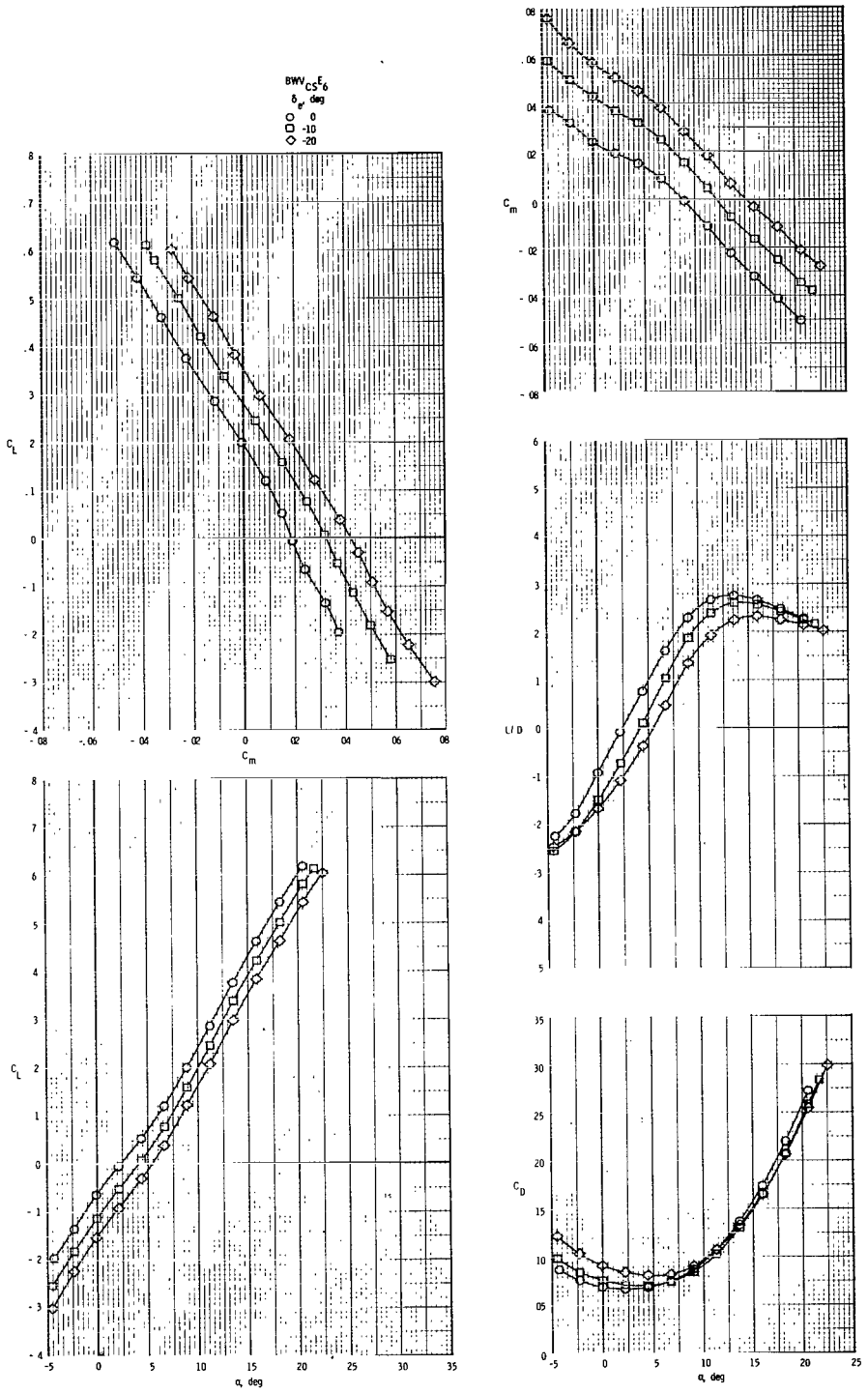
(d) M_∞ = 0.98.

Figure 18.- Continued.



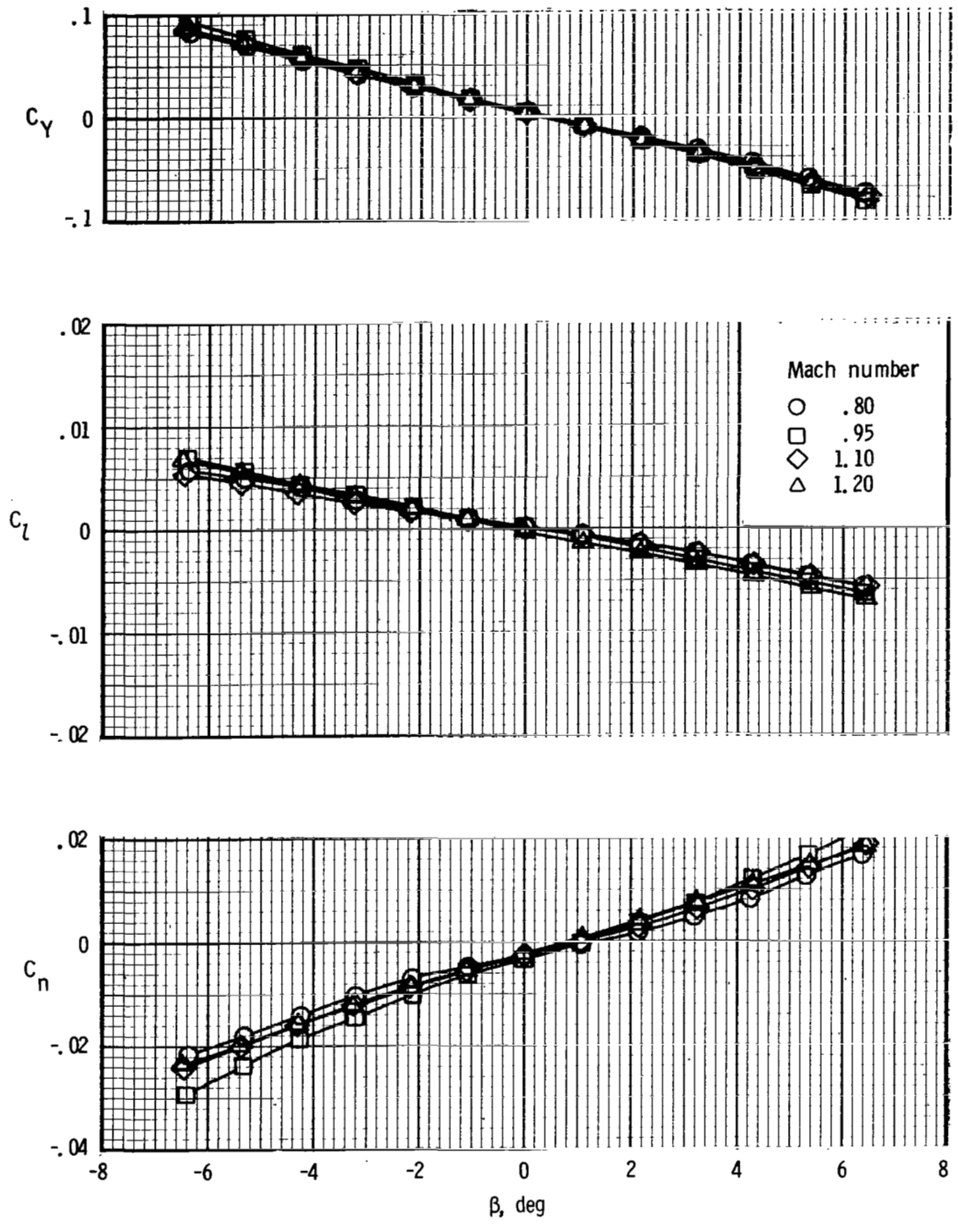
(e) M_∞ = 1.10.

Figure 18.- Continued.



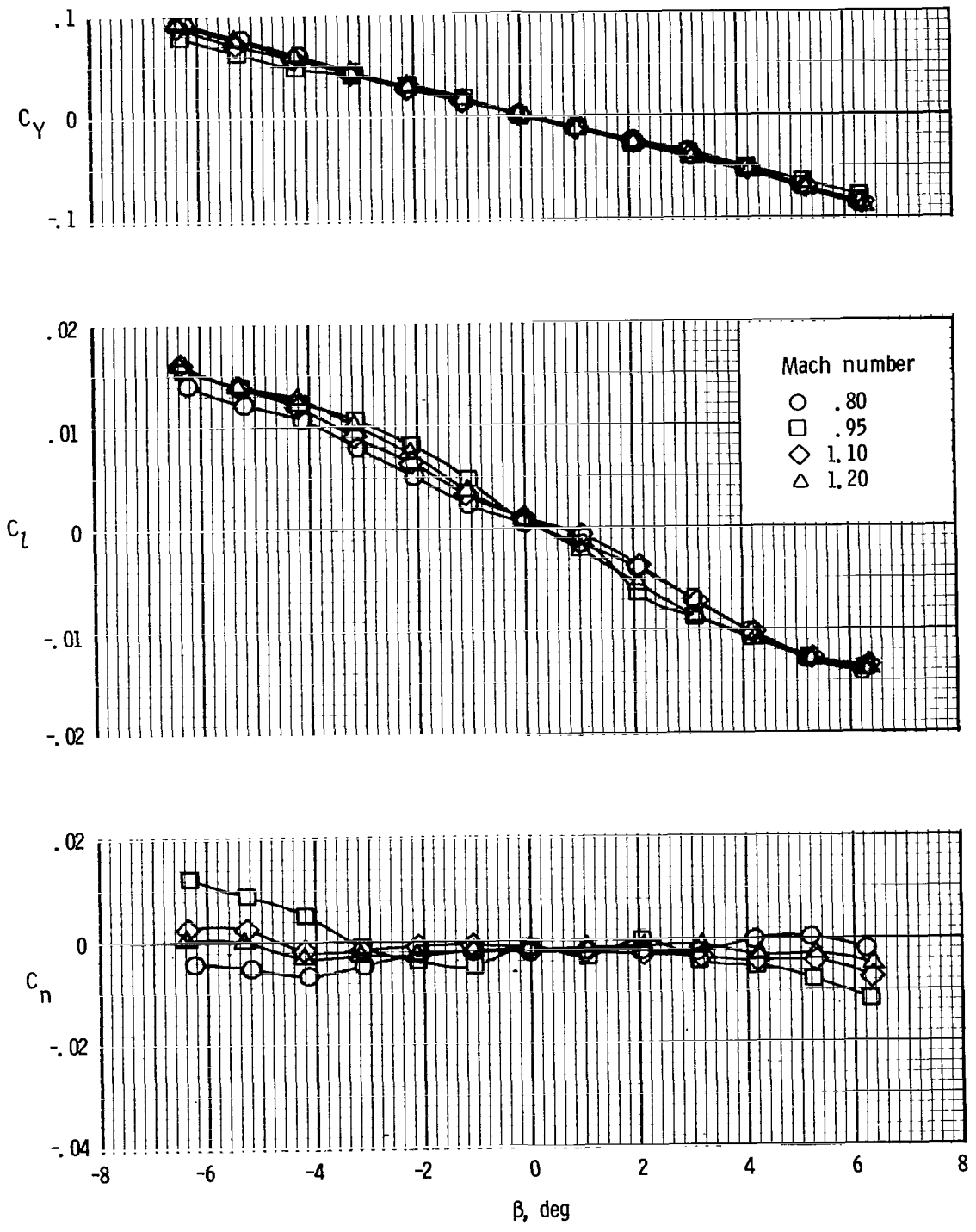
(f) M_∞ = 1.20.

Figure 18.- Concluded.



(a) $\alpha \approx 0^{\circ}$.

Figure 19.- Lateral aerodynamic characteristics of $BWV_{CS}E_6$ configuration.



(b) $\alpha \approx 17^\circ$.

Figure 19.- Concluded.

1. Report No.	2. Government Accession No.	3. Recipient's Catalog No.
NASA TP-1044		

4. Title and Subtitle
AERODYNAMIC CHARACTERISTICS AT MACH NUMBERS FROM 0.33 TO 1.20 OF A WING-BODY DESIGN CONCEPT FOR A HYPERSONIC RESEARCH AIRPLANE

5. Report Date
December 1977

6. Performing Organization Code

7. Author(s)
James L. Dillon and Jimmy L. Pittman

8. Performing Organization Report No.
L-11723

10. Work Unit No.
505-11-31-02

9. Performing Organization Name and Address
NASA Langley Research Center
Hampton VA 23665

11. Contract or Grant No.

13. Type of Report and Period Covered
Technical Paper

12. Sponsoring Agency Name and Address
National Aeronautics and Space Administration
Washington, DC 20546

14. Sponsoring Agency Code

15. Supplementary Notes

16. Abstract

An experimental investigation of the static aerodynamic characteristics of a model of one design concept for the proposed National Hypersonic Flight Research Facility was conducted in the Langley 8-foot transonic pressure tunnel. The experiment consisted of configuration buildup from the basic body by adding a wing, center vertical tail, and a three-module or six-module scramjet engine. The free-stream test Mach numbers were 0.33, 0.80, 0.90, 0.95, 0.98, 1.10, and 1.20 at Reynolds numbers per meter ranging from 4.8×10^6 to 10.4×10^6. The test angle-of-attack range was approximately -4° to 22° at constant angles of sideslip of 0° and 4°; the angle of sideslip ranged from about -6° to 6° at constant angles of attack of 0° and 17°. The elevons were deflected 0°, -10°, and -20° with rudder deflections of 0° and 15.6°.

17. Key Words (Suggested by Author(s))
Aerodynamics
Transonic performance stability and control
Hypersonic aircraft

18. Distribution Statement
Unclassified - Unlimited

Subject Category 02

19. Security Classif. (of this report)	20. Security Classif. (of this page)	21. No. of Pages	22. Price*
Unclassified	Unclassified	73	$5.25

* For sale by the National Technical Information Service, Springfield, Virginia 22161

NASA-Langley, 1977

National Aeronautics and
Space Administration

Washington, D.C.
20546

Official Business
Penalty for Private Use, $300

THIRD-CLASS BULK RATE

Postage and Fees Paid
National Aeronautics and
Space Administration
NASA-451

U.S.MAIL

1 1 1U,A, 110777 S00903DS
DEPT OF THE AIR FORCE
AF WEAPONS LABORATORY
ATTN: TECHNICAL LIBRARY (SUL)
KIRTLAND AFB NM 87117

NASA

POSTMASTER: If Undeliverable (Section 158 Postal Manual) Do Not Return